

Spring 2015

Development of a Practical Visual-Evoked Potential-Based Brain-Computer Interface

Nicholas R. Waytowich
Old Dominion University

Follow this and additional works at: https://digitalcommons.odu.edu/biomedengineering_etds

Part of the [Biomedical Engineering and Bioengineering Commons](#), and the [Neuroscience and Neurobiology Commons](#)

Recommended Citation

Waytowich, Nicholas R.. "Development of a Practical Visual-Evoked Potential-Based Brain-Computer Interface" (2015). Doctor of Philosophy (PhD), dissertation, Biomedical Engineering, Old Dominion University, DOI: 10.25777/wbdc-2v05
https://digitalcommons.odu.edu/biomedengineering_etds/6

This Dissertation is brought to you for free and open access by the Biomedical Engineering at ODU Digital Commons. It has been accepted for inclusion in Biomedical Engineering Theses & Dissertations by an authorized administrator of ODU Digital Commons. For more information, please contact digitalcommons@odu.edu.

DEVELOPMENT OF A PRACTICAL VISUAL-EVOKED POTENTIAL-BASED BRAIN-COMPUTER INTERFACE

by

Nicholas R. Waytowich
B.S. May 2006, University of North Florida
M.Eng. May 2013, Old Dominion University


A Dissertation Submitted to the Faculty of
Old Dominion University in Partial Fulfillment of the
Requirements for the Degree of

DOCTOR OF PHILOSOPHY

BIOMEDICAL ENGINEERING

OLD DOMINION UNIVERSITY

May 2015

Approved by: 

Dean J. Krusienski (Director)

Jiang Li (Member)

Tamer Nadeem (Member)

Alan Rone (Member)

Christian Zemlin (Member)

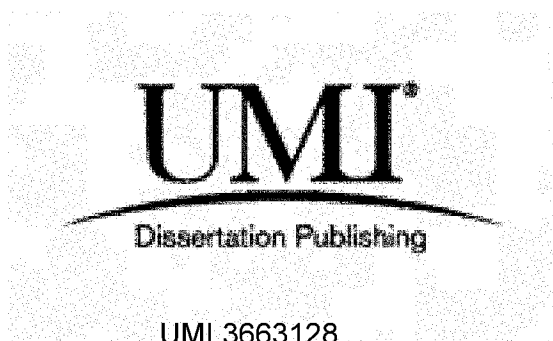
UMI Number: 3663128

All rights reserved

INFORMATION TO ALL USERS

The quality of this reproduction is dependent upon the quality of the copy submitted.

In the unlikely event that the author did not send a complete manuscript and there are missing pages, these will be noted. Also, if material had to be removed, a note will indicate the deletion.

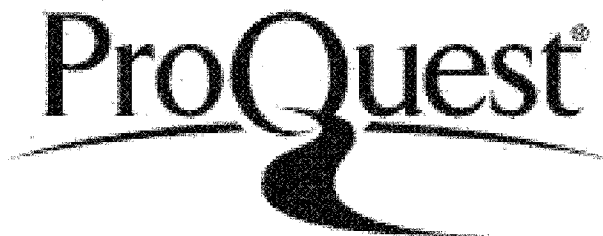


UMI 3663128

Published by ProQuest LLC 2015. Copyright in the Dissertation held by the Author.

Microform Edition © ProQuest LLC.

All rights reserved. This work is protected against
unauthorized copying under Title 17, United States Code.



ProQuest LLC
789 East Eisenhower Parkway
P.O. Box 1346
Ann Arbor, MI 48106-1346

ABSTRACT

DEVELOPMENT OF A PRACTICAL VISUAL-EVOKED POTENTIAL-BASED BRAIN-COMPUTER INTERFACE

Nicholas R. Waytowich
Old Dominion University, 2015
Director: Dr. Dean J. Krusienski

There are many different neuromuscular disorders that disrupt the normal communication pathways between the brain and the rest of the body. These diseases often leave patients in a “locked-in” state, rendering them unable to communicate with their environment despite having cognitively normal brain function. Brain-computer interfaces (BCIs) are augmentative communication devices that establish a direct link between the brain and a computer. Visual evoked potential (VEP)-based BCIs, which are dependent upon the use of salient visual stimuli, are amongst the fastest BCIs available and provide the highest communication rates compared to other BCI modalities. However, the majority of research focuses solely on improving the raw BCI performance; thus, most visual BCIs still suffer from a myriad of practical issues that make them impractical for everyday use. The focus of this dissertation is on the development of novel advancements and solutions that increase the practicality of VEP-based BCIs. The presented work shows the results of several studies that relate to characterizing and optimizing visual stimuli, improving ergonomic design, reducing visual irritation, and implementing a practical VEP-based BCI using an extensible software framework and mobile devices platforms.

Copyright, 2015, by Nicholas R. Waytowich, All Rights Reserved.

“Dedicated to my mother, Dr. Waytowich, who inspired me to pursue my own
doctoral degree so that we may ultimately become a pair-o’-docs”

ACKNOWLEDGMENTS

I would like to thank everyone who has been a part of my life during my Ph.D. studies. I would like to thank my advisor, Dr. Dean J. Krusienski, who first invited me to join his research lab back in 2010, for his unwavering mentorship and support over the past five years. His guidance has been an invaluable asset throughout the course of my dissertation research and has shaped the researcher I am today.

I would like to thank everyone on my dissertation committee, Dr. Jiang Li, Dr. Alan Pope, Dr. Christian Zemlin, and the recent addition of Dr. Tamer Nadeem, for their comments, help, and suggestions that ultimately improved the quality of this dissertation.

I would also like to thank my family for their continual support throughout this entire process. Thank you to my parents, my sister, my grandparents and my aunts and uncles for providing me the encouragement that I needed. I would especially like to thank my Mother, the person who inspired me the most in my decision to pursue a doctoral degree. Thank you for your unconditional love and support.

TABLE OF CONTENTS

	Page
LIST OF TABLES	viii
LIST OF FIGURES	xii
Chapter	
1. INTRODUCTION	1
1.1 CURRENT CHALLENGES FOR BCIS	1
1.2 APPROACH, ORGANIZATION, AND CONTRIBUTIONS	2
2. BACKGROUND	4
2.1 BRAIN-COMPUTER INTERFACES	4
2.2 VISUAL EVOKED POTENTIALS	6
2.3 THE VISUAL SYSTEM AND THE PRIMARY VISUAL CORTEX ..	9
2.4 VEP-BASED BCIS	11
2.5 VEP SIGNAL PROCESSING TECHNIQUES	17
2.6 PERFORMANCE VS. PRACTICALITY	19
3. TEMPORAL CHARACTERIZATION OF THE SSVEP SPECTRUM USING CHIRP-MODULATED STIMULI	21
3.1 INTRODUCTION	21
3.2 METHODOLOGY	22
3.3 RESULTS	27
3.4 DISCUSSION	29
4. MULTICLASS SSVEP FREQUENCY EVALUATION USING CHIRP-MODULATED STIMULI	35
4.1 INTRODUCTION	35
4.2 METHODOLOGY	36
4.3 RESULTS	43
4.4 DISCUSSION	47

5. SPATIAL FREQUENCY CHARACTERIZATION AND OPTIMIZATION OF SSVEP STIMULI	51
5.1 INTRODUCTION	51
5.2 METHODOLOGY	53
5.3 RESULTS	62
5.4 DISCUSSION	69
6. SPATIAL DECOUPLING OF TARGETS AND FLASHING STIMULI FOR VISUAL BRAIN-COMPUTER INTERFACES	72
6.1 INTRODUCTION	73
6.2 METHODOLOGY	75
6.3 RESULTS	86
6.4 DISCUSSION	91
7. LARGE-SCALE TARGET DISCRIMINATION USING SPATIALLY DE- COUPLED STIMULI	94
7.1 INTRODUCTION	94
7.2 METHODOLOGY	95
7.3 RESULTS	97
7.4 DISCUSSION	98
8. PRACTICAL IMPLEMENTATION AND DEVELOPMENT	105
8.1 DEVELOPMENT OF FLEXIBLE SOFTWARE	106
8.2 IMPLEMENTATION AND VALIDATION	113
8.3 FUTURE DIRECTIONS WITH MODERN VISUAL OVERLAY DE- VICES	122
9. CONTRIBUTIONS AND FUTURE DIRECTIONS	126
BIBLIOGRAPHY	130
VITA	143

LIST OF TABLES

Table	Page
1. Classification results for different frequency sets	32
2. Offline Accuracies	86
3. Online Accuracies ($t = 6.3$ seconds) and Visual Irritation Index	91

LIST OF FIGURES

Figure	Page
1. Block diagram of a standard BCI system	5
2. Diagram of the five most common types of Visual Evoked Potentials: Transient, Steady-State, Chirp, Motion and Code-Modulated VEPs	7
3. Diagram showing the major components of the human visual system.	10
4. Diagram of the parallel visual pathways showing the connections from the retina to the visual cortex in the brain.	11
5. Stimulating waveforms and corresponding evoked EEG response of an SSVEP based BCI.	13
6. Diagram of c-VEP based BCI showing time-delayed m-sequence stimulus waveforms and corresponding c-VEP evoked response properties	15
7. Diagram illustrating the use of CCA for SSVEP target detection.	19
8. The EEG electrode montage used for data collection in the SSVEP fre- quency characterization study.	23
9. Diagram of the LED visual stimulator used to display the chirp-modulated waveforms.	24
10. Schematic of the driving circuit for the LED visual stimulator.	25
11. Heat map plot of CCA squared correlation values averaged across all subjects.	30
12. CCA correlation values of the SSVEP response as a function of stimulation frequency averaged across all subjects.	31
13. Histogram plot showing the relative occurrence of each frequency in the optimal frequency sets for all subjects.	33
14. Canonical Correlation Analysis (CCA) squared correlation values aver- aged across the 17 subjects.	38
15. Diagram of standard and proposed genetic algorithm crossover techniques.	42
16. Accuracy and Information Transfer Rate (ITR) of the best solution from the classification error and ECMN optimizations for each N-class condition	44

17.	Comparison of the ECM Norm for the best solutions selected by the Classification Error and ECM Norm optimizations	45
18.	Information Transfer Rate (ITR) performance for the top 10 best optimization solutions for each N-class condition.	46
19.	2-D histogram plots of optimized feature sets for each N-class condition.	48
20.	Electrode montage used for the SSVEP spatial frequency characterization and optimization study.	54
21.	Diagram of checkerboard stimuli with different spatial frequencies used in the SSVEP study.	56
22.	Stimulation paradigm used for the discrete classification task in experiment 1.	58
23.	Stimulation paradigm used for the path-navigation task in experiment 2.	59
24.	Average Classification accuracy for experiment 1 for each spatial frequency condition vs observation length.	64
25.	Average ITR (bits/min) for experiment 1 for each spatial frequency condition vs observation length.	65
26.	Spatial Frequency tuning curves from the discrete classification task in experiment 1.	66
27.	Classification accuracy vs time window length averaged across all subjects from experiment 1.	67
28.	Average subjective evaluation of visual irritation for each spatial frequency condition.	67
29.	Run-duration and path-completion percentage averaged across all subjects for the path navigation task in experiment 2.	68
30.	Ring paradigm used in the c-VEP study showing the workspace, target locations and target groupings.	77
31.	The EEG electrode montage used for the c-VEP study based on the International 10-20 system.	80
32.	Diagram of the online paradigm and timing protocol.	82

33. Simulated average classification accuracies for the offline and online experiments as a function of observation length in # of complete m-sequence cycles.	88
34. Confusion matrices for the three offline 8-class conditions (direct-foveal, near-foveal, parafoveal) for the 6.3 s observation length.....	89
35. The CCA spatial weight topographies and template waveforms for the foveal and parafoveal conditions, respectively, from a representative subject (S1).	90
36. Average classification accuracy and ITR plots for 25-class c-VEP target discrimination.	99
37. Confusion matrix for the 25-class c-VEP target discrimination averaged across all subjects.	100
38. 25-target source characterization plot averaged across all subjects.	101
39. Single channel correlation activations for each of the 25-target positions averaged across all subjects.	102
40. Diagram of the software architecture for the VESSELS platform showing the four major software components.	108
41. Main graphical user interface system for the VESSELS framework.	109
42. Screenshots of several native applications built into VESSELS.	111
43. Screenshots of the SOCS system within VESSELS showing various applications.	112
44. Standard configuration of the Arduino UNO development board with AT-mega328 chip	114
45. Universal Datagram Protocol (UDP) communication architecture.....	116
46. Control-diagram for a motorized wheelchair controlled by an SSVEP based BCI.	117
47. Pictures of the BCI controlled wheelchair and telepresence systems in action.	119
48. Control-diagram for a telepresence wheelchair system controlled by an SSVEP based BCI.	120
49. Pictures showing other developed BCI systems and hardware applications.	121

50.	Schematic diagram of the Google Glass visual overlay device.	123
51.	Diagram of the proposed system setup using a VEP based BCI with a visual overlay device.	125

CHAPTER 1

INTRODUCTION

There are many different neuromuscular disorders that disrupt the normal communication pathways between the brain and the rest of the body. Diseases such as amyotrophic lateral sclerosis (ALS), spinal cord injury, muscular dystrophy, cerebral palsy, etc., are disorders that degrade muscles as well as the neuromuscular pathways that control them. Nearly two-million people suffer from these neuromuscular disorders in the United States alone, with many more worldwide [Ficke and Science Management Corp. Washington, 1992]. The level of degradation can sometimes be severe enough that the affected patients are left in a “locked-in” state, leaving them completely unable to communicate with their environment despite having cognitively normal brain function. One possible intervention for these individuals is to augment or bypass the impaired neuromuscular pathways and communicate directly with the brain. Over the past 25 years, research in the fields of neural-engineering and rehabilitation have focused on restoring communication to these individuals by establishing a direct communication channel between the brain and an external device using a Brain-Computer Interface (BCI). However, despite being demonstrated in laboratory settings for years, BCIs still suffer from many impracticalities that severely limit their widespread adoption by the target population.

1.1 CURRENT CHALLENGES FOR BCIS

BCIs currently face enormous challenges in the ultimate goal of becoming a practical form of augmentative communication. These challenges include but are not limited to: low information transfer rates compared to other forms of communication modalities; low reliability due to noisy and non-stationary EEG data; visual irritation and fatigue due to obtrusive stimulus flashing; lack of self-paced systems due to high synchronous system timing; long calibration times; and general lack of

low-cost hardware and software [Johnson et al., 2011]. Because of these and other issues, BCIs often perform sub-optimally when moving from laboratory settings to real-world applications.

1.2 APPROACH, ORGANIZATION, AND CONTRIBUTIONS

The forefront of BCI research has been to increase performance (i.e. raw accuracy or speed) at the expense of usability, comfort and overall ergonomics of the BCI system. The work and contributions presented in this dissertation focus on the heavily overlooked aspect of BCI practicality. Overall, this work involves optimizing stimulus characteristics, improving the paradigmatic design of visual stimulation, and developing functional software and hardware systems for practical BCI applications. This work helps to make considerable strides for research and development of practical Visual Evoked Potential (VEP)-based BCI systems.

In the development of a practical VEP-based BCI, characterization and optimization of the visual stimulus is needed to improve the fidelity and robustness of the evoked response within the brain. Visual stimuli can have various temporal frequency and spatial frequency characteristics which can vary the signal intensity and fidelity of the evoked response. This first component of this dissertation presents the results of several studies that have been conducted to characterize and optimize both the temporal and spatial components of visual stimuli that are commonly used in SSVEP-based BCIs. The second component presents two studies that introduce a novel paradigmatic concept that separates targets from flashing stimuli for VEP-BCIs. The final component implements flexible software and hardware for practical VEP-BCI deployment.

Chapter 2 outlines all of the background information preluding the work presented in this dissertation. Chapters 3 and 4 describe two studies that characterize the temporal frequency profile of the SSVEP response spectrum using chirp-modulated stimulation. The overall contribution is a novel characterization of the SSVEP response as a function of frequency. Additionally, Chapter 4 provides a performance optimization of stimulus frequency selection for multiclass SSVEP BCIs.

Chapter 5 details a study that evaluates SSVEP BCI performance using stimuli with different spatial frequencies. The contribution of this chapter is a novel characterization of SSVEP performance over the functional spatial frequency range and the determination of a spatial frequency optimization profile for flashing stimuli in an online 4-class SSVEP BCI. Additionally, chapter 5 demonstrates that accurate BCI performance can be achieved using less fatiguing, high spatial frequency stimuli.

Chapters 6 and 7 detail two studies that introduce and investigate the spatial decoupling of BCI targets from their respective flashing stimuli. These studies resulted in a major contribution that breaks the traditional notion of one-to-one stimulus-target correspondence by demonstrating comparable classification performances with indirect fixation of spatially decoupled stimuli. This results in reduced visual irritation as stimuli are not required to be directly fixated on. Additionally, spatial decoupling reduces the number of overall flashing stimuli compared to traditional approaches.

Chapter 8 outlines the development and implementation of an extensible software platform that can be used for a wide variety of VEP BCI applications. The main contributions of this chapter are: 1) a fully functional and extensible software platform known as the Visual Evoked Stimulation and SElection Software (VESSELS) and 2) a working prototype of a practical BCI-controlled wheelchair application with mobile device implementation.

The final chapter concludes this dissertation by summarizing the main findings and contributions and proposing future directions of this work.

CHAPTER 2

BACKGROUND

2.1 BRAIN-COMPUTER INTERFACES

A brain-computer interface (BCI) is an augmentative communication device that decodes brain activity to reveal user intent and translates that intention into useful device commands [Wolpaw et al., 2002, Wolpaw and Wolpaw,]. BCIs consist of three major components: signal acquisition, signal processing, and application. Figure 1 shows a block diagram of a typical BCI system. The brain activity of the user can be acquired using a number of different methods which can be classified as either invasive or non-invasive. Invasive methods, such as electrocorticography (ECoG), record electromagnetic potentials generated from brain activity using electrodes placed either on the surface or deep inside the brain. Non-invasive methods, such as electroencephalography (EEG), record the electromagnetic potentials from the surface of the scalp. ECoG signals have high spatial and temporal resolution; however, they require brain surgery for electrode implantation. EEG does not require any surgery; however, it suffers from comparatively poor signal quality as the brain signals are blurred and attenuated by volume conduction through the skull and scalp tissue. There are several other non-invasive recording techniques such as functional magnetic resonance imaging (fMRI), magnetoencephalography (MEG) and Positron Emission Tomography (PET); however, due to their expense and size, EEG remains the most commonly used signal acquisition method for BCIs.

Once the signals are acquired, they are analyzed and decoded in a signal processing module. This typically involves two steps: feature extraction and feature classification. Feature extraction is the process of reducing signal dimensionality by extracting certain characteristics or features from the brain signal that reflect the

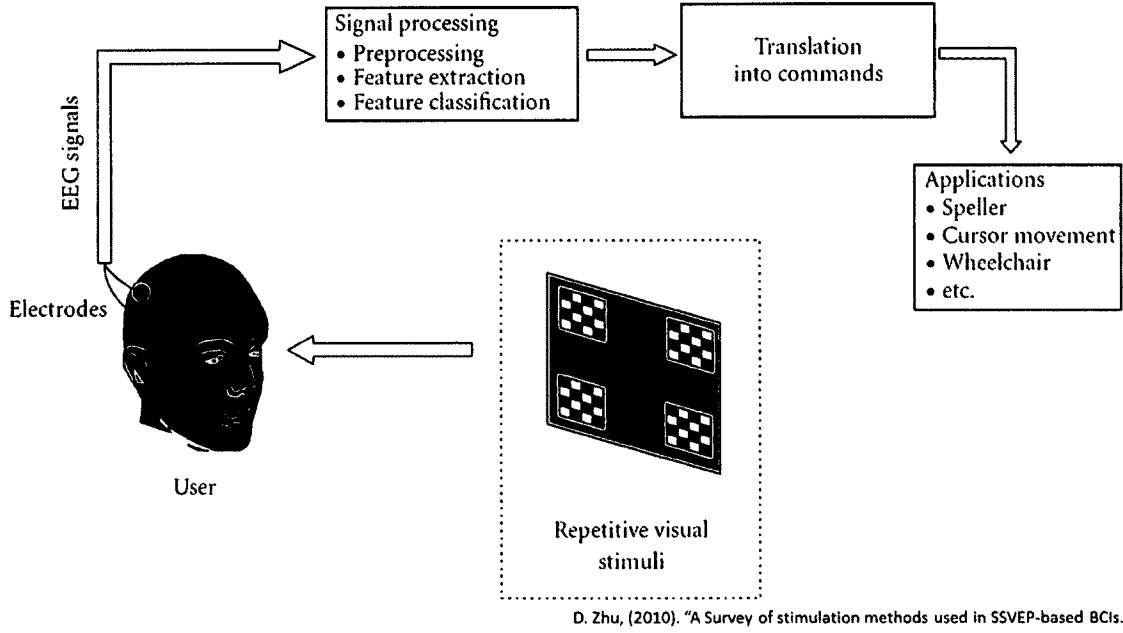


FIG. 1: A block diagram showing a standard BCI system [Zhu et al., 2010]. Brain-activity is recorded and digitized (usually in response to exogenous stimuli). The digitized signals are then processed using feature extraction and classification algorithms. The output of the signal processing components are translated to device commands that reflect user intent which are used to control the BCI application.

task being performed. The features are then classified using machine learning techniques to reveal underlying user intent. EEG signals often require a pre-processing step in which temporal or spatial filtering techniques are applied to boost the signal to noise ratio (SNR) of the EEG. Once the signals are finally classified, they are sent to a BCI application for control of the computer via a virtual keyboard or mouse or for control of an external peripheral device such as a motorized wheelchair or neuro-prosthetic limb [Pfurtscheller et al., 2010, Li et al., 2013].

There are several different types of BCI modalities that can be broadly classified under two distinct classifications: Independent BCIs and dependent BCIs. The former type represent BCIs that are independent of any external stimuli and do not require any exogenously evoked brain-signals. These types of BCIs rely purely on endogenous, or self-generated, brain-signal modulation. Such endogenous BCI control signals include slow-cortical potentials (SCPs) and sensory motor rhythms (SMRs).

In the SCP BCI, a user can be trained to slowly modulate the resting EEG potentials over the frontal lobe to slightly increase or decrease EEG amplitude for a 2-class yes/no communication paradigm [Hinterberger et al., 2004, Kubler et al., 2004]. The SMR BCI utilizes a sensory-motor cortex phenomenon known as event-related synchronization/de-synchronization in which 12-16 Hz oscillating rhythms over the motor-cortex, known as the mu rhythm, de-synchronize and re-synchronize after imagined limb movement onset and offset, respectively. This type of modulation is again self-generated and can be trained to control a 2-class yes/no BCI [Wolpaw et al., 1991]. Dependent BCIs are BCIs which rely on external stimuli to evoke brain-signal modulations. These exogenously generated signals can be elicited through different modalities such as visual, auditory, or tactile stimulation, with visual stimulation being the most common and widely used. Dependent BCIs driven by visual stimuli utilize innately generated visual evoked potentials (VEPs), which are robust in nature and have been found to provide a more consistent and reliable signal for communication and control compared to other BCI modalities [Wolpaw et al., 2002].

2.2 VISUAL EVOKED POTENTIALS

Visual Evoked Potentials (VEPs) are involuntary electro-physiological potentials that arise in the visual cortex of the brain in response to a flashing stimulus [Galloway, 1990]. Background EEG (naturally occurring EEG activity) can mask VEP responses; thus, averaging and spatial filtering techniques are utilized to enhance the VEP response. VEPs have been heavily researched by cognitive and clinical neuroscientists to diagnose visual system deficiencies.

There are several different types of VEPs, namely: transient VEPs, steady-state VEPs, chirp-VEPs, motion VEPs and code-modulated VEPs [Galloway, 1990, Sutter, 1992].

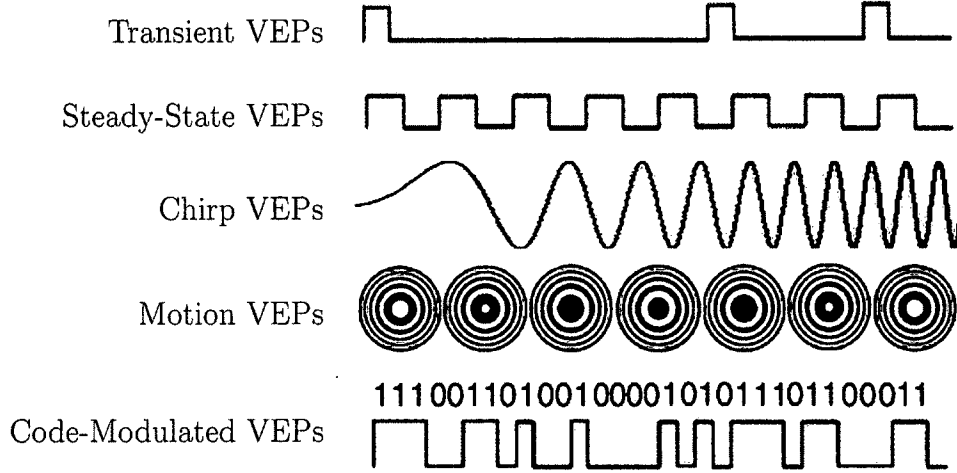


FIG. 2: Diagram of the five most common types of Visual Evoked Potentials: Transient, Steady-State, Chirp, Motion and Code-Modulated VEPs

Transient VEPs:

Transient VEPs (TVEPs) are electrical potentials resulting from a transient response in the brain due to an intermittent visual stimulus [Celesia et al., 1982]. TVEPs are typically evoked from either low-frequency stimuli ($< 2\text{Hz}$) or single flash stimuli. These VEPs are characterized by a transient deflection in the EEG that returns to baseline a short period after stimulus onset [Tobimatsu et al., 1993].

Steady-State VEPs:

Steady-state VEPs (SSVEPs) are sustained, oscillatory responses from steady-state, repetitively flashing stimuli ($> 5\text{Hz}$). SSVEPs have distinct fundamental and harmonic frequency components that correspond to the fundamental frequency of the attended stimulus [Celesia et al., 1982, Middendorf et al., 2000].

The SSVEP response can be elicited from stimuli with steady-state frequencies in the range of 1-100 Hz [Herrmann, 2001]. However, most SSVEP BCI studies utilize flashing stimuli from the more functional 5-45 Hz range [Chen et al., 2014, Ng et al., 2012, Zhang et al., 2012, Zhu et al., 2010]. Higher frequency stimulation produces weaker responses as EEG power is inversely proportional to frequency

[Vialatte et al., 2010]. When the visual stimulus is a combination of two frequencies f_1 and f_2 , the SSVEP will produce responses at the average frequency $[f_1 + f_2]/2$ in addition to responses at f_1 and f_2 [Hwang et al., 2013]. SSVEPs tend to have a high inter-subject variability in response strength across frequencies [Vialatte et al., 2010].

Chirp VEPs:

Chirp-VEPs are VEPs elicited from a signal with linearly changing frequency (chirp signal) [Tu et al., 2012]. Chirp-VEPs have embedded frequency components that correspond to the central frequency and chirp rate of the chirp stimulus. Chirp VEPs have been elicited using chirp rates of 4-8Hz/s [Tu et al., 2012]. Chirp-VEPs have similar frequency matching characteristics as SSVEPs, such that they can be considered a generalization of SSVEPs (i.e. Chirp-VEPs are SSVEPs when the chirp rate is zero).

Motion-Onset VEPs:

Motion-onset VEPs (MVEPs) are VEPs that respond to the slight onset of motion of visual stimuli [Guo et al., 2008]. MVEPs are often coupled with SSVEPs to produce responses with spatio-temporal characteristics. Xie et al., used steady state oscillations between concentric rings to elicit the SSMVEP (a combination of both the SSVEP and MVEP) [Xie et al., 2012].

Code-Modulated VEPs:

Code-modulated VEPs (c-VEPs) are VEPs elicited from a pseudo-random stimulus sequence. The response characteristics of the c-VEP are largely dependent on the characteristics of the underlying stimulus code. c-VEPs generated from a maximum-length sequence (m-sequence) will have embedded broadband frequency components and will have a characteristically sharp autocorrelation [Bin et al., 2009a].

2.3 THE VISUAL SYSTEM AND THE PRIMARY VISUAL CORTEX

The human visual system is a very complicated and intricate system consisting of components such as the retina, optic nerves, optic chiasm, optic tracts, thalamus, lateral geniculate nucleus, and the visual cortex that all work together to process and make sense of all visual stimuli [Rentschler et al., 1975]. The retina itself contains approximately 100 million photoreceptor cells known as rod and cone cells, the latter of which are primarily used to distinguish color. These photoreceptor cells contain light-sensitive proteins that induce thresholded action-potentials. The optic nerve is a bundle of approximately 1 million electrically excitable fibers that carry information from the retinal photoreceptor cells to the visual cortex. The optic nerve passes through the lateral geniculate nucleus (LGN) which is a sensory relay station that resides in the thalamus. The visual cortex is the largest system in the brain that handles all of the visual sensory information for image processing. The visual cortex consists of the primary visual cortex (V1) and secondary visual cortices (V2, V3, V4, V5). Information travels from excited retinal cells, through the optic tract via optic nerve fibers to the LGN. The LGN relays the visual information to the primary visual cortex which then gets distributed about the secondary visual cortices. Due to the contralateral nature of the optic chiasm, information from the left visual field gets processed by the right occipital lobe of the visual cortex while information from the right visual field gets processed by the left occipital lobe. Figure 3 shows a general diagram of the visual system. Information flow in the visual system is composed of two major visual pathways (Parvocellular and Magnocellular pathways shown in Figure 4) that convey visual aspects of what is seen from the retina to the brain. The Parvocellular pathway (PC) is responsible for conveying sustained responses of high spatial contrasts and color information to the brain, whereas the Magnocellular pathway (MC) is responsible for conveying motion and depth information. [Tanaka, 1996]. VEP research exploring these two pathways has found that, in response to a flashing stimulus, the PC pathway, made up of slow cells, is responsible for the first harmonic response and the MC pathway, made up of fast cells, is responsible for the second

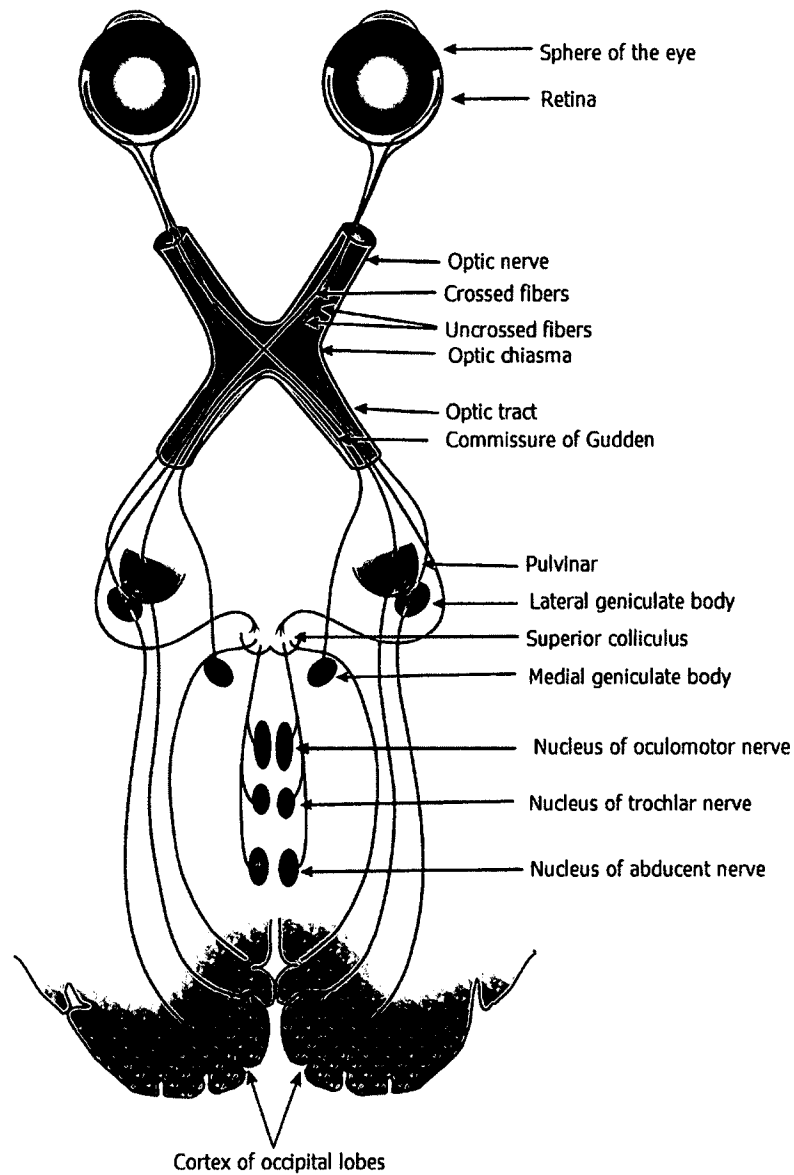


FIG. 3: Diagram showing the major components of the visual system. Light enters through the cornea of the left or right eye to excite the photosensitive rod and cone cells in the retina. The corresponding activity travels through the optic tract along optic nerve fibers, through the optic chiasm and towards the lateral geniculate nucleus in the thalamus. The information then gets relayed to the primary visual cortex for hierarchical processing. [Schroeder, 2014].

harmonic response [McKeefry et al., 1996, Lalor et al., 2007, Lalor and Foxe, 2009].

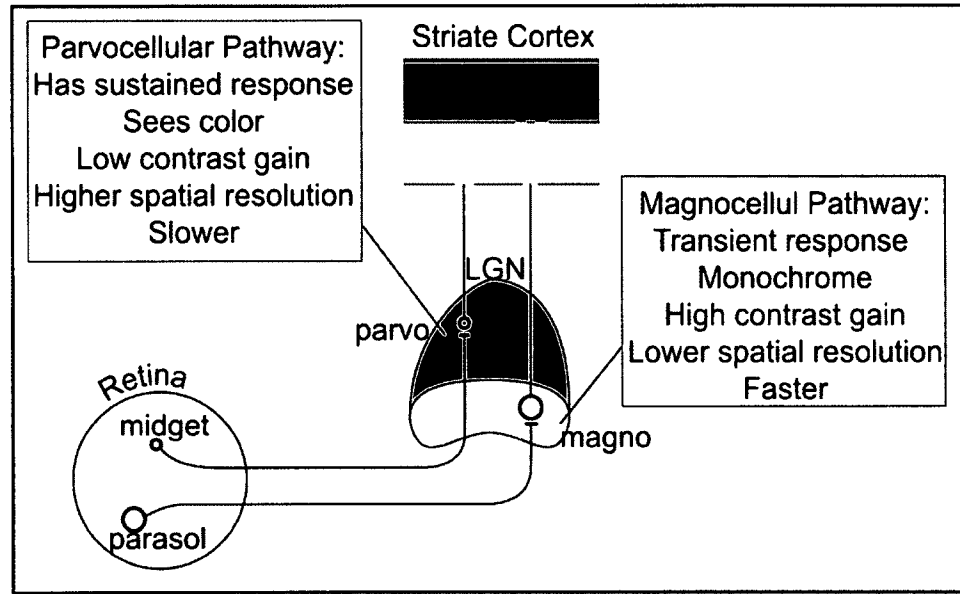


FIG. 4: The connections from the retina to the visual cortex in the brain can be grouped into two parallel visual pathways. The Magnocellular (MC) pathway processes fast moving stimuli with high contrast. The Parvocellular (PC) pathway processes fine detailed stimuli with high spatial resolution. The PC pathway also processes color information. [Haslwanter, 2011].

2.4 VEP-BASED BCIS

The innate and reliable response characteristics of VEPs have made them a desirable signal for use in BCIs. As such, VEP-based BCIs have become very popular in BCI research as they exhibit superior communication speeds and classification accuracies compared to other BCI modalities [Wang et al., 2008]. In a VEP based BCI, one or more visual stimuli are utilized to elicit characteristic VEP responses unique to each stimulus. Decoding techniques can be used to extract the VEP and find the corresponding stimulus target which can represent any command or action for the user. VEPs of each type have been incorporated into a BCI [Hwang et al., 2013, Tu et al., 2012, Guo et al., 2008, Bin et al., 2009a]; however, the most popular and widely used VEP based BCI is the SSVEP BCI [Diez et al., 2013, Allison et al., 2008, Bakardjian et al., 2010, Burkitt et al., 2000,

Cheng et al., 2002, Jin et al., 2011]. Recently, an improvement to the SSVEP BCI has been the implementation of the c-VEP BCI [Bin et al., 2011, Spüler, 2012]. C-VEP BCI research is relatively new, and the dynamics of the c-VEP are not as well understood as SSVEP dynamics. Initial studies have shown that the c-VEP has multiple advantages over the SSVEP as a BCI control signal [Bin et al., 2009a].

2.4.1 SSVEP BCIS

The SSVEP BCI was first implemented by Middendorf et al., in 2000 using a cathode ray tube computer monitor [Middendorf et al., 2000]. This initial attempt using SSVEPs for a BCI consisted of two virtual buttons on a monitor for a two-target system in which each target flashed at a distinct frequency (23.42Hz and 17.56Hz). Their system, which measured frequency response amplitudes from channels O_1 and O_2 , achieved an average accuracy of 92% with an average selection time of 2.1s. Since then, numerous improvements have been made to SSVEP-BCIs in both performance and in usability. These performance and usability enhancements have come in the form of novel stimulus design, improved signal processing and classification algorithms and novel application paradigms.

The fundamental principle of multiple target selection for SSVEP-BCIs has been based on the frequency-division multiple access strategy (FDMA), in which each target is allotted a distinct frequency so that selections can be made based on detecting responses from those frequencies. Figure 5 illustrates the FDMA principle for an SSVEP BCI by showing example stimulating sequences (Figure 5a) and the power spectrum of the evoked SSVEP response in (Figure 5b) from a 10Hz stimulus. This sets a limitation on the number of targets that can be employed in an SSVEP-BCI as LCD monitors with a 60Hz refresh rate, which are frequently utilized in practice, are limited in the number of distinct frequencies they can produce. This limitation can bottleneck the overall performance an SSVEP-BCI can achieve as the information-transfer rate (ITR) is dictated by the accuracy of the system, the time required for the system to make a selection and the number of targets employed in the system. One solution to this problem is combining both frequency and phase

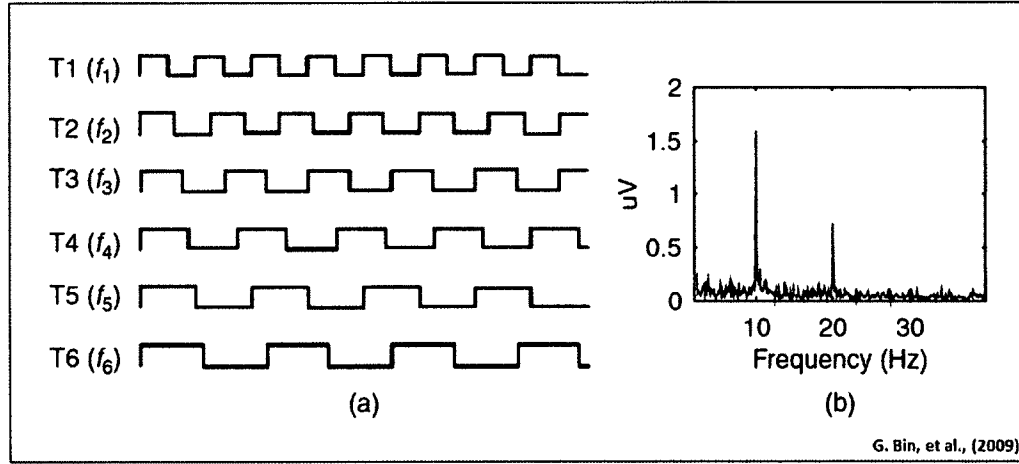


FIG. 5: Part (a) shows example SSVEP stimulating waveforms for 6 different targets, where each target is encoded with a different frequency. Part (b) shows the power spectrum of the evoked SSVEP response from a 10Hz stimulus. [Bin et al., 2009a].

information to increase the number of available targets. Jia et al. implemented a 15 target system with only three distinct frequencies and achieved an average ITR of 60 bits/min with 10 subjects [Jia et al., 2011]. Other attempts at improving the stimulation scheme have been the development of dual-frequency coded targets [Hwang et al., 2013, Srihari Mukesh et al., 2006] and frequency-space coded targets [Yan et al., 2011]. Zhu et al. outlined a review consisting of numerous BCI studies which tested the effect of stimuli shape, color, pattern, and intensity on SSVEP-BCI performance [Zhu et al., 2010].

Visual irritation and fatigue from prolonged visual stimulation is a significant practical issue for SSVEP-BCIs (or any VEP-BCI) as it can hinder performance and dramatically reduce practicality in real-world use [Boksem et al., 2005, Hong et al., 2009]. To address this, researchers have made several attempts to reduce visual fatigue, increase usability, and improve overall ergonomic design. The main attempt at reducing visual fatigue has been to reduce the saliency or obtrusiveness of the visual stimuli. This can be done in a number of different ways such as utilizing high-frequency stimulation ($> 35\text{Hz}$) [Müller et al., 2011, Diez et al., 2013], high duty-cycle stimulation ($\geq 50\%$ duty cycle) [Lee et al., 2011], or low-contrast

stimulation (0-10% contrast) [Lalor and Foxe, 2009]. Although these attempts do reduce visual fatigue, they come at the expense of reduced performance. For example, with high-frequency stimulation, Muller et al. showed accuracies around 69% with an average ITR of 46.8 bits/min [Müller et al., 2011] with frequencies greater than 30Hz.

SSVEP BCIs that utilize peripheral stimulation have also been developed. These BCIs are termed gaze-independent BCIs because they do not require direct visual fixation, as opposed to traditional (gaze-dependent) VEP-BCIs in which overt visual fixation is required. Gaze-independent SSVEP BCIs were originally developed for individuals suffering from late-stage ALS [Lesenfants et al., 2011]. These individuals have lost all muscle control including eye movements and therefore cannot utilize traditional SSVEP BCIs. Typically, the user’s eye-gaze is positioned between two flashing stimuli that are on opposite sides of the user’s peripheral vision. While maintaining gaze on the fixation cross in the middle, the user focuses attention on either the left or the right stimulus to endogenously produce an SSVEP response according to the attended stimulus. Since SSVEP BCIs of this type do not require direct visual stimulation, visual fatigue is reduced; however, the endogenous attention to peripheral stimulation produces much weaker and less discriminable SSVEP responses. As a result, these BCIs suffer from a dramatic drop in performance even when only implementing a few targets [Lalor et al., 2007, Lesenfants et al., 2011, Kelly et al., 2004].

2.4.2 THE C-VEP BCI

The c-VEP BCI utilizes evoked responses generated from stimuli flashing according to a pseudorandom binary sequence. The most popular pseudorandom sequence is the maximum-length sequence (m-sequence) which is created using maximum linear feedback shift registers that give it unique properties for studying linear and non-linear systems. The autocorrelation of the m-sequence nearly approximates an impulse function that is 1 at the zero time-lag and $1/N$ for all other time-lags (where N is the length of the m-sequence which is usually 63 for c-VEP BCIs). As such, the c-VEP BCI system can employ multiple time-lagged versions of a single m-sequence

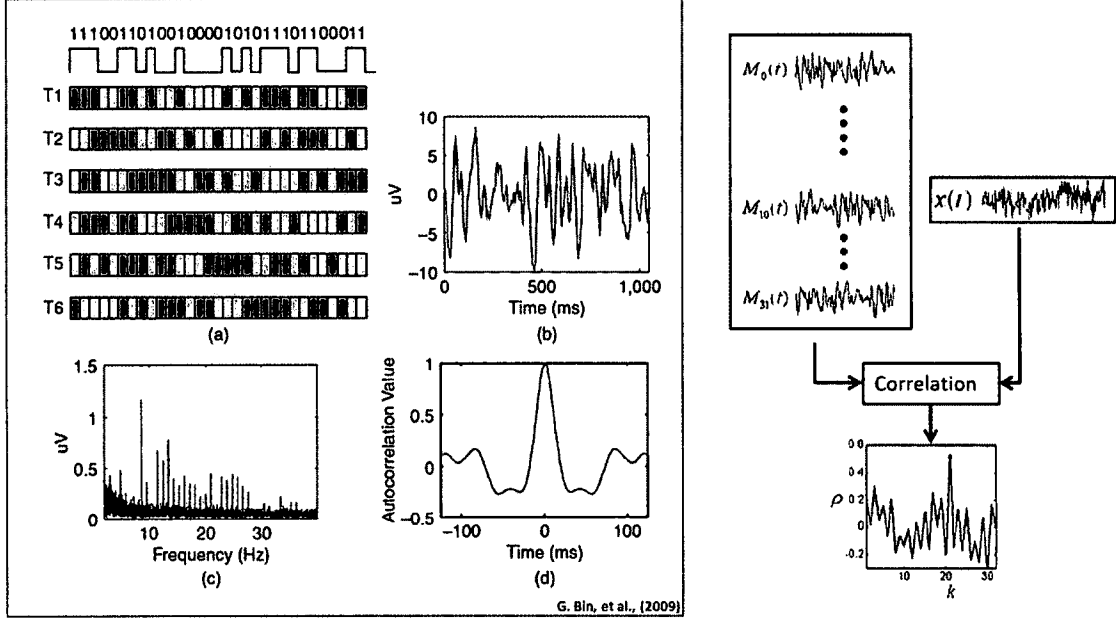


FIG. 6: LEFT: (a) shows example time-delayed m-sequence stimulus waveforms for six targets, (b) shows an evoked c-VEP response in the time-domain, (c) shows the frequency spectrum of the c-VEP response and (d) shows the autocorrelation of the c-VEP response. RIGHT: Target selection method for the c-VEP BCI. Unknown observations are classified by assigning the predicted class label whose template waveforms produce the strongest correlation with the unknown observation.. [Bin et al., 2009a].

that are shifted by a small delay τ . Since each shifted m-sequence is nearly orthogonal with all other shifted versions, the c-VEP response from attending to a given m-sequence driven stimulus is nearly uncorrelated with other corresponding c-VEP targets. This forms the basis of target selection for the c-VEP BCI as the correlation coefficient can be computed to select the attended target. The left sub-figure in Figure 6 shows time-delayed m-sequence stimuli for six targets in (a). The c-VEP waveform in the time-domain is shown in (b), the frequency spectrum of the c-VEP is shown in (c) and the autocorrelation of the c-VEP response is shown in (d). The right portion of Figure 6 is the target selection method for the c-VEP BCI.

To perform target selection for the c-VEP BCI, c-VEP response templates $M_k(t)$ from each stimulus are correlated with EEG observations $x(t)$, where k is the number

of targets (typically 32). This is done by acquiring training data as a subject attends to one of the c-VEP stimuli over N cycles. The template for that target is then made by averaging over the N cycles. This initial c-VEP template is referred to as the reference template. Training data only needs to be collected from one target as the c-VEP templates for all other targets can be made by circularly shifting the reference template. For example, given a 32 target c-VEP BCI, each c-VEP template can be made as:

$$M_k(t) = M_{ref}(t - (\tau_k - \tau_{ref})), \quad for \quad k = 1, 2, \dots, 32.$$

Once all c-VEP targets are made, a new c-VEP observation $x(t)$ can be classified by linearly correlating $x(t)$ with each c-VEP template using Pearson's correlation function:

$$\rho_k = \frac{\langle M_k(t), x(t) \rangle}{\sqrt{\langle M_k(t), M_k(t) \rangle \langle x(t), x(t) \rangle}}.$$

The target selection is made by assigning the template with the highest correlation:

$$C = \max_k \rho_k, i = 1, 2, \dots, 32.$$

The c-VEP BCI has been shown to outperform the SSVEP BCI in accuracy and in ITR [Bin et al., 2009a]. Although the exact reasons for this performance increase have not been thoroughly investigated, several characteristics of the c-VEP are advantageous compared to the SSVEP. First, the c-VEP utilizes time-shifted m-sequences and, as such, it can generally employ more targets than the SSVEP BCI using an LCD monitor. Secondly, c-VEP stimuli can be arranged in a spatial configuration that achieves symmetric time-lag relationships between any stimulus and its neighbors. This is called the principle of equivalent neighbors, and its implementation effectively alleviates any inter-stimuli interference issues that the traditional multi-target VEP-BCIs are affected by [Bin et al., 2011]. Finally, the m-sequence, which has broad-band frequency components, has the same frequency spectra for each m-sequence target. This therefore nullifies any inter-subject frequency response

variations as the response to a particular frequency is unimportant in c-VEP target selection. On the other hand, SSVEP target selection is extremely vulnerable to inter-subject frequency variations.

2.5 VEP SIGNAL PROCESSING TECHNIQUES

The strength, or detectability, of the VEP response is one of the key factors for improving VEP-BCI performance. As such, many signal processing techniques have been developed to better extract and classify VEP responses from background EEG. Common signal processing techniques include common average references (CAR), Laplacian filters, principle component analysis (PCA), independent component analysis (ICA) and common spatial patterns (CSP) [Garcia-Molina and Zhu, 2011, Mackay et al., 2003]. These are often coupled with machine learning techniques such as linear discriminant analysis (LDA), artificial neural networks (ANNs), support vector machines (SVMs) and Bayesian classifiers [Lotte et al., 2007]. Recently, a multivariate signal processing technique called Canonical Correlation Analysis (CCA), was applied to SSVEP-BCIs in which CCA was used to find optimal time-domain correlations between multichannel EEG and reference sinusoidal signals [Bin et al., 2009b]. The CCA achieves a significant improvement in performance compared to traditional frequency domain analysis techniques [Lin et al., 2007]. An additional benefit from the CCA is that it is a calibration-less classifier; thus, it improves practical feasibility as lengthy training sessions are not required beforehand for BCI control. The CCA, explained further in section 2.5.1, currently stands as the de-facto signal processing technique for SSVEP-BCIs.

2.5.1 CANONICAL CORRELATION ANALYSIS

To quantify the level of VEP responses in the EEG signals, a multivariate processing technique known as Canonical Correlation Analysis (CCA) can be utilized to find linear correlations between EEG data and a stimulating signal. CCA has recently been adopted for multidimensional EEG analysis and has been shown to be

extremely effective for SSVEP signal processing [Lin et al., 2007, Bin et al., 2009b].

CCA is a multi-dimensional correlation analysis technique that finds underlying correlations between two sets of data. It finds linear combinations of two multi-dimensional data sets such that the mutual projection between the two data sets is maximized. Given two multi-dimensional data sets, X and Y , and their respective linear combinations, $x = X^T W_x$ and $y = Y^T W_y$, the CCA finds the weight vectors W_x and W_y that produce the maximum correlation between x and y . The projected vectors x and y are known as canonical variants, and their correlation is known as the canonical correlation. The weight vectors W_x and W_y that produce the highest canonical correlation are found by solving the optimization problem:

$$\max_{W_x, W_y} \rho(x, y) = \frac{E[x^T y]}{\sqrt{E[x^T x]E[y^T y]}} = \frac{E[W_x^T X Y^T W_y]}{\sqrt{E[W_x^T X X^T W_x]E[W_y^T Y Y^T W_y]}}. \quad (1)$$

In practice this can be solved using the singular-value decomposition method to diagonalize the covariance matrices as the maximum canonical correlation corresponds to the square-root of the largest eigenvalue. For SSVEP signal processing, the multidimensional EEG data, X , can be canonically correlated with a multivariate set of reference signals Y_f . The reference signals Y_f are a set of sine and cosine signals derived from N_h harmonics:

$$Y_f = \begin{pmatrix} \sin(2\pi f t) \\ \cos(2\pi f t) \\ \vdots \\ \sin(2\pi N_h f t) \\ \cos(2\pi N_h f t) \end{pmatrix}. \quad (2)$$

Each set of reference signals corresponds to the fundamental frequency of each of the SSVEP targets. The multi-channel EEG and reference signals are used in the CCA to produce a canonical correlation for each target frequency. The correlation

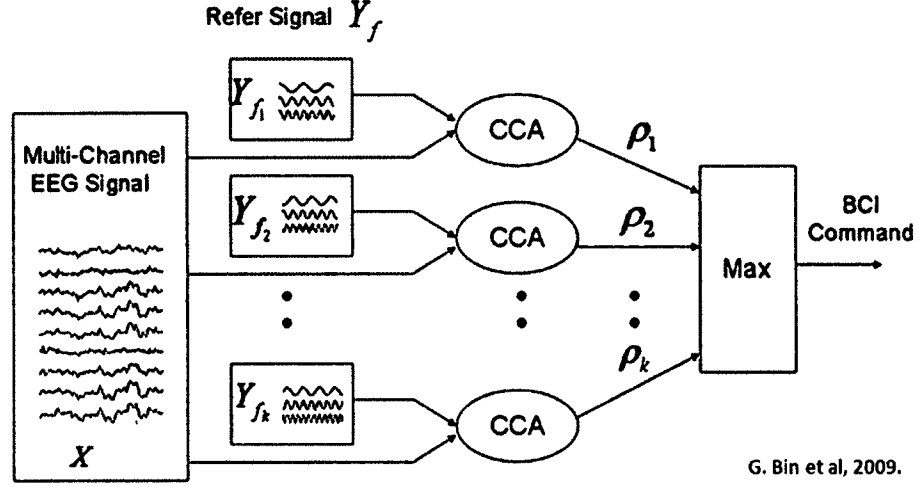


FIG. 7: Diagram illustrating the use of CCA for SSVEP target detection. The CCA between a multichannel EEG signal X and the reference signals Y_f for each SSVEP target is performed. The maximum correlation is selected as the classified target. For a c-VEP-BCI, the reference signals Y_f are replaced by the c-VEP templates for each target. [Bin et al., 2009b].

output of the CCA provides a quantitative metric of the strength of the SSVEP response from background activity. Additionally, since the canonical correlation values are inherently bounded between -1 and 1 , they can be directly used for SSVEP classification. For an SSVEP BCI, the output class is determined as

$$C = \arg \max_i \rho_i, \quad i = 1, 2, \dots, K, \quad (3)$$

where K is the total number of classes or target frequencies in the SSVEP BCI. Figure 7 illustrates the use of CCA for SSVEP target detection. The CCA has also been adopted for use in a c-VEP-BCI [Bin et al., 2011]. For c-VEP processing, the CCA is utilized similarly except that the sinusoidal reference signals (Figure 7) are replaced with c-VEP template signals.

2.6 PERFORMANCE VS. PRACTICALITY

Given the wide range of challenges that VEP-based BCIs face, solutions to these challenges are generally developed with either the goal of increasing performance or

the goal of increasing practicality, with the former traditionally receiving the most attention in the field.

Performance

Enhancing performance is the typical objective of most academic research. Incremental improvements that attempt to increase BCI performance have dominated and saturated the current research for VEP-based BCIs. These improvements focus solely on increasing the raw accuracy and/or the raw information transfer rate (ITR) of the BCI system. The ITR for BCI systems is commonly calculated using the following equation:

$$ITR = \left(\log_2 M + P \log_2 P + (1 - P) \log_2 \left[\frac{1 - P}{M - 1} \right] \right) * \left(\frac{60}{T} \right).$$

In this equation, M is the number of targets in the BCI system, P is the probability of a correct selection, and T is the time (amount of data) needed for target selection. Thus, there are essentially three factors that contribute to improving ITR for a BCI: increase the number of targets, decrease the selection time, or increase the accuracy.

Practicality

There are a several different avenues for advancement that focus on increasing the practicality of a BCI system. Although not an exhaustive list, the primary areas of advancement are in improving the ergonomic design, reducing visual fatigue from obtrusive stimulation, reducing system calibration time, improving asynchronous control, reducing obtrusiveness of EEG sensors, and utilization of ubiquitous technologies. All of these areas for increased practicality will help to increase the overall pervasiveness of BCI technology.

CHAPTER 3

TEMPORAL CHARACTERIZATION OF THE SSVEP SPECTRUM USING CHIRP-MODULATED STIMULI

While SSVEPs have proven to be very consistent signals for rapid EEG-based brain-computer interface (BCI) control, due in part to perceptual and neurophysiological aspects, SSVEP signal detection biases exist for different stimulation frequencies. Furthermore, these biases tend to differ across subjects. In this chapter, in order to provide a better characterization of the SSVEP spectrum for BCI applications, 22 subjects were stimulated with an LED array that flashed according to a chirp signal having a frequency that varied over the typical functional range of SSVEP from 5.5-34.5 Hz. The resulting EEG was analyzed using CCA to elucidate the stimulus frequencies that produce the best discriminability for practical use. Subjects achieved an average accuracy of 72.2% using a six-class paradigm with a standardized set of stimulus frequencies. However, when using a subject-specific frequency set (i.e. frequencies optimized for each subject), the average accuracy significantly increased to 83.7% ($p = 0.03$). The results show that inherent SSVEP response differences exist between subjects, which can have a significant effect on performance. This approach also establishes a framework for a rapid optimization of subject-specific frequency profiles.

3.1 INTRODUCTION

Multichannel SSVEPs have been used online with Canonical Correlation Analysis (CCA) producing a robust BCI system that achieves good performance with little to no training data [Lin et al., 2007, Bin et al., 2009b]. CCA is generally a preferred detection method for SSVEP BCIs because of its inherent channel harmonic analysis capabilities, relative simplicity, and robust performance. However, individuals

generally have SSVEP responses in the range of 5-45 Hz, and the optimal stimulus frequencies within this range can vary greatly across individuals. This study aims to establish a novel characterization of the SSVEP using CCA and to quantify the BCI performance differences between subject-optimized stimulation frequencies and standard, pre-selected stimulation frequencies. The results show that the brain responses over the SSVEP spectrum can vary drastically across subjects and frequencies and that subject-specific optimization can greatly improve the performance of SSVEP BCIs.

3.2 METHODOLOGY

3.2.1 DATA COLLECTION

EEG data were collected from 22 healthy volunteers (5 women, 17 men; age range 18-42 years) from a single session. All subjects were free of any neurological or psychiatric disorders and had either normal or corrected-to-normal vision. Each subject gave written informed consent prior to participation, and all aspects of the study were reviewed and approved by Old Dominion University's Institutional Review Board.

EEG data were recorded using 16 active electrodes and a g.USBAmp biosignal amplifier (g.tec Medical Engineering). Electrodes were positioned primarily over the occipital and parietal regions at locations based on the International 10-20 system [Sharbrough et al., 1991]: Fz, Pz, POz Oz, O1, O2, PO3, PO4, PO7, PO8, POO1, POO2, POO3, POO4, OI1h, OI2h, as shown in Figure 8. All EEG data were band-pass filtered from 0.1 Hz to 100 Hz, notch filtered at 60 Hz, and digitized at 512 Hz. Data recording and timing were controlled by BCI2000 general purpose BCI software. [Schalk, 2004].

3.2.2 EXPERIMENTAL PARADIGM

Each subject sat in a dark room in front of a custom-built SSVEP stimulator

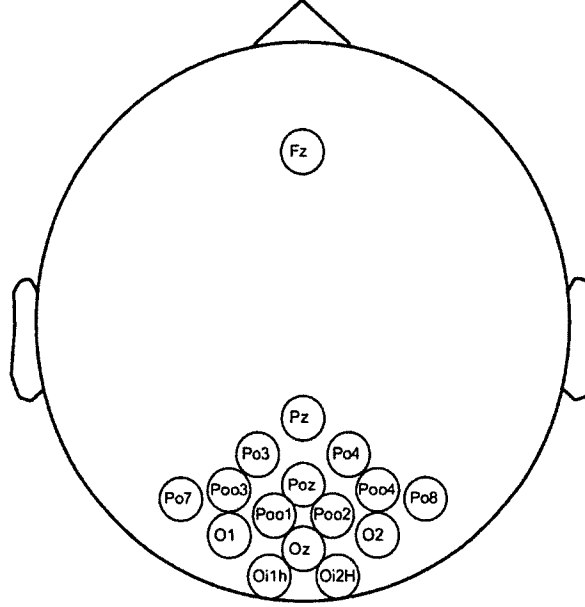


FIG. 8: The EEG electrode montage used for data collection for the SSVEP study. The positions are based on the International 10-20 system.

composed of an 8×8 array of green LEDs. A schematic of the LED stimulator array is shown in Figure 9. Green LEDs were used as they generate among the highest SNR responses for SSVEPs compared to other colors [Zhu et al., 2010]. Each LED in the array was wired together so that all LEDs illuminated simultaneously with the preprogrammed stimulus. The LED stimulator has dimensions of 5.84 cm x 5.84 cm and was placed in the center of the subjects' visual field approximately 60 cm away so that the stimulation spanned visual angles of 5.25 degrees vertically and horizontally. The stimulator was driven by an Arduino Mega microcontroller board with an output stimulation frequency of 500 Hz and a 10-bit intensity resolution. LED luminosity was linearized over the operating range to ensure a uniform intensity distribution, and the LED array was tested using a photo-diode to verify consistent stimulation frequencies. All stimulation signals were generated using Matlab software (Mathworks, Nattick, MA) and loaded onto the microcontroller before stimulation. A circuit diagram of the visual stimulator is shown in Figure 10.

During the experiment, the subject's task was to visually attend and keep focus

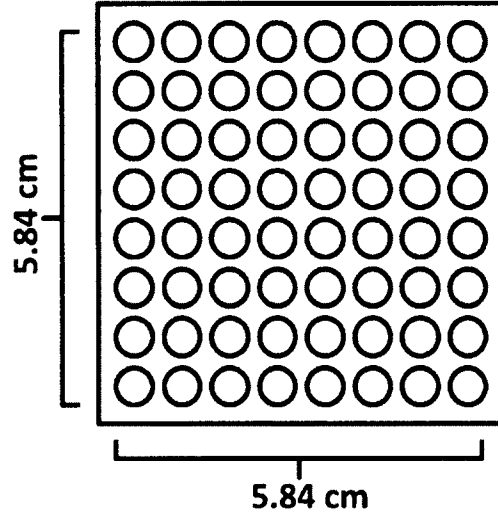
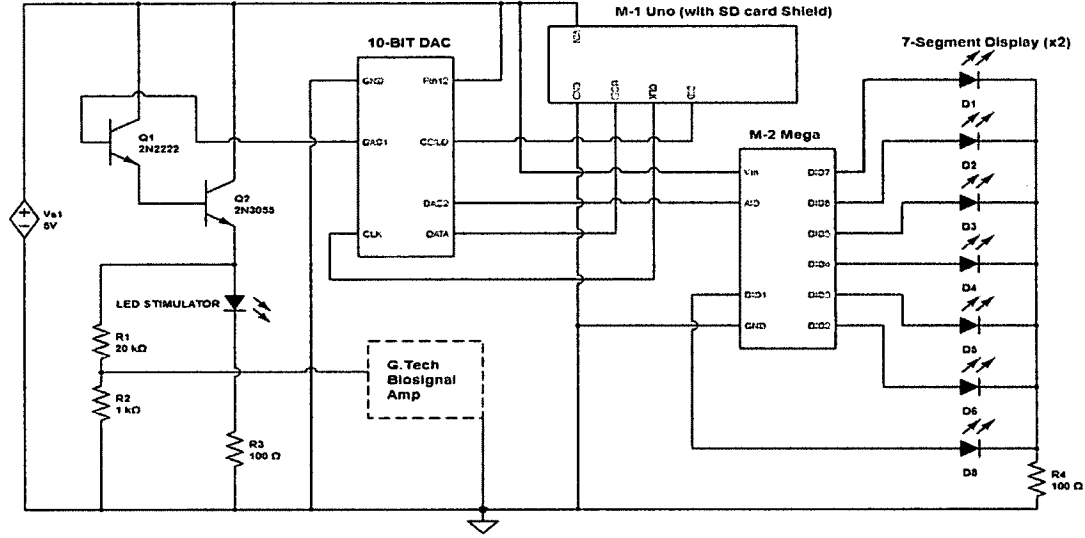


FIG. 9: The LED stimulator consists of an 8 x 8 array of green LEDs driven by a microcontroller with a 10-bit DAC. The physical dimensions of the stimulator are 5.84 cm x 5.84 cm.

on the flashing stimulator. During the course of a single session, subjects performed several runs of attending to 30 seconds of continuous stimulation followed by 15 seconds of rest. Runs were repeated five times for each of four different chirp-modulated stimulus waveforms. The waveforms that were presented were composed as follows: 1) square waveform with a chirp increase from 5.5-20.5 Hz, 2) square waveforms with a chirp increase from 19.5-34.5 Hz, 3) square waveform with a chirp decrease from 20.5-5.5 Hz, and 4) square waveform with a chirp decrease from 34.5-19.5 Hz. Each chirp-modulated waveform (increase and decrease) had a chirp rate of $\Delta_f = 0.5$ Hz per second. This provided approximately two seconds centered on each integer frequency and is sufficiently slow enough to emulate a fixed frequency over a short time window.

A total of 5 trials per waveform were presented, giving a total of 20 trials. The waveforms were presented in a counterbalanced order to account for possible fatigue issues. Baseline EEG with the stimulator turned off and the subjects' eyes kept open was collected for approximately two minutes before and after the session. Each subject participated in a single experimental session lasting approximately 30 minutes.



data from the 19.5-34.5 Hz waveform to produce an SSVEP response signal from 5.5-34.5 Hz. The decreasing chirp signals (20.5-5.5 Hz and 34.5-19.5 Hz) were concatenated to produce a 34.5-5.5 Hz response and then time-reversed to match the previous 5.5-34.5 Hz.

Fixed frequencies were approximated from the chirp signal by using a sliding window with a length of two seconds and a one-second overlap. This corresponds to frequencies starting from 6 Hz to 34 Hz in increments of 0.5 Hz (55 total distinct frequencies), which covers the functional range of the SSVEP spectrum with sufficient resolution.

CCA was performed on each window of the EEG response and on each frequency from the SSVEP reference signals. Each target frequency (i.e. the current time window corresponding to the frequency from the chirp stimuli) was canonically correlated with each reference signal frequency. This results in a quantitative measure of target discrimination from background EEG activity for each of the selected frequencies.

SSVEP Classification

For BCI applications, it is common to select a somewhat arbitrary set of stimulation frequencies based on hardware restrictions or EEG spectral characteristics (e.g., alpha-band overlap). To assess the discriminative capacity of CCA for the broad range of stimulus frequencies provided by the chirp signals, an offline BCI classification scheme was set up using 6-classes. As a reference, 13 Hz, 14 Hz, 15 Hz, 16 Hz, 17 Hz and 18 Hz were evaluated based on Bin et al., 2009 [Bin et al., 2009b], which is the landmark SSVEP CCA study. This reference frequency set represents typical, generic stimulus frequencies that are not optimized for each subject. Using the SSVEP response data due to the chirp stimuli, the time windows centered at these six frequencies were extracted to set up a simulated BCI classifier.

To compare with the classification performance of this frequency set, 1600 unique frequency sets were extracted and used in the off-line classification. Each subject's SSVEP stimulus frequencies were optimized by finding the combination that maximized the individual classification performance. The value of 1600 frequency sets

was selected to provide comprehensive combinations of six stimulus frequencies over the range of 6-34 Hz (55 distinct frequency choices). The theoretical number of frequency permutations for a set of 6 out of 55 is approximately 28 million combinations. Since it is impractical and unnecessary to test all of these frequency combinations in a exhaustive optimization, selected uniformly-spaced and randomly-determined frequency sets were evaluated. The 1600 different sets were generated as follows: 100 frequency sets of 6 frequencies starting from 6 Hz to 34 Hz with spacings of 0.5 Hz, 1 Hz, 2 Hz, and 2.5 Hz (i.e., Set 1: 6, 6.5, 7, 7.5, 8, 8.5; Set 2: 6.5, 7, 7.5, 8, 8.5, 9, 9.5; etc.). The uniform sets cover the entire range of the SSVEP spectrum of frequencies. The next 1500 frequency sets were generated by selecting 500 random frequency permutations each in the low (6-15.5 Hz), medium (16-25 Hz) and high (25.5-34.5 Hz) frequency ranges.

To optimize the frequency set for each subject, 70% of the data were used for training and the remaining 30% were used for testing. The accuracies for the training data were evaluated, and the frequency set that performed the best for each subject was recorded. In the event of ties (i.e. cases where multiple frequency sets provided the equivalent best performance) the frequency set for each tie was recorded. The testing data was then used to evaluate the performance of the frequency set optimization. For ties, each set was individually evaluated and the results were averaged. To assess the prevalence of optimal frequencies across subjects, a histogram was created showing the proportion of times a particular frequency was included in the optimal frequency set. The contributions from each subject to the histogram were normalized to adjust for subjects with ties.

3.3 RESULTS

3.3.1 SSVEP SPECTRUM CHARACTERIZATION

The SSVEP Spectrum Characterization is shown in Figure 11. This figure shows a time-frequency plot of the CCA correlation values of the reference signals and the

EEG across the 60 s of concatenated chirp signal. The CCA was repeated using three different combinations of progressive harmonics: the first (fundamental) harmonic only, the first two harmonics, and the first three harmonics. Each time-frequency plot represents the average across all subjects. Since the EEG signal is in response to a linearly increasing chirp signal, the prominent diagonal lines in Figure 11 represent the expected strong correlation of the EEG signal with the target frequency.

The diagonal line representing the fundamental frequency is present in all three graphs. Likewise, the second and third harmonics are also pronounced in each plot, though not as nearly as prominent as the fundamental. What appear to be sub-harmonics in the lower two plots are actually the result of performing CCA with harmonics. For instance, if the EEG is oscillating at 20 Hz due to a 20 Hz stimulus, there will be a correlation with a 10 Hz reference signal when the harmonics are included in the CCA. This is an important consideration when evaluating harmonic frequencies.

Figure 12 shows the CCA correlation values of the SSVEP response as a function of stimulation frequency averaged across all subjects. A second-order polynomial is fit to the correlation data. It is observed that the correlation values generally increase as more harmonics are added.

3.3.2 SSVEP CLASSIFICATION

The SSVEP classification results are shown in Table 1. The first column shows the performance using the reference frequency set from [Bin et al., 2009b]. This frequency set resulted in an average classification accuracy of $72.2\% \pm 20.7\%$ across subjects.

For the 1600 uniform/random frequency sets, the frequency set that maximized the average performance across all subjects was determined to be: 6, 7, 7.5, 8.5, 9.5, and 11 Hz. The performance of this group-wise set is given in the second column. This set produced an average classification accuracy of $77.2\% \pm 17.6\%$ across subjects. Although the average accuracy of the group-wise set is greater than the reference set, a two-tailed t-test indicates that the increase is not statistically significant ($p = 0.38$).

Lastly, individually optimized frequency sets were determined by selecting the set with the highest classification accuracy for each individual subject. These individually-optimized frequencies represent the best classification performance that a subject can obtain given the range of available frequency values. The individually-optimized frequency sets produced an average classification accuracy of $83.7\% \pm 15.0\%$ across subjects. The accuracies produced using individually optimized frequencies resulted in significantly higher accuracies compared to the reference set ($p = 0.03$). Compared to the group-wise set, the individual accuracies were better on average, although the increase was not statistically significant ($p = 0.19$).

The individual frequency sets varied greatly across each of the 22 subjects, indicating that each subject has a rather unique frequency response profile that should be individually optimized. To illustrate the commonly selected frequencies, Figure 13 shows a histogram of the relative occurrence of frequencies in the optimized frequency sets. This figure shows two distinct frequency ranges that were most commonly selected as frequencies for the optimized sets. The majority of the optimized frequencies tend to be in the lower frequency range from 6 to 15 Hz, with a smaller grouping in the higher frequency range from 22 to 34 Hz and very few frequencies selected from the mid range (16-21 Hz).

3.4 DISCUSSION

While it is generally known that subject-specific stimulation frequencies should produce superior performance, there has been little work to quantify and evaluate optimal frequencies. This study represents a fairly comprehensive analysis and characterization of the full SSVEP spectrum and its effect on SSVEP BCI performance.

The results shown in Figures 11 and 13 indicate that lower stimulus frequencies (i.e., 6-15 Hz) generally produce the best SSVEP discrimination. This is likely the result of the higher signal-to-noise ratio (SNR) of the lower frequencies due to the $1/\text{frequency}$ power characteristic of the EEG, which impacts the correlations as shown in Figure 12. Additionally, the histogram plot in Figure 13 shows that frequencies in the high range (22-34 Hz) more often contributed to optimal BCI performance

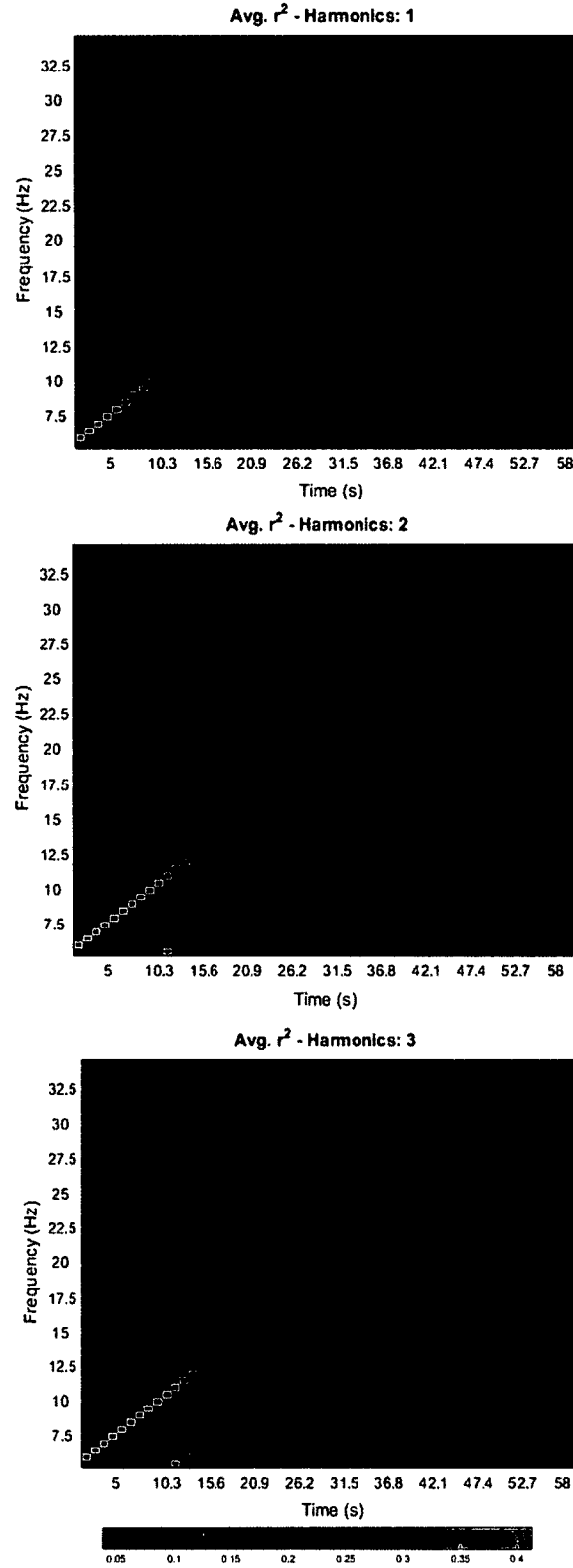


FIG. 11: CCA squared correlation values using for first harmonic (top), first two harmonics (middle), and first three harmonics (bottom), averaged across all subjects.

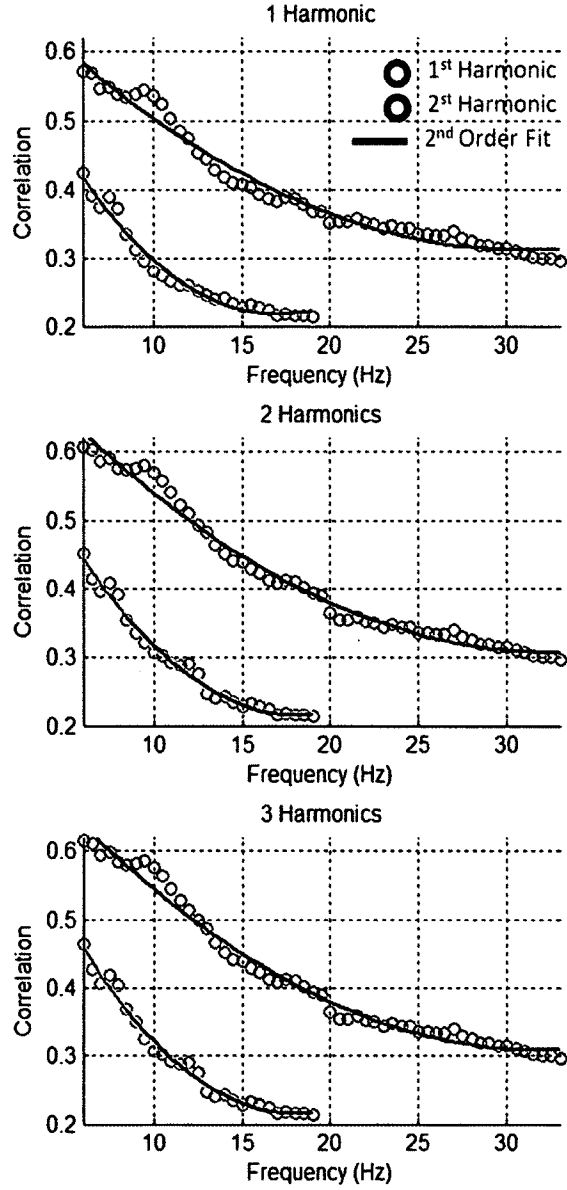


FIG. 12: CCA correlation values of the SSVEP response as a function of stimulation frequency averaged across all subjects. Top: first harmonic, middle: first two harmonics, bottom: first three harmonics

TABLE 1: Classification results for different frequency sets

Subject	Reference	Group-wise	Individual
1	95.8	100	98.3
2	83.3	95.8	95.8
3	54.2	66.7	64.6
4	70.8	95.8	94.4
5	66.6	83.3	80.8
6	45.8	75	78.12
7	37.5	87.5	87.5
8	91.6	54.2	94.4
9	70.8	87.5	83.3
10	37.5	45.8	61.1
11	100	87.5	95.8
12	87.5	70.8	75
13	75.0	87.5	95.8
14	73.5	37.5	41.6
15	41.7	45.8	58.3
16	87.5	83.3	87.5
17	83.3	91.7	88.6
18	91.7	75.0	95.8
19	83.3	91.7	88.4
20	75.0	70.8	87.5
21	79.2	83.3	94.4
22	91.7	83.3	95.0
Avg	72.2	77.3	83.7

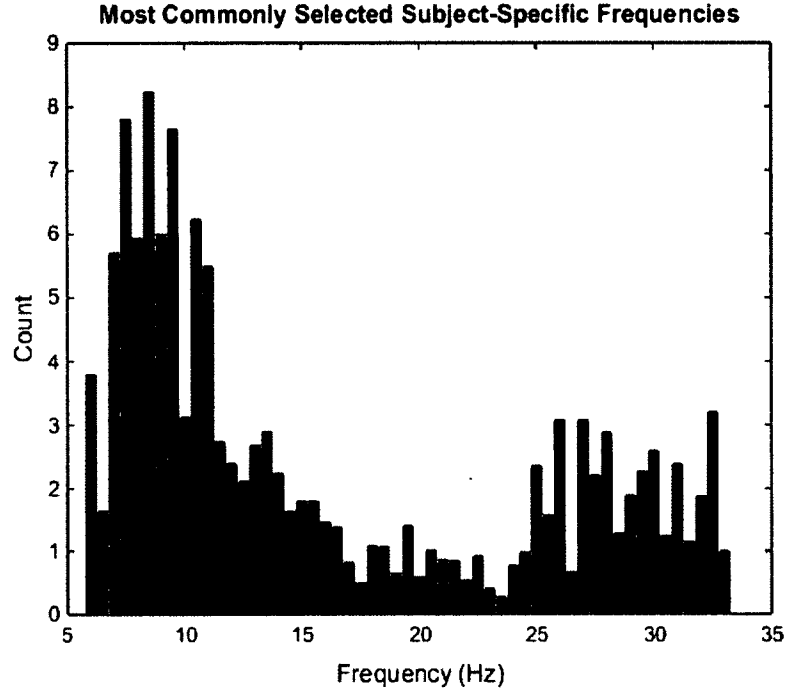


FIG. 13: Histogram plot showing the relative occurrence of each frequency in the optimal frequency sets for all subjects.

compared to the mid-range (16-21 Hz). Since this higher range has a lower SNR compared to the key lower-range frequencies, the higher frequencies may serve as an “outlier condition” that serves to boost discrimination; although this must be validated through further analysis.

The classification results indicate that frequency selection can have substantial impact on overall BCI performance, increasing from 72.2% to 83.7% ($p = 0.03$). To date, there is no widely accepted stimulus frequency set or standardized methodology for obtaining subject-specific stimulus frequencies. As a result, most studies use sub-optimal frequencies, although this can still lead to acceptable performance - particularly in individuals with strong SSVEP responses.

If a subject-specific frequency optimization is not feasible for a particular scenario, the results show that frequencies in the lower frequency range (particularly from 6-11 Hz) provide the best performance. These findings are consistent with the results from [Allison et al., 2010], indicating that the majority of subjects have an

SSVEP response innately present in the EEG, while a small percentage of subjects will naturally have a weaker or even no detectable SSVEP response.

The method utilized in the study can be used as an efficient way to characterize the response of the SSVEP spectrum for an individual. The chirp stimulus displayed at a rate of 0.5 Hz/s can be achieved much more rapidly than evaluating individual frequencies independently. Additionally, only several passes of the chirp signal would be required, leading to calibration times on the order of minutes.

Because of the continuous nature of the chirp signals and the limitation of monitor refresh rates, this study was done using LED stimulation and not the more convenient LCD stimulation. An identical follow-up study using an LCD monitor is planned, although it is not expected that the results will significantly differ from the present study. Additionally, the long-term stability of the SSVEP spectrum has yet to be assessed and longitudinal online experiments need to be conducted. Nevertheless, the present offline results serve as a strong indicator of the potential impact of optimized SSVEP frequencies and efficient characterization of the SSVEP spectrum.

CHAPTER 4

MULTICLASS SSVEP FREQUENCY EVALUATION USING CHIRP-MODULATED STIMULI

While a subject-specific SSVEP stimulus frequency optimization is ideal, this can be a tedious and time-consuming process. Thus, many studies select SSVEP stimulation frequencies somewhat arbitrarily. Not only is there no standardized set of SSVEP stimulus frequencies or frequency selection method, some studies even claim conflicting frequency ranges for optimal performance. In this work, 17 subjects were stimulated with an LED array that flashed according to a chirp-modulated signal having a frequency that varied linearly over the typical functional range of SSVEP. The resulting EEG was analyzed using canonical correlation analysis (CCA) and a genetic algorithm (GA) was implemented to determine generalized stimulation frequency sets over a continuum of simulated multiclass BCI classification scenarios. The results show that distinct frequency feature groupings exist over the different multiclass scenarios, and that these groupings result in different information transfer rates. These offline results can provide a guide for generalized stimulus frequency selection for SSVEP-based BCIs with an arbitrary number of targets.

4.1 INTRODUCTION

Due to physiological differences between subjects, there tends to be high intersubject variability in terms of SSVEP response power at different stimulation frequencies. While a subject-specific SSVEP stimulus frequency optimization is ideal, this can be a tedious and time-consuming process. Thus, many studies select SSVEP stimulation frequencies somewhat arbitrarily. Not only is there no standardized set of SSVEP stimulus frequencies or a standardized frequency selection method, some studies even claim conflicting frequency ranges for optimal

performance. A detailed review of SSVEP stimulation techniques by Zhu et al. [Zhu et al., 2010] showed that most studies not only varied greatly in the stimulus frequencies used but also varied the number of classes used. The majority of studies did not perform stimulus frequency optimization prior to the study, nor provided a justification for the selected frequencies. This generally arbitrary selection of stimulus frequencies leads to suboptimal fixed-frequency results (i.e., not subject-specific) and makes performance comparisons across SSVEP studies difficult. Several recent studies have performed fairly comprehensive evaluations of various SSVEP stimulus parameters, including stimulus size, shape, color, and pairwise comparisons of stimulus frequencies based on signal-to-noise ratio [Kuś et al., 2013, Duszyk et al., 2014, Waytowich and Krusienski, 2014]. However, these studies did not examine optimal sets of frequencies for multiclass SSVEP applications.

Whereas the previous chapter explored individualized optimization of SSVEP stimulus frequencies using CCA, this chapter uses the same data set to investigate generalized stimulation frequency sets over a continuum of simulated multiclass BCI classification scenarios. Subjects were visually stimulated with an LED array that flashed according to a chirp-modulated signal [Tu et al., 2012] having a frequency that varied linearly over the typical functional range of SSVEP from 5.5-34.5 Hz. The resulting EEG was analyzed using canonical correlation analysis (CCA), and a genetic algorithm (GA) was implemented to determine the generalized stimulation frequency set that maximizes classification performance for numbers of classes (i.e., simulated flashing target groupings) ranging from 2 to 36.

4.2 METHODOLOGY

4.2.1 DATA COLLECTION AND EXPERIMENTAL PARADIGM

The data collection and experimental paradigm are described in the previous chapter. After a screening of the EEG data for discriminable SSVEP responses using

a visual evaluation of the subject-specific CCA characterization similar to Figure 14, five subjects were excluded because they produced little or no detectable SSVEP response. Thus, 17 (3 women, 14 men; age range 18-36 years) of the 22 subjects were included in the subsequent analysis.

4.2.2 DATA PREPROCESSING

All SSVEP data was first bandpass filtered using a zero-phase, IIR filter from 0.5-40 Hz. All data were segmented by trial for each chirp stimulus condition and inter-trial data (i.e. rest periods) were discarded. The data elicited from the chirp signals were then analyzed using the CCA method. Reference signals Y_f were created and centered around each frequency from 6 to 33.5 Hz, spaced every 0.5 Hz for a total of 56 reference signal sets that spanned the chirp signal. All reference signals were created using only the fundamental frequency ($N_h = 1$) for this study.

The chirp data from the 5.5-20.5 Hz waveform was concatenated with the chirp data from the 19.5-34.5 Hz waveform to produce an SSVEP response signal from 5.5-34.5 Hz. The decreasing chirp signals (20.5-5.5 Hz and 34.5-19.5 Hz) were concatenated to produce a 34.5-5.5 Hz response and then time-reversed to match the previous 5.5-34.5 Hz. Fixed frequencies were approximated from the chirp signal by using a sliding window with a length of two seconds and a one-second overlap. The data representing the 34-34.5 Hz was discarded due to a recording inconsistency at the beginning or end of the decreasing or increasing chirp trials, respectively. Thus, the frequency features used in this study range from center frequencies of 6 Hz to 33.5 Hz in increments of 0.5 Hz (56 total distinct frequencies). This covers the functional range of the SSVEP spectrum with sufficient resolution.

For all 17 subjects, the CCA was performed on each window of the EEG response and on each frequency from the SSVEP reference signals. Each target frequency (i.e. the current time window corresponding to the frequency from the chirp stimuli) was canonically correlated with each reference signal frequency. This results in a quantitative measure of target discrimination from background EEG activity for each of the selected frequencies (shown in Figure 14).

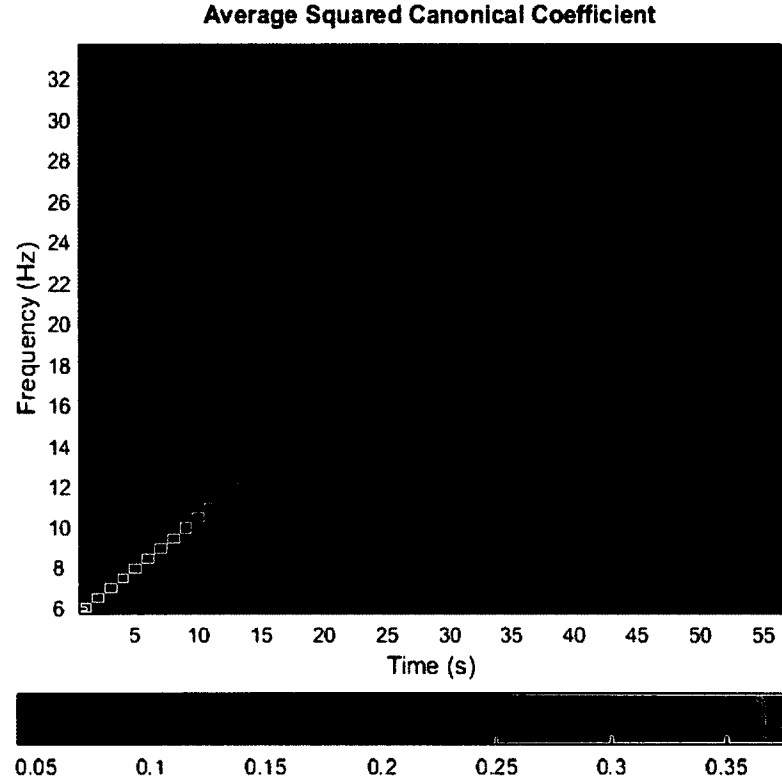


FIG. 14: Canonical Correlation Analysis (CCA) squared correlation values averaged across the 17 subjects. The x-axis shows the timescale based on the chirp stimulus. Each column represents a 2-second segment of the chirp signal that is approximated as a fixed frequency. The strong diagonal correlations represent a correspondence of the EEG and the stimulation frequency and its harmonics across the windowed time segments.

The data from the 17 subjects were combined into a single set consisting of 170 observations per frequency. The combined subject set is used to build an average SSVEP classifier for the optimization to produce a generalized solution for each N-class condition.

4.2.3 FEATURE SELECTION USING A GENETIC ALGORITHM

Genetic algorithms (GAs) are powerful search algorithms that simulate natural evolution for optimization problems [Goldberg and Others, 1989]. GAs have been used for wrapper-based feature selection problems and have been utilized to optimize feature selection in BCIs [Peterson et al., 2005]. In this study, the GA is used to find

optimal sets of SSVEP frequency features using CCA for a range of simulated N-class classification problems. The N-class conditions simulated in this study range from 2 to 36 classes in order to compare the performance between practical class sizes and determine generalized feature sets that optimize performance for each N-class condition. Each 0.5 Hz increment of the chirp stimulus ranging from 6 Hz to 33.5 Hz was used to generate a simulated frequency feature. This resulted in 56 total frequency features, which constitutes an extremely vast search space for feature selection that is not practical for exhaustive evaluation for most of the N-class conditions.

Initial Population

An independent GA optimization was performed for each of the 35 N-class BCI conditions (i.e., 2-36 classes). For each condition, an initial population of 1000 individuals (candidate solutions) is created. Each individual is a binary string of length 56, where the ones represent the features that are to be included in the model and zeros represent the features to disregard. For each N-class condition, the number of selected features is constrained to match N, as each feature represents a frequency target.

For the initial population, the majority of individuals are randomized with N ones and $(56-N)$ zeros using a uniform random distribution. After 50 generations, the population was reinitialized with uniform random distribution and 5-10% of the population was seeded with a combination of the 10 best solutions from the previous GA optimization and random 1-bit permutations of these solutions. These permutations were selected to minimize the Hamming distance from the best solutions since the best solutions were generally found to be completely or partly contiguous over frequency spans. This was done in order to fine tune the search near the best solution while still maintaining diversity of the search.

Fitness Evaluation

The fitness of each individual is evaluated by classifying the EEG using the CCA algorithm. Each individual is assigned a fitness value based on its respective classification performance. In this study, two fitness evaluation schemes are compared: the overall classification error and empirical confusion matrix norm (ECMN).

Classification Error Optimization: The GA was tuned to select and reproduce individuals with features that minimize the classification error from the CCA classifier. The overall classification error metric is calculated from the confusion matrix as:

$$\text{classification error} = 1 - \frac{\sum_i H_{ii}}{N_C}, \quad (4)$$

where H_{ii} is the number of correctly classified observations for class i and N_C is the total number of observations in the confusion matrix.

Empirical Confusion Matrix Norm Optimization: This approach minimizes the norm of the empirical confusion matrix (ECM) $\|C_s\|$ [Ko, 2013, Ralaivola, 2012]. For this scheme, the diagonals (correct classifications) of the standard confusion matrix are zeroed out to create the empirical confusion matrix C_S . The ECMN is calculated as:

$$\|C_S\| = \sqrt{\lambda_{\max}(C_S^* C_S)} \leq \sqrt{\text{Tr}(C_S^* C_S)}, \quad (5)$$

where C_S^* denotes the conjugate transpose of C_S , λ_{\max} is the maximum eigenvalue and $\text{Tr}()$ is the sum of the diagonal elements. The latter equation constitutes the upper bound of the confusion matrix norm. The value of $\|C_S\|$ will be higher for confusion matrices with miss-classifications that bias towards a certain set of classifier outputs. Unlike classification error optimization, which seeks to find the set of SSVEP features that provide the overall best classifier performance, the confusion norm optimization seeks features that provide the best classifier balance. This is particularly important for practical BCI implementations since lower frequencies tend to produce responses

with higher signal-to-noise ratios (SNRs) that can dominate the classifier output, which may be masked for higher class conditions if only the overall accuracy is evaluated.

Selection and Reproduction

For the GA selection procedure, the population is ranked and sorted according to the individuals' fitness, and the top 150 individuals are labeled the elite group. Individuals from the elite group are randomly selected for mating with a randomly selected member of the entire population (i.e., at least one parent is always from the elite group). This elitist procedure is done to speed convergence of the GA [Baluja and Caruana, 1995]. Thus, 850 children are generated in each generation of the GA.

Crossover and Mutation

The crossover of two parent genes (i.e., binary strings) to form a child gene is performed using bitwise logical AND and bitwise logical OR. Given the binary strings from two parents, the bitwise OR operation is used to select the feature from each parent providing a total of R features that will be transferred to the child gene. This results in $R \geq N$; thus, an n subset of R must be selected. The bitwise AND is then used to select the S features that are common to both parents. If $S < N$ then the remaining $N - S$ features are randomly selected from the original set of R features. The final child has N features derived from the parent features. A mutation rate of 5% was applied to the children genes after reproduction and crossover. For each generation, 5% of the children's genes were randomly selected for mutation where one random bit was flipped from 1 to 0 and another random bit was flipped from 0 to 1 to maintain the desired number of features. Figure 15(b) shows a visual representation of the modified crossover method implemented in this study compared to the traditional crossover method shown in Figure 15(a).

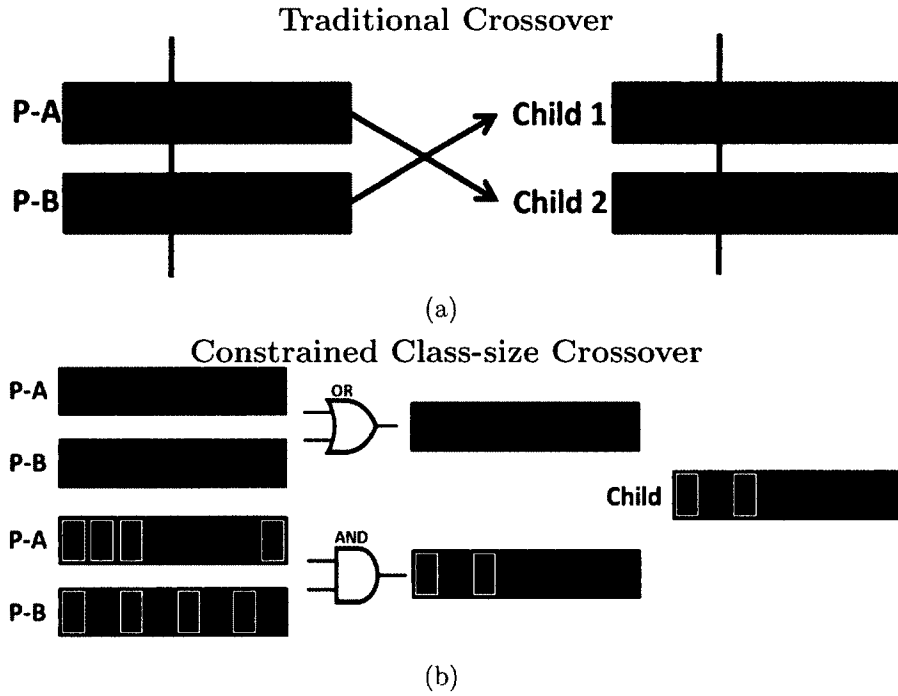


FIG. 15: Part (a) shows the traditional crossover technique which may result in varying number of features that will survive to the next generation. Part (b) shows the modified crossover technique used in this study that guarantees a fixed number of features will survive based on a desired class size. The child gene is composed of the S features from the AND operation and $N - S$ features randomly chosen from R features resulting from the OR operation. The child gene results in N total selected features.

Batch Processing and Evaluation

The combined EEG data set from the 17 subjects was used for the GA optimizations. A separate GA optimization was performed for each of the 35 different N-class conditions (2 through 36-class) for both the classification error and ECMN optimization, resulting in a grand total of 70 distinct GA optimizations. The runtime of each GA was fixed to 100 generations (i.e., 50 generations for determining the best seeds and 50 generations for fine tuning the solution) to provide a sufficient search. For each GA evaluation, the features and fitness values were stored for each individual and generation to evaluate the convergence and sensitivity of the solutions.

The resulting performances are quantified using the overall classification accuracy and the corresponding information transfer rate (ITR). The ITR, or bitrate, is a common metric for evaluating performance of a BCI that accounts for speed, accuracy, and class-size. The ITR in bits/min is computed as:

$$ITR = \left(\log_2 N + P \log_2 P + (1 - P) \log_2 \left(\frac{1 - P}{N - 1} \right) \right) * \frac{60}{T}, \quad (6)$$

where N is the number of possible classes, P is the classification accuracy and T is the selection time used to obtain the classification. The nominal selection time is 2 seconds based on the length of each SSVEP observation used in this study. In order to simulate a practical ITR, an inter-epoch duration of 0.3 seconds was utilized based on the recent SSVEP study from [Chen et al., 2014] which estimates the time required to shift eye-gaze from one target to the next. These simulated ITRs are intended to provide a relative performance comparison between the optimization methods rather than a completely realistic estimate of ITR.

4.3 RESULTS

To compare the GA solutions for each of the N-class conditions, the performance results are plotted as line plots for each N-class condition. The GA solutions (best feature set) for both the classification error and the ECMN optimization approaches

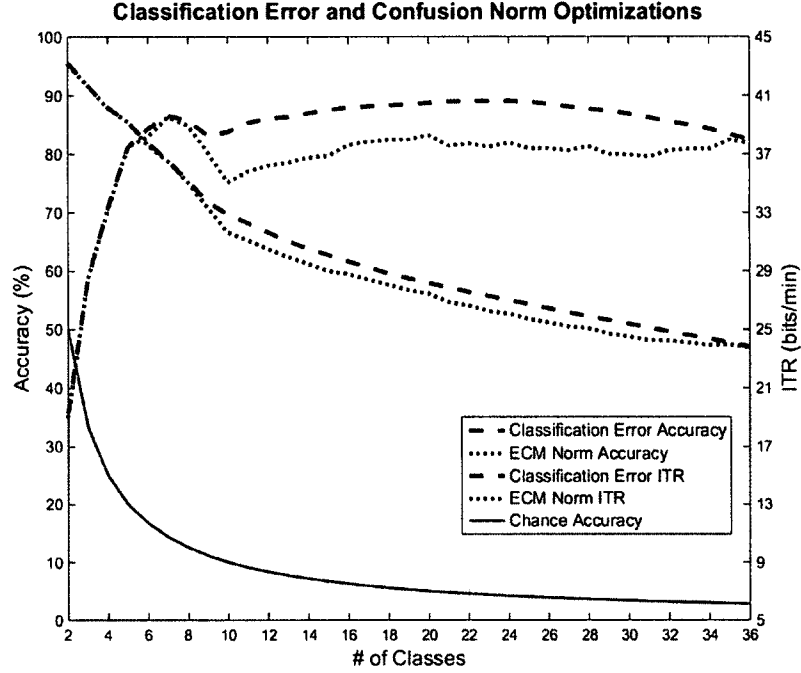


FIG. 16: Accuracy and Information Transfer Rate (ITR) of the best solution from the classification error and ECMN optimizations for each N-class condition. The red and blue accuracy line plots correspond to the left y-axis scale and the green and purple ITR line plots correspond to the right y-axis scale. Chance accuracy for each N-class condition is plotted as the solid gray line.

are compared in Figure 16. The resulting overall accuracy and ITR of the best individual from both approaches are plotted against each of the N-class conditions. The results in Figure 16 show the expected decrease in accuracy of the optimization solutions for increased number of classes. All accuracies produced are significantly higher than chance. The accuracy of the best solution from the ECMN optimization shows a slight decrease in accuracy compared to the best solution from the classification error optimization. The drop in accuracy only becomes apparent after a class size of 9 and exists until an class size of 35. The ITR plots in Figure 16 show an even more pronounced degradation in performance of the ECMN optimization compared to the classification error optimization for class sizes 9-34. For both optimization conditions, an inflection point in accuracy and ITR is observed around 9-10 classes, indicating suboptimal performance for these conditions. In order to quantify and

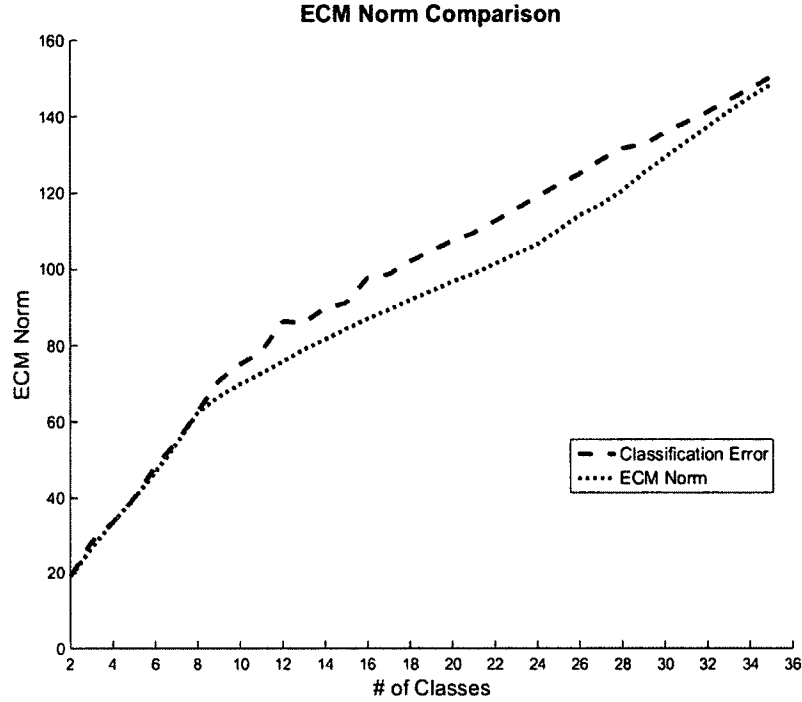
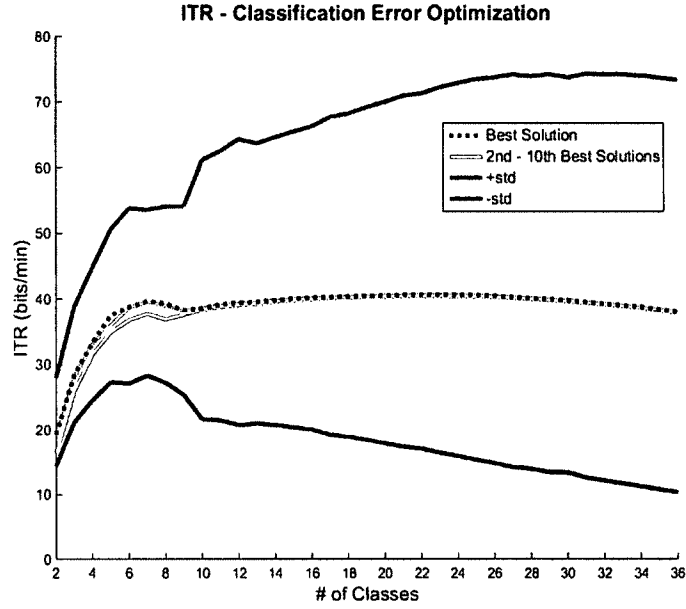


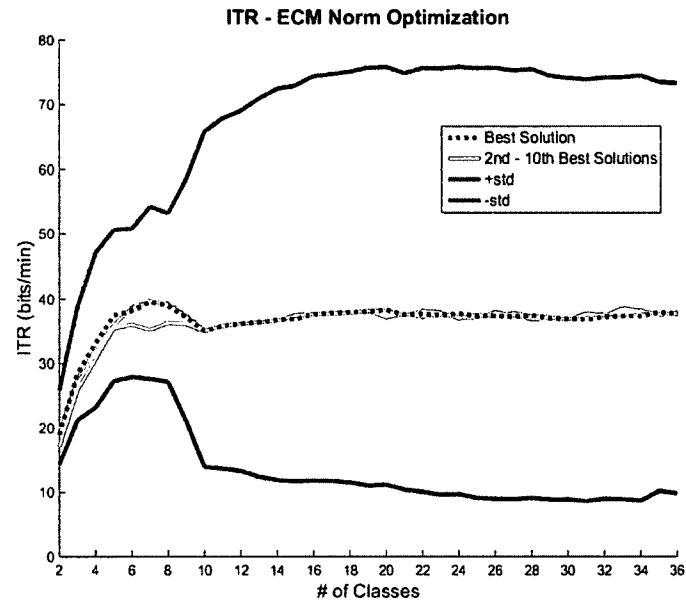
FIG. 17: A comparison of the ECM Norm for the best solutions selected by the Classification Error and ECM Norm optimizations, respectively. The ECM Norm provides a measure of classification accuracy imbalance across target frequencies, where a lower ECM Norm indicates more balanced accuracies across target frequencies.

compare the accuracy imbalance across target frequencies, the ECMN for both approaches is shown in Figure 17, where a lower ECM Norm indicates more balanced accuracies across target frequencies. Similar to accuracy and ITR in Figure 16, it is observed that the differences in approaches occur for class sizes 9-34.

To illustrate the level of solution uniqueness and sensitivity from each GA evaluation, the ITR of the solution is plotted with the ITRs of the 10 next-best solutions in the population history as shown in Figure 18. Figure 18(a) shows the top 10 solutions for each N-class condition from the classification error optimization and Figure 18(b) shows the top 10 solutions for each N-class condition from the ECMN optimization. The performance difference between the best solution and the 9 next-best solutions is most apparent for the lower N-class conditions between 2 and 10. The higher N-class conditions show very similar ITR performances between the best



(a)



(b)

FIG. 18: Information Transfer Rate (ITR) performance for the top 10 best optimization solutions for each N-class condition. (a) shows the top 10 results from classification error optimization and (b) shows the top 10 results from the ECMN optimization. For each plot, the dotted line indicates the best solution and the solid lines bound the 2nd-10th best solutions. The \pm -std indicates the standard deviation of accuracy across subjects converted to ITR.

and 9 next-best solutions. For the ECMN optimization in Figure 18(b), the next-best solutions sometime show a slight increase in ITR for a few of the higher N-class conditions. This is due to the fact that the ECMN is optimizing the norm of the empirical confusion matrix and not overall accuracy.

Figure 19 shows the selected features from GA optimization for each N-class condition as 2-dimensional histograms. Figure 19(a) shows the selected feature distribution from the classification error optimization, and Figure 19(b) shows the selected feature distribution from the ECMN optimization. Each column represents an N-class condition (i.e., number of simulated SSVEP targets) and each row represents a possible frequency feature. For each GA evaluation, the best set of features is plotted using white dots where the number of dots corresponds to the N-class condition and the location of each dot corresponds to the selected frequency feature. A histogram distribution of the selected features from the 9 next-best solutions for each N-class condition is plotted with a color scale corresponding to the number of times each frequency feature was selected for the next-best solutions. This gives a rough indication of the usefulness of a given feature with respect to the N-class condition.

4.4 DISCUSSION

The feature selection histograms for both optimization methods in Figures 19(a) and 19(b), respectively, indicate the optimal features for lower N-class conditions come from lower frequencies. In both figures, there is a distinct change in selected features from the 6-9 Hz range to the 15-20 Hz range as the N-class condition increases from 8 to 9, which is also near the performance inflection point. This can be explained by examining the CCA plot in Figure 14. This plot shows that the frequencies from 6-10 Hz have a higher CCA coefficient across this entire band compared to the diagonals at higher frequencies. This is partly due to the higher power and SNR in this low frequency range, particularly in the alpha band. It should be noted that the alpha band and its second harmonic are generally avoided in the frequency selection due to the innate nature of this rhythm, independent of stimulation in this range.

Of further interest, no N-class conditions that are greater than N=9 contain

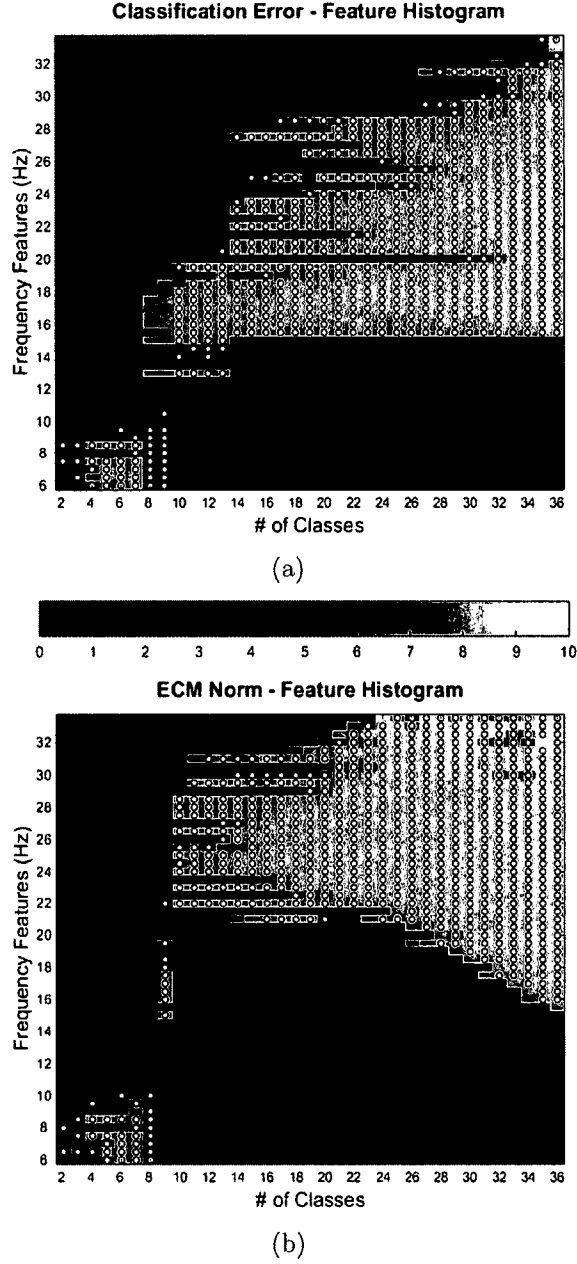


FIG. 19: 2-D histograms of optimized feature sets for each N-class condition. Each column is a different N-class condition that spans the possible feature range (6-33.5 Hz). For a given N-class condition, the features from the best optimized solution are superimposed as white circles indicating the selected feature. Each column has N dots corresponding to each N-class condition. The 9 next-best solutions are plotted as histograms where the color corresponds to the occurrence rate of the selected feature. (a) shows the feature distributions for the classification error optimization and (b) shows the feature distributions for the ECMN optimization.

any low frequency features in the final optimized set. For the classification error optimization, Figure 19(a) shows a bias towards the middle frequency range (15-19.5 Hz) which gradually includes higher frequencies as the N-class condition increases. However, for the ECMN optimization, Figure 19(b) shows another sharp change in selected features from the mid range (15-19.5 Hz) to the higher range (22-32 Hz) at the 10-class condition. This is likely due to the fact that these ranges of frequencies have more similar SNRs. This would result in a more balanced classification (i.e., minimizing the ECM norm), which is desirable for practical BCIs.

The contiguous nature of the majority of the selected feature sets can also be, in part, explained by the relative SNR across particular frequency bands. For the classification error, it is observed that the features are generally contiguous and after the inflection point, the added features come from the next highest frequency (i.e., next highest SNR). The ECMN optimization follows a similar contiguous pattern, except the initial range after the inflection point is (22-28 Hz) and roughly alternating lower and higher frequency contiguous features are included to maintain the class balance. Another contributing factor to the observed contiguous ranges is that the harmonic frequencies play a role in the CCA as depicted in Figure 14. Particular frequency features, especially in the lower frequencies, will tend to dominate the CCA at the respective harmonic frequencies. Thus, it is unlikely for frequencies to be selected that have competing harmonics. Future work will examine the inclusion of harmonic frequencies in the CCA and its impact of on the selected feature sets.

In terms of maximizing the ITR across the population, the results indicate that a peak ITR near 40 bits/minute is achieved for the seven-class condition for both optimization schemes. Additionally, both optimization schemes selected contiguous frequency features from 6-9 Hz (0.5 Hz increment) for this condition. Aside from the inflection point, the ITR is generally flat above the 10-class condition due to the steady decrease in accuracy for higher classes. It should be noted that a fixed inter-stimulus interval was used across N-class conditions to compute the simulated ITRs. It is likely that longer inter-stimulus intervals would be needed for adequate scanning time in the higher-class conditions, which would further degrade the ITR.

as the number of classes increases. Figure 17 shows the expected improvement in balanced classification across target frequencies for the ECMN optimization for class sizes 9-34. Ultimately, if all target frequencies should be equi-probable for a given interface design, the ECMN optimization will provide a more balanced scheme for more than 8 classes with marginal decreases in overall classification performance.

The proposed approach has some limitations in terms of generalizing to an online BCI. The SSVEP responses were collected serially using a fairly large single-stimulus LED array. For an actual multi-class online implementation, simultaneous stimuli at different frequencies would be presented, generally with smaller physical dimensions. The present analysis does not account for the potential simultaneous interference or attentional issues present in a practical online scenario. Another limitation is that the chirp signal, while slowly varying over the selected time windows, is not of a fixed frequency and had a limited duration. Thus, there may not have been adequate time to fully entrain certain frequencies, and the CCA may have a slight bias due to the variation in frequency over the time windows. Another consideration is that the selected features may be specific to the CCA approach and may be suboptimal if other SSVEP feature extraction and classification schemes are employed. Through examination of the sensitivity of the ITR and selected features to the near-optimal solutions shown in Figure 18, the selected next-best feature histograms generally have overlapping densities with the best solutions, and slight changes in the selected features lead to comparable ITR performances. Nevertheless, it is believed that the present analysis provides a comprehensive evaluation of the most discriminable frequency feature sets for a given number of classes, which should serve as a reference and a guide for standardization of generalized SSVEP stimulus frequencies.

CHAPTER 5

SPATIAL FREQUENCY CHARACTERIZATION AND OPTIMIZATION OF SSVEP STIMULI

Most traditional SSVEPs implement solid rectangular stimuli, flashing at different frequencies, to elicit the SSVEP response. This is a binary flashing technique in which the stimulus alternates between one solid color and another solid color (usually white and black). However, it is also common to use spatial checkerboard patterns as visual stimuli. The checkerboard stimuli are pattern reversed at a constant frequency using alternating checker colors to elicit the SSVEP response. The pattern reversal from a checkerboard stimulus creates a similar SSVEP response to the solid rectangular stimulus, although there is debate over which stimulation type is superior.

5.1 INTRODUCTION

The effect of spatial frequency has been tested thoroughly in the clinical fields with the elicitation of pattern electroretinograms (PERGs) and pattern VEPs (PVEPs) [Armington, 1977]. These pattern responses are usually elicited using a single pattern reversal checkerboard stimulus or a vertical square wave grating stimulus. In 1985, Leguire and Rogers recorded ERGs as a function of spatial frequency and contrast and showed that an increase in either spatial frequency or contrast resulted in an increase in the amplitude of the pattern ERG [Leguire and Rogers, 1985]. These results, however, are not in concurrence with results from previous investigators that have found an increase in spatial frequency produces a decrease in amplitude response [Armington et al., 1971]. Likewise, other investigators have shown that an increase followed by a decrease in pattern ERG amplitude results from increased spatial frequencies from 0.5 arc-min/cycle to 1.5 arc-min/cycle EEG and ERG amplitude peaking at 1 arc-min/cycle [Armington et al., 1967]. In 1991, Tomoda et al.

recorded simultaneous ERGs and VEPs and showed that ERGs exhibited a bandpass tuning with a peak amplitude at 1.5 cycles/degree while VEPs had a bimodal spatial frequency function with peaks at 3 c/deg and 1 c/deg [Tomoda et al., 1991]. Overall, these conflicting results confirm that the true nature of the visual system response elicited from pattern stimuli from various spatial frequencies is not conclusive and may depend on the individual subject [Sokol and Bloom, 1977].

Similar to these contradictory results found in the clinical and neuroscience fields, recent BCI studies have also found conflicting results on the effect that checkerboard stimuli have on the performance of SSVEP BCIs. Some studies have found that the checkerboard stimuli produce stronger SSVEP responses than solid stimuli [Lalor et al., 2005], while others have found conflicting results which conclude that solid flashing stimuli perform better than checkerboard pattern reversal stimuli for SSVEP BCIs [Allison and Sugiarto, 2008, Saetang et al., 2013, Zerafa et al., 2013]. Not only is it unclear whether or not checkerboard pattern reversal is superior to solid flashing stimuli, the effect of checkerboard's spatial frequency (i.e. size of the individual checks) on SSVEP performance has also never been studied in the context of BCIs where multiple stimuli are presented simultaneously.

A study characterizing and optimizing the spatial frequency of visual stimuli was conducted using checkerboard stimuli in a BCI paradigm. In this study, stimuli of four different temporal frequencies were tested with varying spatial frequencies. This study tests the entire spatial frequency range from a 1x1 (0 c/deg) checkerboard (solid stimuli) and doubling in spatial frequency (i.e. 2x2 (0.15 c/deg), 4x4 (0.3 c/deg), 8x8 0.6 c/deg, etc) up to a 256 x 256 checkerboard (single pixel check sizes with a spatial frequency of 19.2 c/deg) providing 9 total spatial frequency conditions. A four-class SSVEP BCI paradigm was used online to test the 9 total spatial frequency conditions where each condition was tested as a separate BCI to evaluate the effect of spatial frequency on SSVEP performance. Additionally, an online path-navigation task was performed with each of the 9 total spatial frequency conditions.

It is hypothesized that subjects have various degrees of detectable response to each of the different spatial conditions and thus will obtain varying levels of BCI

performance for each condition. Similar to how stimuli flashing at high temporal frequencies (30-50Hz) appear less obtrusive and visually fatiguing to the user [Müller et al., 2011], stimuli with high spatial frequency also have the effect of reduced perceptibility, which may also lead to reduced visual fatigue. High spatial frequency stimuli may provide a novel way to reduce stimulus saliency with limited degradation on VEP-BCI performance. The aim of this study is to characterize these differences amongst the spectrum of spatial frequencies and determine which spatial frequency provides superior performance in the context of SSVEP-BCIs. The outcomes of this study can potentially provide a method for presenting less irritating or fatiguing stimuli.

5.2 METHODOLOGY

5.2.1 DATA COLLECTION

A total of 11 subjects (7 male, 4 female, ages 24-32) participated in the experiment. Each subject gave informed consent prior to the study and were free of any known neurological conditions. All subjects had normal or corrected-to-normal vision and had varying levels of previous BCI experience, with 6 subjects having no previous BCI experience. The study was approved by the Old Dominion University Institutional Review Board.

Data were collected from a 16-channel g.USBamp amplifier with active electrodes (Guger Technologies, Austria). Electrodes were placed primarily over the occipital, parietal-occipital and parietal regions of the brain (Figure 20) according to the international 10-20 system [Sharbrough et al., 1991]. Electrodes were referenced to the right earlobe and grounded to the right mastoid. All data were collected using a sampling rate of 256 Hz, bandpass filtered from 2-30 Hz and stored on a hard disk. All aspects of the data collection were controlled using BCI2000 general-purpose BCI recording software [Schalk, 2004].

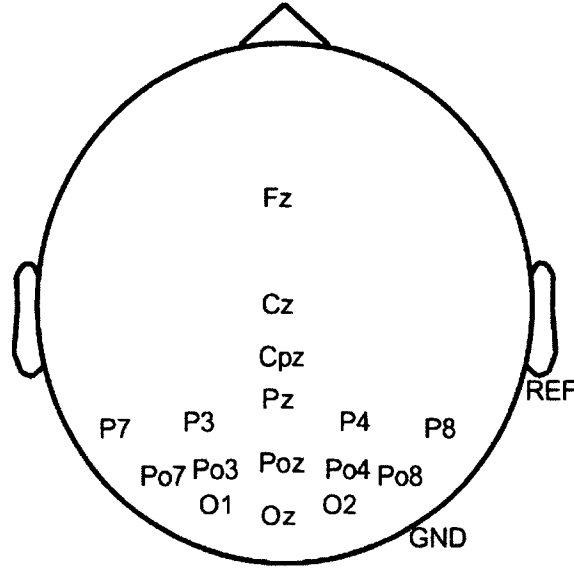


FIG. 20: Electrode montage used for this study. Data were recorded from all 16 electrodes shown, however, data from only 8 channels (Oz, O1, O2, POz, PO3, PO4, PO7, PO8) were utilized in the online and offline analysis.

An Arduino Uno microcontroller board with an ATMEL ATMEGA328P microcontroller chip was used to synchronize the stimulus onsets with the EEG signals. A custom Matlab script was written to apply canonical correlation analysis (CCA) in real-time to classify the attended target and present feedback to the subject.

All subjects participated in a single session consisting of two experiments lasting 30 minutes each for a total session length of 1 hour. All subjects completed the experiments in the same order.

5.2.2 EXPERIMENTAL PARADIGM

Stimulus Parameters

All stimuli were rendered using DirectX (Microsoft Inc.) and displayed on a 24" LCD monitor with a 60Hz refresh rate and a 1920 x 1080 resolution. Subjects sat comfortably in dark room and were centrally seated in front of the monitor at a distance of 55 cm. Nine different spatial frequency stimulus conditions were tested: 0 cycles/degree (1x1 checkerboard), 0.15 c/deg (2x2)), 0.3 c/deg (4x4), 0.6 c/deg

(8x8), 1.2 c/deg (16x16), 2.4 c/deg (32x32), 4.8 c/deg (64x64), 9.6 c/deg (128x128), and 19.2 c/deg (256x256). Figure 21 shows the 9 checkerboard conditions with their respective pattern reversed forms. The 1x1 represents a checkerboard that has 1 row and 1 column (i.e. a solid square), and the 256x256 is a checkerboard with 256 rows and 256 columns. Each checkerboard condition is an image with the size of 256x256 pixels. Therefore, the 256x256 checkerboard condition has checker sizes that are composed of single pixels.

Subjective Evaluation

Before the start of the experimentation session, subjects participated in an evaluation of the visual stimuli. Subjects were placed 55 cm away from a 24" LCD monitor where all 9 spatial frequency conditions were displayed simultaneously on the screen. Each of the spatial frequency conditions were flashing with the same temporal frequency of 6 Hz. During this time, subjects were asked to subjectively evaluate the different conditions in terms of visual irritation, by ordering each spatial frequency from 1 to 9 where 1 indicated the least visually irritating spatial frequency and 9 indicated the most visually irritating spatial frequency. Subjects provided a written response to the statement: "Please order each condition from 1-9 indicating how visually irritating it is to continuously start at the stimulus where 1 represents the least irritating and 9 represents the most irritating". The subjective evaluation was performed prior to the experiment to avoid potential biases in preferences after performance feedback during the experimental sessions.

Experiment 1: Discrete Classification

The first experiment consisted of a standard 4-class BCI paradigm in which four stimuli were presented simultaneously in the top, bottom, left and right portions of the screen and were flashed at four temporal frequencies of 6, 6.66, 7.5 and 8.571 Hz (shown in Figure 22). The experiment consisted of 18 runs each with 8 trials. Within each run, one of the 9 spatial frequency conditions were tested in which

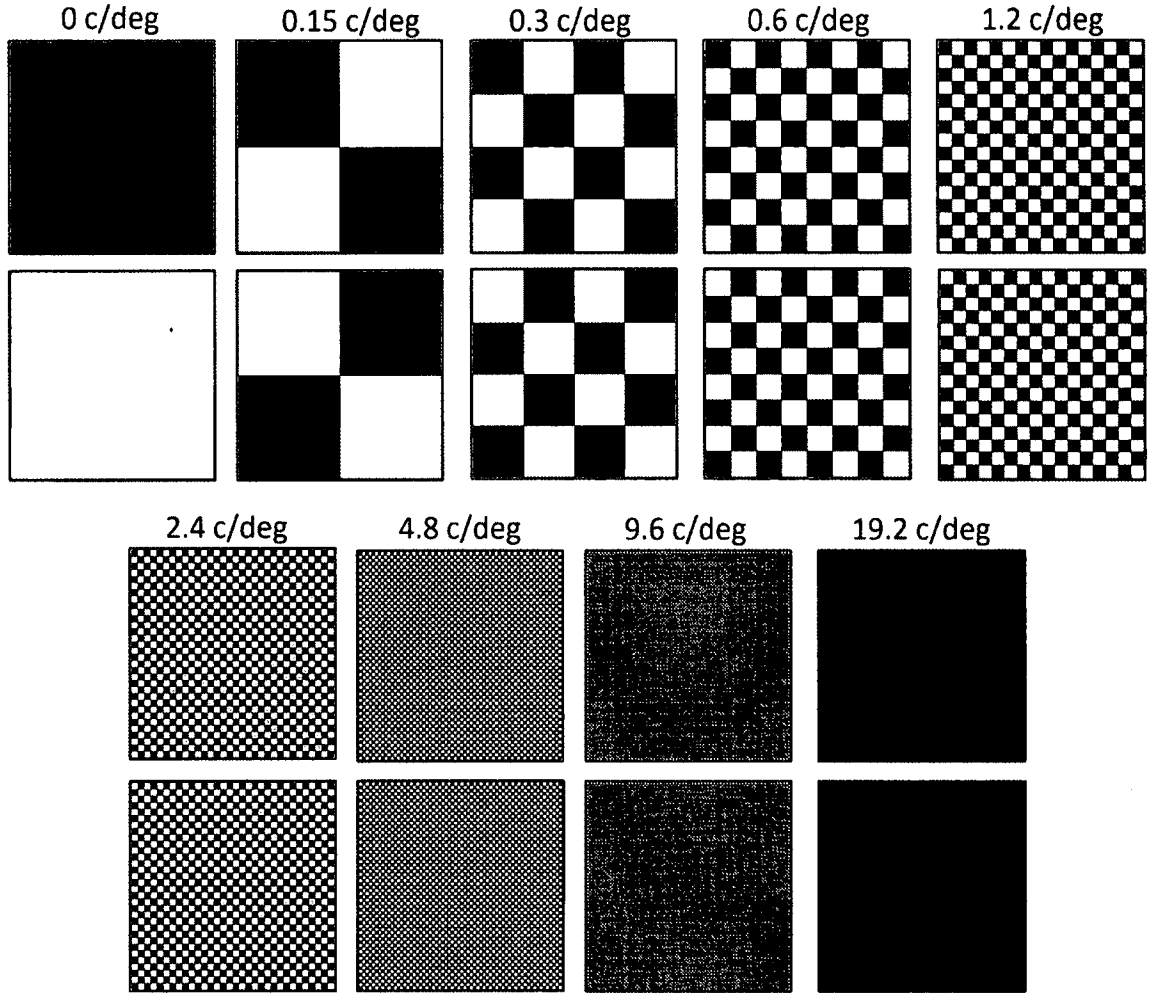


FIG. 21: Checkerboard stimuli used in the study. Each of the 9 checkerboard spatial frequency conditions is displayed with its respective pattern reversal shown beneath. The corresponding spatial frequencies in cycles per degree (# of rows and cols) going from top left to bottom right are: 0 c/deg (1x1), 0.15 c/deg (2x2), 0.3 c/deg (4x4), 0.6 c/deg (8x8), 1.2 c/deg (16x16), 2.4 c/deg (32x32), 4.8 c/deg (64x64), 9.6 c/deg (128x128) and 19.2 c/deg (256x256).

the 4 stimuli were populated with the checkerboard pattern from that condition. Each trial began with a 2-second cue period where an arrow indicated the current target stimulus from a random sequence as shown in Figure 22(a). The task for each subject was to centrally fixate gaze and attend the target stimulus for 6 seconds during the stimulation portion of the trial. The trial concluded with a 2-second feedback period where the predicted target was encompassed by either a green or red square corresponding to a correct or incorrect classification (Figure 22(b)). During the feedback period, text was also displayed to the subject indicating the current condition and trial as well as the running classification accuracy.

A single trial lasted 10 seconds and all trials were presented in immediate succession of one another making the duration of a single run equal to 80 seconds (10 seconds x 8 trials). After each spatial frequency condition a short rest period was given to the subjects lasting approximately 30-60 seconds. Each of the 9 spatial frequency conditions was tested twice during the 18 runs and was presented in random order to avoid any fatiguing or order-on-performance biases. The total length of Experiment 1 was approximately 30 minutes. After completion, subjects were given a small break before proceeding to experiment 2.

Experiment 2: Continuous Path-Navigation

In experiment 2, subjects used the 4-target configuration from experiment 1 to complete a path-navigation task using a familiar PacMan avatar (shown in Figure 23). The four stimulus targets controlled the four directions the avatar could move (up, down, left and right). Two different paths were utilized which contained no bifurcations to provide a unique path from the starting point to the ending point.

Each path took exactly 48 total moves to complete, where each movement direction was equally represented with 12 moves each. The goal of the navigation task was to move the PacMan avatar from the starting point to the coinciding ending point of the path which was represented by a blue square (Figure 23). The avatar could not cross the path walls and the movement was unconstrained so the avatar could move in the correct or opposing directions depending on the predicted classification.

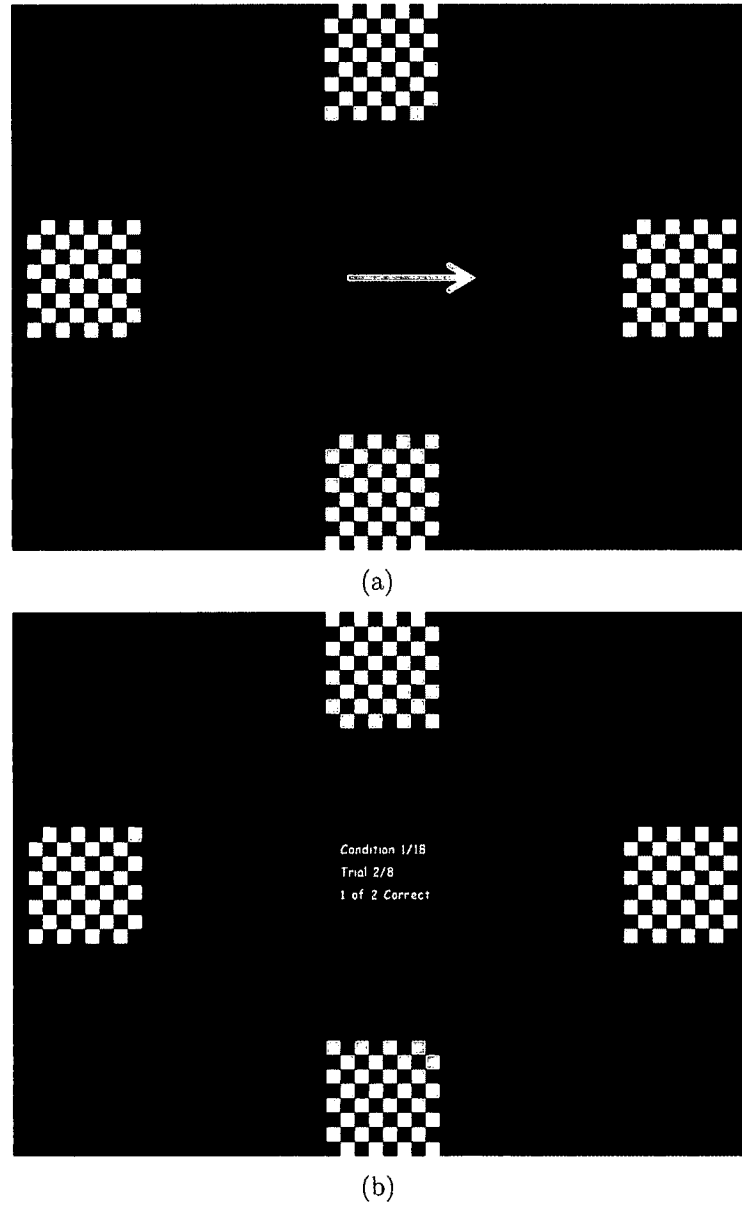
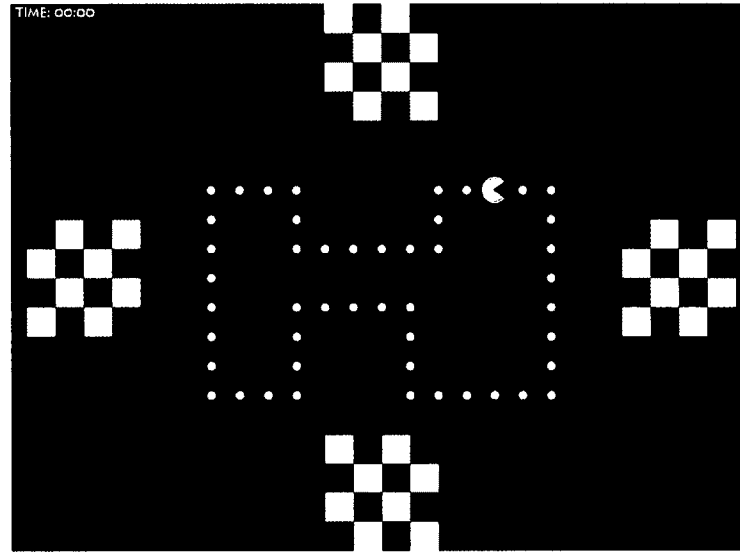
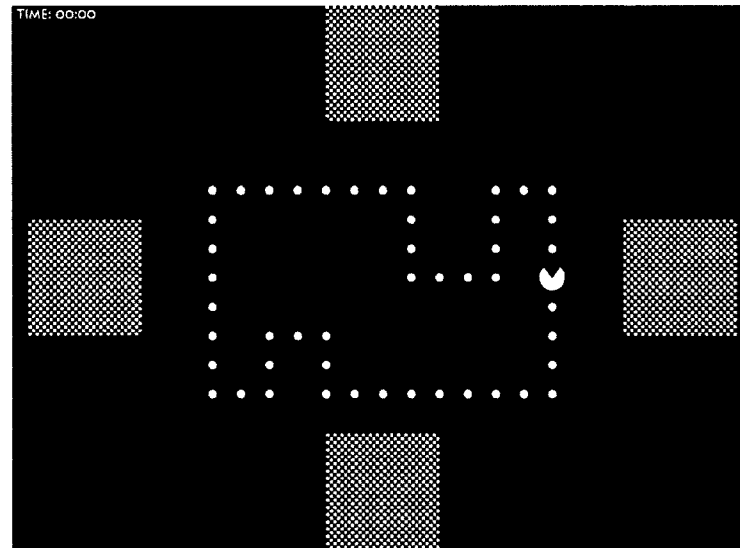


FIG. 22: Stimulation paradigm used for experiment 1 with currently the 0.6 c/deg (8x8) spatial frequency condition shown. Each trial starts with a 2-s cue period to indicate the current fixation target, shown in part 22(a). After a 6-s stimulation period, feedback is given as box surrounding the predicted target (part 22(b)). Correct predictions were shown with a green box while incorrect predictions were shown with a red box. The left stimulus flashed at 6 Hz, the right flashed at 7.5 Hz, the top at 8.57 Hz and the bottom at 6.66 Hz.



(a)



(b)

FIG. 23: Stimulation paradigm used for experiment 2. The four stimuli match the same shape and position as experiment 1. The path used in PacMan path navigation task was placed in the center of the four stimuli, contained no bifurcations and took 48 moves to complete where each direction had 12 moves. The blue square indicates the start/end position which was randomized for each run. Parts 23(a) and 23(b) show the two path variants that were randomly presented. The top panel currently shows the 0.3 c/deg (4x4) spatial frequency condition and the bottom panel shows the 2.4 c/deg (32x32) spatial frequency condition. The run time was shown at the top left which counted upwards starting from 0. If the path was not completed after 3 minutes, the run was terminated.

This represents a practical use-case for an online BCI as incorrect classifications must subsequently be corrected in-order to complete the path.

Subjects performed the path-navigation task for each of the 9 spatial frequency conditions for a total of 9 runs of the path navigation task. The conditions were presented randomly to the subjects. The minimum time to complete the path was approximately 48 seconds. The maximum time allotted for path completion was 180 seconds. If the subject was unable to complete the path in the allotted time, the run ended, and the next run was presented.

To better keep the subject engaged throughout the session, two different paths were used. Each path had a different starting and ending location, as well as different starting and ending directions. This also served to mitigate any spatial biases or learning effects as the presentation order of each path and each starting position was randomized for each of the 9 spatial frequency conditions. The overall direction of path navigation (clockwise or counterclockwise) was indicated by the starting direction of the PacMan avatar. Figure 23(a) shows an example of path 1 with a starting location that indicates clockwise navigation, and Figure 23(b) shows path 2 with a starting location indicating counter-clockwise navigation.

For the path-navigation task, EEG signals were classified using a continuously updating signal buffer with a fixed buffer length of 2 seconds of EEG data that was classified using a committee of CCA classifiers. The 2-second buffer was split into three 1-second sub-windows which overlapped every 0.5 seconds (i.e. sub-windows were from 0-1 s, 0.5-1.5 s and 1-2 s). A separate CCA classification was performed on each of the 1 s sub-windows resulting in three predictions of the target direction. A committee scheme was utilized for final prediction by way of majority voting in which the target direction was chosen when at least two of the three CCA classifiers agreed on the same target. If no mutual agreement was reached between the three classifiers then no selection was made representing a null state in which the avatar did not move. This classification scheme continuously analyzed the 2-second long data buffer which updated every second with a new second of data. Therefore, movement decisions and actions were made every second using the previous 2-seconds of data.

For each subject, each movement decision and the total path completion time was recorded for each of the 9 spatial frequency conditions.

5.2.3 DATA ANALYSIS

Experiment 1: Discrete Classification

For the online classification, data from the 6-second stimulation period were classified in real-time using CCA. A target template was created for each of the four temporal frequencies using two harmonics ($N_h = 2$) each.

Additional offline analysis was performed to compare the different spatial frequency conditions. Data were already filtered at the time of recording with a 2-30 Hz hardware bandpass filter; thus, no additional filtering was performed. Data from each of the spatial frequency conditions were extracted providing a total of 96 seconds of SSVEP data for each spatial frequency condition corresponding to 24 seconds of data for each of the four target stimuli. To test for any spatial adaptation that the visual system may be experiencing, CCA classification analysis was performed for different observation lengths varying from six seconds to single trial observation lengths of one second. To simulate the smaller observation lengths, data from the original 6-second runs were from 1 to 6 second in 0.5-second increments, starting from the stimulus onset to better represent actual online performance using shorter window lengths.

The Information-Transfer Rate (ITR) was calculated for each spatial frequency and observation length using Equation 7.

$$ITR = \left(\log_2 N + P \log_2 P + (1 - P) \log_2 \left(\frac{1 - P}{N - 1} \right) \right) * \frac{60}{T} \quad (7)$$

The classification accuracy and ITR as a function of overall spatial frequency were calculated by averaging over all observation lengths tested. In the case of ITR, only the lengths from 1-3 seconds were used in the averaging as ITR places emphasis on smaller time-windows.

The visual irritation index from each subject during the subjective evaluation survey was aggregated and averaged for each spatial frequency condition.

Experiment 2: Continuous Maze-Navigation

Analysis for the online experiment was handled in real time with the majority vote classification of a 2-second data buffer that was sub-divided into three 1-s sub-windows with an overlap of 0.5 s. CCA was performed on each window; a classification was made only when two of the 3 sub-windows agreed.

Using the online results, the average path completion time for each spatial frequency condition was computed across all subjects to give an indication of task performance as a function of the spatial frequency. Subjects that were not able to complete a path in the allotted 180-s limit were recorded with path completion time of 180 s. To further differentiate the task performance for each condition, the percentage of path that was traversed before time expired was calculated as a ratio of the farthest traversed point divided by the total number of moves. For example, a completion percentage of 50% (24/48) represents a condition where the subject only made it to the halfway point around the path before completion. The average path completion percentage across all subjects was computed for each spatial frequency condition.

5.3 RESULTS

5.3.1 EXPERIMENT 1: DISCRETE CLASSIFICATION

Figures 24 and 25 show the average classification accuracies and ITRs for each spatial frequency condition and observation length. These results are shown as 2-dimensional heat-plots where the color is mapped to either accuracy or ITR. Each column represents a different observation length and each row represents a spatial frequency condition. The accuracies in Figure 24 show that, overall, the 0 c/deg spatial

frequency condition (solid stimulus) achieves the highest average classification accuracy of 97.7% amongst all conditions for observation lengths ≥ 3.5 s. Additionally, the accuracy plot in Figure 24 shows two other distinct patterns. First, a bimodal distribution can be seen column-wise where a decrease in accuracy is exhibited for spatial frequency conditions between 0.15-0.6 c/deg as well as for conditions greater than 9.6 c/deg. Accuracies are greater for the conditions between 1.2 and 4.8 c/deg with a secondary peak forming at the 2.4 c/deg condition. Second, the observation length shows a considerable effect on the accuracy, especially for the conditions from 0.3 c/deg to 9.6 c/deg. Normally, an increased observation length ensures an increase in accuracy performance; however, the rows in Figure 24 show an interesting decrease in performance given observation lengths longer than 4.5 seconds with peak accuracies ranging from 2.5-3.5 seconds.

The average ITR results in Figure 25 show a similar column-wise bimodal distribution across the spatial frequency conditions with a peak in the 0 c/deg condition and a peak over the 2.4 - 4.5 c/deg conditions. Additionally, the 2.4 c/deg spatial frequency condition achieves the highest average performance among all conditions with an average ITR of 45.3 bits/min which exceeds the 35.7 bits/min ITR achieved by the solid stimulus condition (0 c/deg).

Figures 26(a) and 26(b) show 1-dimensional line plots of accuracy vs. spatial frequency and ITR vs. spatial frequency, respectively. In each figure, the accuracies and ITRs were averaged across multiple observations lengths. Both figures show a bimodal spatial tuning pattern where the performance peaks can be seen at the 0c/deg and 2.4c/deg spatial frequency conditions.

The level of spatial frequency adaptation over time is shown in the accuracy vs time plots in Figure 27. The 0 c/deg condition (solid stimulus) in blue, shows the typical accuracy vs. time profile where accuracy monotonically increases as the observation length increases until a ceiling is reached. The 2.4 c/deg (the best performing checkerboard stimulus) shows a similar proportional relationship between accuracy and observation length up to 2.5 s, after which, the relationship becomes

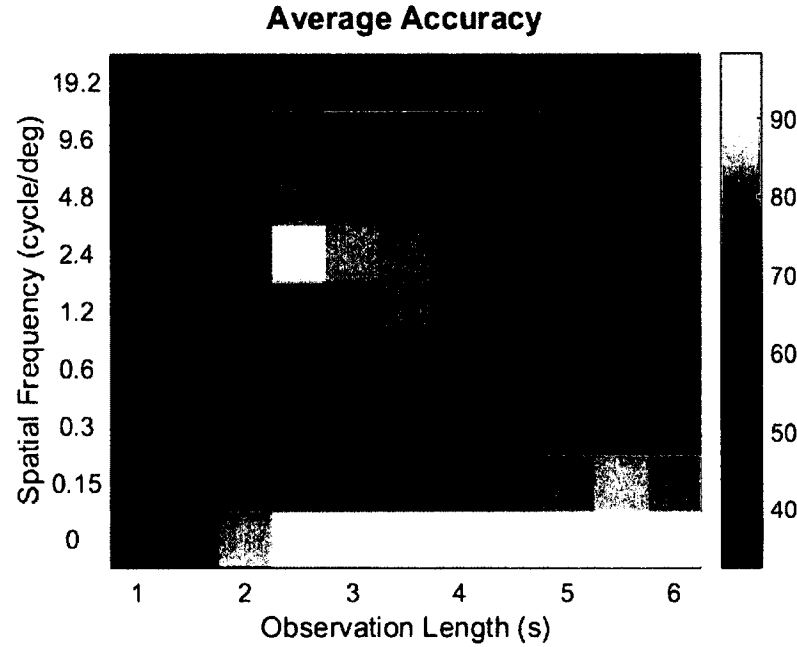


FIG. 24: Average Classification accuracy for experiment 1 for each spatial frequency condition vs observation length. where columns show the different observation lengths and rows show the different spatial frequencies.

inversely proportional and accuracy starts to decrease as the observation length continues to increase. The dashed black line in Figure 27 shows accuracy versus time averaged over all spatial frequency conditions. With the exception of the 0 c/deg solid stimulus condition, the remaining spatial frequency (checkerboard) conditions all follow a similar unimodal pattern where the accuracy peaks between observation lengths between 2 and 4 seconds, and longer observation lengths result in significant decreases in accuracy.

Figure 28 shows average rated irritation index for each spatial frequency from the subject evaluation questionnaires. The subjective irritation index generally follows the expected trend where level of visual irritation decreases as the spatial frequency increases, with the exception of a slight increase in the 1.2 c/deg increase.

5.3.2 EXPERIMENT 2: CONTINUOUS PATH-NAVIGATION

Figure 29 shows the performance results from the continuous path-navigation

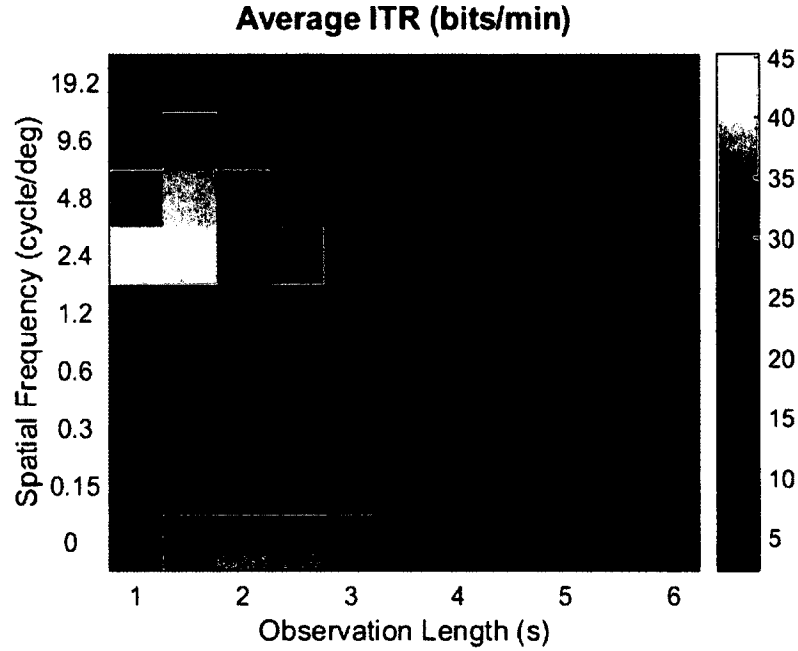
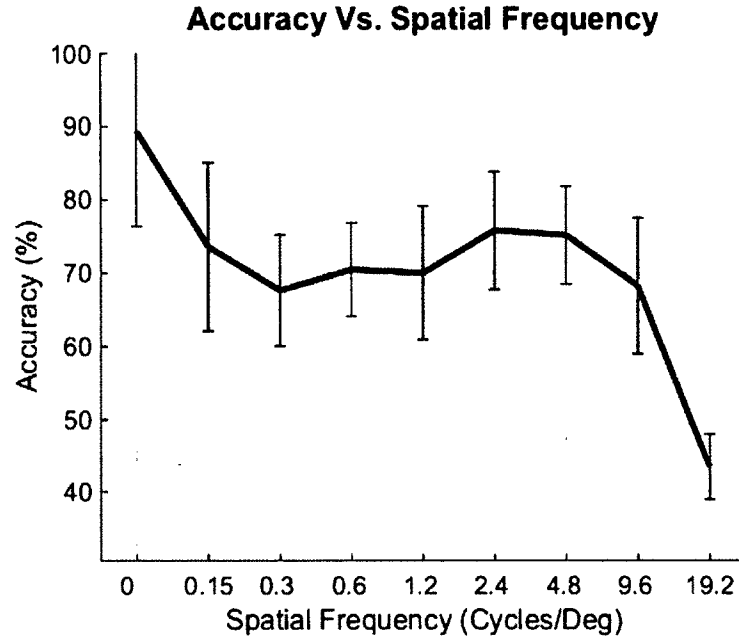
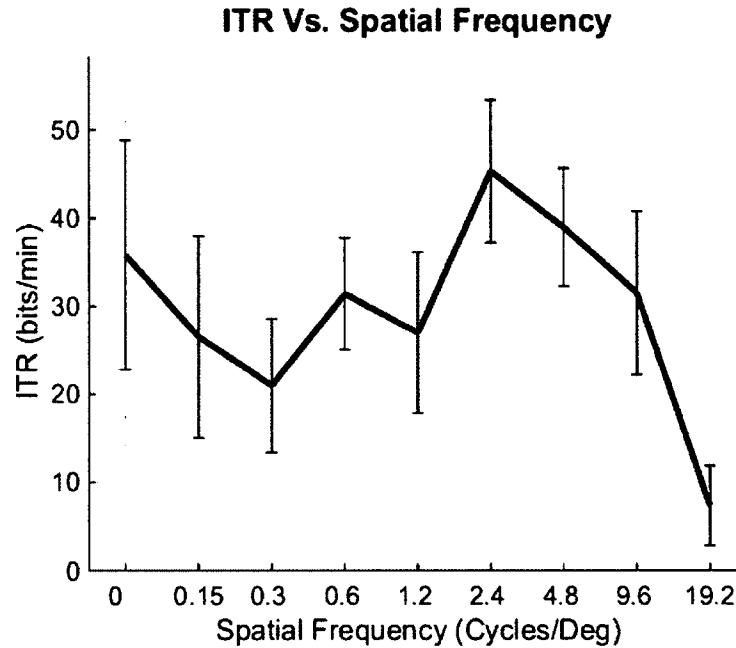


FIG. 25: Average ITR (bits/min) for experiment 1 for each spatial frequency condition vs observation length. Each column shows represents a different observation length and each row represents a different spatial frequency condition.

task. The average run duration is shown in Figure 29(a) where a shorter duration corresponds to better BCI performance as less time was required to fully navigate the path. Note that run duration time does not always imply completion of the as run duration lengths were capped to a maximum of 180 seconds and therefore some subjects were unable to complete the for some of the spatial frequency conditions. Figure 29(b) shows the amount of completion for each spatial frequency condition averaged over all subjects. The 0 c/deg and 2.4 c/deg spatial frequency conditions were the only conditions where all subjects were able to fully complete the in the allotted time. These results agree with those obtained from experiment 1 which showed performance peaks at the 0 c/deg and 2.4 c/deg conditions. Additionally, both the run-duration and the path-completion performance curves show bimodal distributions with the emergence of two distinct peaks; one at 0 c/deg and one at 2.4 c/deg.



(a)



(b)

FIG. 26: Spatial Frequency tuning curves from experiment 1. (a) shows classification accuracy as a function of spatial frequency averaged across all subjects. (b) shows the ITR as a function of spatial frequency averaged across all subjects. For both 26(a) and 26(b) the averages were computed using the maximum value over the range of observation lengths.

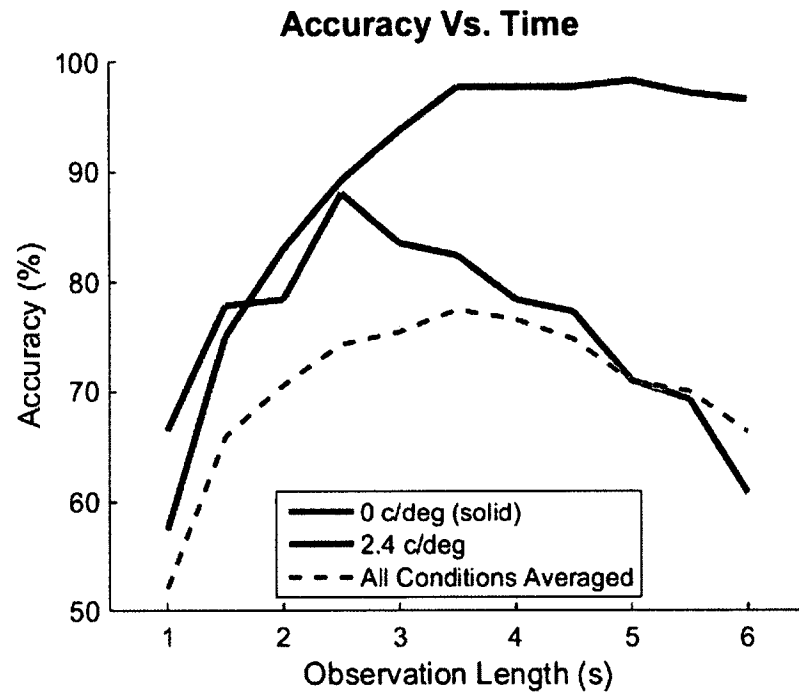


FIG. 27: Classification accuracy vs time window length averaged across all subjects from experiment 1. The solid blue line shows the accuracy vs time for the 0 c/deg (solid) spatial frequency condition and the solid red line shows the accuracy for the 2.4 c/deg condition. The dotted black line is the accuracy vs time averaged over all 9 spatial frequency conditions.

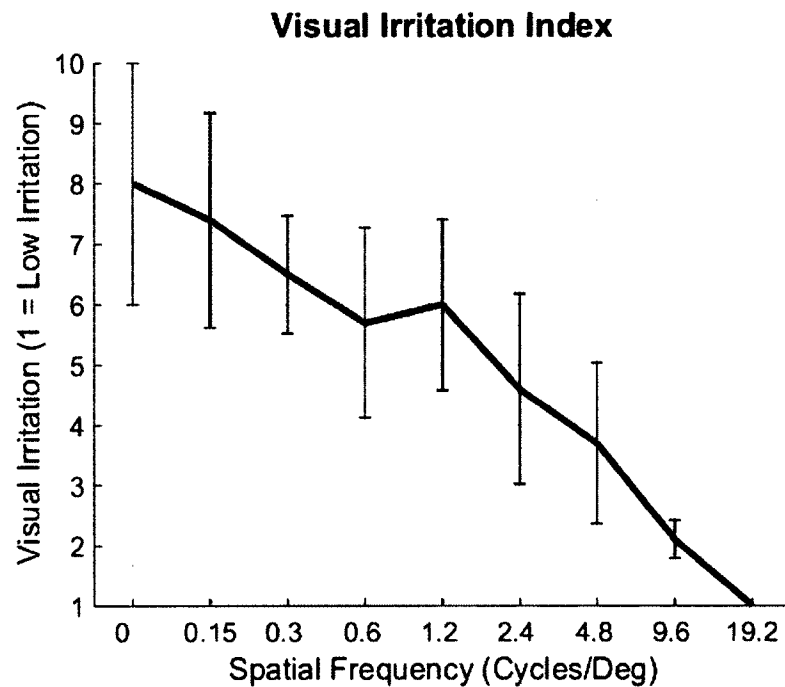


FIG. 28: Average subjective evaluation of visual irritation for each spatial frequency condition.

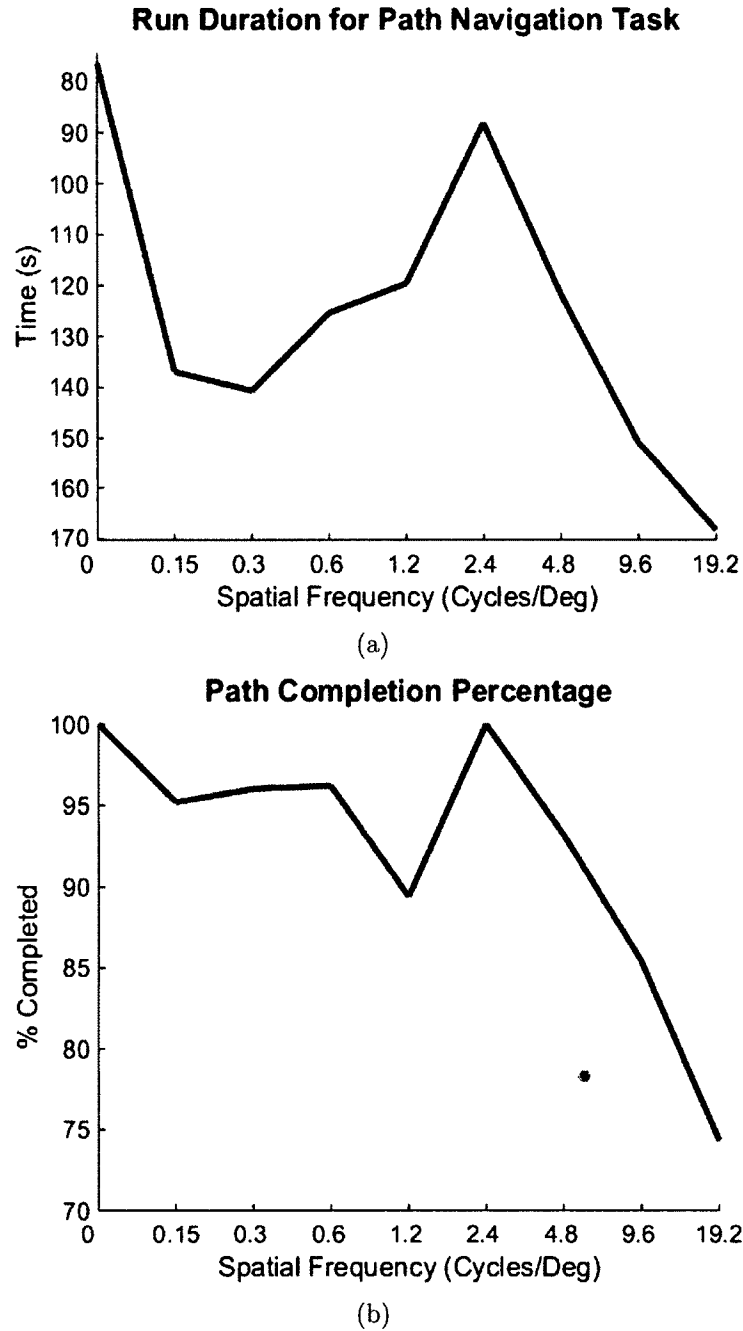


FIG. 29: Part (a) shows the average run-duration from experiment 2 across all subjects for each of the spatial frequency conditions. Part (b) shows the average path-completion percentage for each of the conditions. On average, the subjects were able to complete the path the fastest with the 0 c/deg and 2.4 c/deg conditions which is reflected in (b) as those were the only two conditions where all subjects were able to completely finish the path.

5.4 DISCUSSION

As the effect of spatial frequency on BCI performance has not been explored, most studies arbitrarily select stimuli using either a solid image or a generic checkerboard pattern in the range of 0.15-0.3 c/deg. This study demonstrates that spatial frequency can have a dramatic effect on SSVEP performance that is consistent across subjects. The results in Figure 24 show that the solid 0 c/deg condition is able to achieve an average accuracy of 97.7% given observation lengths greater than 3.5 s. The 2.4 c/deg spatial condition is also able to achieve a reasonable accuracy of 85.1% using a shorter observation length of 2.5 s. Even though the 2.4 c/deg accuracy is not as high as that obtained from the solid condition, the responses generated from the 2.4 c/deg spatial frequency condition require a shorter time window for excitation. This is reflected in Figure 25 where the 2.4 c/deg condition obtains an averaged ITR of 45.3 bits/min which is significantly higher compared to 35.7 bits/min with the solid stimulus condition ($p=0.02$).

The results from both the discrete classification and the continuous navigation experiments show a clear bimodal distribution of SSVEP performance across the spatial frequency conditions. Figures 24, 25, and 26 from the discrete classification experiment all reflect a similar bimodal spatial tuning where performance peaks are exhibited around the 0 c/deg and 2.4 c/deg conditions. For the accuracy plots, the peaks at the 0 c/deg condition are higher than the peaks at the 2.4 c/deg, whereas the opposite is seen from the ITR plots where the 2.4 c/deg peaks exceed the 0 c/deg peaks. The continuous navigation experiment confirms the results from experiment 1 as Figure 29 shows that the performance of the navigation task averaged across all subjects exhibits a similar bimodal distribution across spatial frequency conditions. The 0 c/deg and 2.4 c/deg peaks were the only conditions where all subjects were able to fully complete the path, thus giving a strong indication that these two spatial frequency conditions provide superior response characteristics and can result in optimal SSVEP performance compared to other spatial frequencies. These results concur with the findings in [Tobimatsu et al., 1993, Tomoda et al., 1991] where

similar bimodal spatial tuning curves were found when measuring VEP amplitude during stimulation from a single stimulus. This study shows for the first time that a similar bimodal relationship occurs between SSVEP BCI performance and spatial frequency even when multiple stimuli are flashed simultaneously at different temporal frequencies.

Interestingly, the 0 c/deg condition resulted in a faster completion time on average, compared to the 2.4 c/deg condition despite the fact that the 2.4 c/deg achieves an overall higher ITR than 0 c/deg condition. This may be due to the decrease in accuracy exhibited by the 2.4 c/deg condition for longer observation lengths, as seen in Figure 27. Additionally, all of the spatial frequency conditions, except for the solid condition, show a substantial decrease in accuracy for observation lengths longer than 3 seconds that continues to decrease as the observation length increases. This suggests that a mechanism of spatial adaptation might be occurring in the visual system from the stimulation of these spatial frequency conditions during the SSVEP BCI tasks. It is a known phenomenon that there exists a reduction of neural activity when stimuli are continuously repeated [Grill-Spector et al., 2006]; however, the underlying neural mechanisms of this phenomenon are still unknown. In the case of spatial frequency adaptation, there exists spatially tuned neuronal populations (or spatial channels) that can adapt during stimulation of spatial stimuli in which the strength of the spatial channel response declines throughout adaptation [Blakemore and Sutton, 1969, Klein et al., 1974, Movshon and Lennie, 1979]. The results from this current study show a similar pattern of spatial frequency adaptation over the time-course of stimulation that agrees with previous EEG studies that use a single stimulus [Heinrich and Bach, 2001, Baas et al., 2002]. The results from this current study show that the mechanisms of spatial adaptation similarly occur in the context of SSVEP BCIs where multiple simultaneously flashing stimuli are presented to the visual system. These have important implications for VEP-based BCIs where simultaneously flashing stimuli are common. Thus, when using spatial frequency stimuli, the target detection accuracy over prolonged durations of stimulation can decrease due to spatial adaptation – a fact that is generally overlooked in

VEP-BCI studies.

The results in Figure 28 of the subjective evaluation of visual irritation for each spatial frequency condition show that subjects, on average, perceive less overall irritation for higher spatial frequencies compared to lower spatial frequencies. Specifically, for the two top performing conditions, the average irritation index was 8.1 for the 0 c/deg condition, whereas the irritation index was roughly half that at 4.5 for the 2.4 c/deg condition. This has favorable implications which show that practical VEP-based BCIs can be employed with less visually irritating stimuli to achieve comparable performance with the traditional, more obtrusive solid stimuli.

Although these results demonstrate that spatial frequency exhibits a distinct pattern on the accuracy and performance of SSVEP BCI target detection, additional analysis is still needed to further characterize these effects. A longitudinal study is needed to determine the stability of subject-specific spatial frequency tuning and adaptation. Further, the relationship between spatial frequency and the temporal flashing (or pattern reversal) frequency needs to be studied as the effect of temporal frequency on spatial frequency tuning and adaptation is not well-understood. Overall, these results demonstrate that the clinically studied mechanisms of spatial frequency tuning and adaptation are present in the context of multi-target stimulation, showing that spatial frequency plays a significant role in SSVEP performance. This characterization can potentially be utilized for the development of more practical and robust BCIs.

CHAPTER 6

SPATIAL DECOUPLING OF TARGETS AND FLASHING STIMULI FOR VISUAL BRAIN-COMPUTER INTERFACES

Recently, paradigms using code-modulated visual evoked potentials (c-VEPs) have proven to achieve among the highest information transfer rates for noninvasive brain-computer interfaces (BCIs). One issue with current c-VEP paradigms, and visual-evoked paradigms in general, is that they require direct foveal fixation of the flashing stimuli. These interfaces are often visually unpleasant and can be irritating and fatiguing to the user, thus adversely impacting practical performance. In this study, a novel c-VEP BCI paradigm is presented that attempts to perform spatial decoupling of the targets and flashing stimuli using two distinct concepts: spatial separation and boundary positioning. For the paradigm, the flashing stimuli form a ring that encompasses the intended non-flashing targets, which are spatially separated from the stimuli. The user fixates on the desired target, which is classified using the changes to the EEG induced by the flashing stimuli located in the non-foveal visual field. Additionally, a subset of targets is also positioned at or near the stimulus boundaries, which decouples targets from direct association with a single stimulus. This allows a greater number of target locations for a fixed number of flashing stimuli. Results from 11 subjects showed practical classification accuracies for the non-foveal condition, with comparable performance to the direct-foveal condition for longer observation lengths. Online results from 5 subjects confirmed the offline results with an average accuracy across subjects of 95.6% for a 4-target condition.

The work from this chapter is published in the Journal of Neural Engineering [Waytowich and Krusienski, 2015]

The offline analysis also indicated that targets positioned at or near the boundaries of two stimuli could be classified with the same accuracy as traditional superimposed (non-boundary) targets. The implications of this research are that c-VEPs can be detected and accurately classified to achieve comparable BCI performance without requiring potentially irritating direct foveation of flashing stimuli. Furthermore, this study shows that it is possible to increase the number of targets beyond the number of stimuli without degrading performance. Given the superior information transfer rate of c-VEP paradigms, these results can lead to the development of more practical and ergonomic BCIs

6.1 INTRODUCTION

Brain-Computer Interfaces (BCIs) are systems that directly decode brain activity to communicate user intent [Wolpaw et al., 2002]. One of the most promising approaches for scalp electroencephalogram (EEG)-based BCIs utilizes flashing stimuli to elicit visual-evoked potentials (VEPs) over the occipital cortex. BCIs based on steady-state visual evoked potentials (SSVEPs) have been extensively studied and have proven to be among the most flexible and robust approaches [Middendorf et al., 2000]. The performance and reliability of SSVEP detection have been improved with advanced multichannel analysis techniques such as canonical correlation analysis (CCA) [Bin et al., 2009b]. A variation known as the code-modulated VEP (c-VEP) [Bin et al., 2011] employs stimuli that flash according to binary, pseudo-random sequences known as m-sequences. Because m-sequences have an autocorrelation of nearly zero for non-zero shifts of the sequence, each target can be flashed using distinct time-shifted versions of a single reference m-sequence. This eliminates potential steady-state stimulus frequency biases and allows for straightforward extension to larger numbers of targets compared to standard SSVEP. Thus, c-VEP paradigms have provided among the highest information transfer rates (ITRs) for noninvasive BCIs [Spüler et al., 2012].

Visual irritation and fatigue from prolonged visual stimulation is an often overlooked issue that can significantly affect usability of VEP-BCIs in real-world scenarios [Boksem et al., 2005, Hong et al., 2009]. In the seminal study that yielded impressively high noninvasive BCI information transfer rates (ITRs), Bin et al. used a matrix of 32 targets that simultaneously flashed according to a time-shifted m-sequence [Bin et al., 2011]. The matrix was additionally encompassed by 28 complementary flashing non-target stimuli for a total of 60 simultaneously flashing stimuli. Although this paradigm produced a comparatively high ITR for a noninvasive BCI, it generates a visual cacophony that is not visually pleasing or desirable for long-term use. Traditional solutions to this problem have been to reduce the saliency or obtrusiveness of the visual stimuli such as utilizing high-frequency stimulation ($> 35\text{Hz}$) [Müller et al., 2011, Diez et al., 2013], high duty-cycle stimulation ($<50\%$ duty cycle) [Lee et al., 2011], or low-contrast stimulation (0-10% contrast) [Lalor and Foxe, 2009]. Although these approaches can reduce the reported visual fatigue, they generally compromise performance. For example, with the high-frequency stimulation, Muller et al. [Müller et al., 2011] reported average accuracies near 69% with an average ITR of 46.8 bits/min with frequencies greater than 30 Hz, compared to average accuracies of 91% and an average ITR of 92.8 bits/min using c-VEP [Bin et al., 2009a].

SSVEP BCIs that do not require direct foveation of the flashing stimuli have also been developed. These paradigms are ultimately designed for individuals who are unable to control their gaze, such as with locked-in syndrome [Lesenfants et al., 2014]. Typically, these paradigms require the user to fixate their eye-gaze on a central, inactive position while focusing covert attention on a flashing target located in their parafoveal vision (i.e., $2 \simeq 5$ degrees of visual angle from foveal center [Westheimer, 1982]). While these paradigms achieve some degree of effectiveness, they generally suffer from a dramatic drop in performance compared to direct-gaze approaches, even when implementing a small number of targets [Lesenfants et al., 2014, Allison et al., 2008, Lalor et al., 2007, Kelly et al., 2004].

The present study proposes a novel c-VEP paradigm that incorporates two distinct concepts that spatially decouple the targets from the flashing stimuli. The first concept spatially separates the targets from the stimulus such that fixation of the target does not require direct foveation of the flashing stimuli, nor does it require covert attention. For the second concept, while traditional SSVEP and c-VEP paradigms generally require a unique stimulus per target location, the proposed paradigm allows for target locations associated with the boundaries of the stimuli. This effectively decouples the targets from association to a single stimulus and increases the number of possible targets for a fixed number of distinct stimuli.

To evaluate both of these concepts, the flashing stimuli form a ring that encompasses the spatially-separated non-flashing targets, i.e., the user’s “workspace”. Targets are also uniquely positioned at or near the boundaries of adjacent stimuli. The user attends to a non-flashing target, and the non-foveal flashing stimuli modulate the EEG. Several target configurations are evaluated and compared to the traditional direct-foveal (i.e., superimposed) target approach using the same interface. The results indicate that comparable performance can be attained using the traditional direct-foveal and the proposed non-foveal approaches and that boundary targets can be as effectively discriminated as traditional non-boundary targets. These findings provide important insights for the development of more ergonomic and practical visual flashing paradigms for BCIs.

6.2 METHODOLOGY

6.2.1 EXPERIMENTAL PARADIGM

The proposed paradigm utilizes c-VEP stimuli that form a circular ring encompassing the non-flashing targets as shown in Figure 30. The ring is segmented into four distinct arcs that are each flashed according to time-shifted versions of a single m-sequence. An m-sequence length of 63 was selected for purposes of comparison to the results from Bin et al. [Bin et al., 2011]. While a shorter m-sequence can be used

for this four- stimulus configuration, the length 63 m-sequence was implemented to maintain the same stimulus interval and temporal dynamics as Bin’s landmark study. Because there are only four stimuli in the present paradigm, the m-sequence was circularly shifted by 15 bits (0.25 s) for each adjacent stimulus to minimize undesirable EEG correlations due to smaller temporal shifts. During flashing, the segments of the ring alternate between pure black and white according to the shifted m-sequence. The background is 50% gray tone.

Both offline and online experiments were conducted to evaluate the new paradigm. In the offline experiment, EEG data were collected during foveal fixation on 25 different target locations (see Figure 30a) to test the effects of target position and distance from the stimuli on performance. Fixation crosses were placed in three concentric rings (eight crosses per ring) at varying radii from the center of the ring. Eight of the 25 targets were superimposed directly on the stimuli for direct comparison of traditional direct-foveal stimulation and parafoveal stimulation. Targets were also placed at or near the boundaries of adjacent stimuli to determine if the combination of these stimuli could create discriminable EEG patterns and effectively double the number of possible targets for a given number of stimuli.

Target Location Grouping

The stimulus-ring design allows for unique characterization of c-VEP stimulation by exploiting spatial asymmetries produced by the surrounding ring stimuli and the encompassed target locations. The targets shown in Figure 30a can be grouped by location such that attending to a particular location will elicit either direct-foveal (<1 degree of visual angle from foveal center), near-foveal ($1 \simeq 2$ degrees of visual angle from foveal center), or parafoveal ($2 \simeq 5$ degrees of visual angle from foveal center) visual stimulation. While there is no precise delineation of these foveal categorizations, the prescribed visual angles fall within the generally accepted ranges for foveal vision [Westheimer, 1982].

Additionally, targets can also be grouped as *boundary*, being on or adjacent to the boundary of two c-VEP stimuli; or *non-boundary*, on or adjacent to a single stimulus.

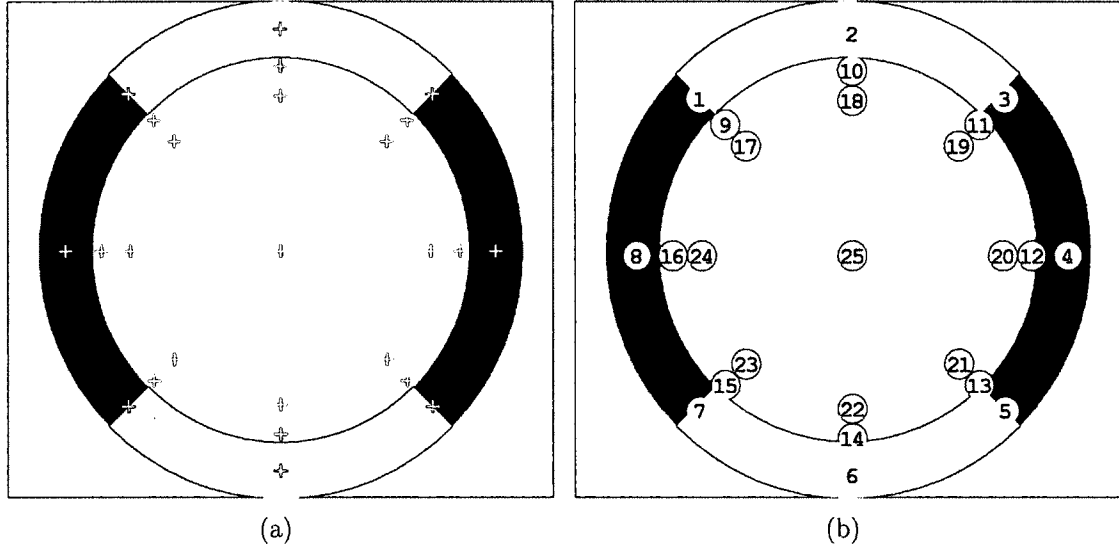


FIG. 30: Workspace and target locations/groupings. (a) Four flashing c-VEP stimuli form a ring that encompass non-flashing targets indicated by the fixation crosses (+). During flashing, the segments of the ring alternate between pure black and white according to the shifted m-sequence. All 25 target locations used for offline evaluation are shown. Target locations are also placed directly over the stimuli to represent traditional direct-gaze stimulation. Only a single target is visible at any time for the offline experiments. (b) Target numbering for groupings. The odd numbers in blue represent the boundary targets and the even numbers in green represent the non-boundary targets. This numbering scheme is used to designate the concentric rings and the various 4- and 8-class classification configurations. (c) Target groupings for classification according to (b).

As can be seen in Figure 30a, the targets that are in the boundary group lie on the diagonals of the ring, and the non-boundary targets are on the horizontals and verticals of the ring. These boundary conditions were included to explore the effects of having two distinct, equally prominent stimuli representing the target, which has implications for increasing the number of possible target locations for a fixed number of flashing stimuli. The center target is equidistant from all ring stimuli and was included for comparison purposes but was not included in the present analysis.

Based on this categorization scheme, several 8-target and 4-target classification groupings were considered; they are listed in Figure 30c. These 8- and 4-class configurations were used in the offline analysis to assess the quality of non-foveal c-VEP stimulation as a control signal for a BCI, as well as to explore the utility of the boundary targets in the 8-class configuration. While a wide variety of other groupings can be considered, particularly for offline analysis, the focus of the present study is to examine the effects of target distance from the stimuli and the impact of targets at or near the stimulus boundaries.

6.2.2 DATA COLLECTION

A single experimental session was collected from twelve able-bodied subjects (five females and seven males, ages 21 to 28) for offline evaluation of the proposed paradigm. The subjects varied in previous BCI experience with seven subjects having no prior experience. This study was approved by Old Dominion University's Institutional Review Board and each subject gave informed consent before participating. Subjects reported no history of epilepsy or seizures, which can be induced in susceptible individuals by flashing stimuli. Data for one subject was excluded because the subject failed to comply with the task; thus, data from eleven subjects were analyzed. Five subjects (three females, two males) participated in a second session for an online evaluation of the proposed c-VEP paradigm in which real-time target selection feedback was provided.

For both the online and offline sessions, EEG was recorded using a 16-channel g.USBamp amplifier and active electrodes (Guger Technologies, Austria) primarily

placed over the occipital and parietal-occipital regions of the brain as shown in Figure 31. Signals were digitized at 600 Hz and stored on a hard disk. All EEG channels were referenced to the left ear-lobe, and FPz was used as the ground. The EEG data recording was synchronized with the c-VEP task using UDP communication protocol with BCI2000 general-purpose BCI software [Schalk, 2004].

Stimulus onsets for each m-sequence were synchronized using a digital trigger signal generated from an Arduino Mega microcontroller board with an Atmel ATmega1280 microcontroller that was connected to the recording computer. All m-sequence stimuli were displayed using DirectX (Microsoft Inc.). In both sessions, the c-VEP ring paradigm was displayed on a 40-inch LCD monitor with a refresh rate of 60 Hz.

Subjects sat in a darkened room in a comfortable chair, approximately 60 cm from the monitor. The stimulus ring subtended 45.2H X 45.2W (radius = 50 cm) from the center. The parafoveal targets (locations 17-24) were centered 4.2 cm (4.0 degrees of visual angle) from the inner edge of the stimulus ring. The near-foveal targets (locations 9-16) were centered 1 cm (1.0 degree of visual angle) from the inner edge of the stimulus. The location of each subject's gaze was recorded and verified using a TOBII X60 eye tracker, which was positioned directly below the monitor. The average radial standard deviation of the eye gaze for each target location and subject was computed to be 0.54 cm, which confirms that the subjects' gaze remained consistently fixated on the prescribed target locations.

Offline Experiment

For the offline experiment, EEG data were collected for all 25 target locations. During the experiment, a single white fixation cross (i.e., target) was displayed at a time. Subjects were instructed to maintain visual fixation and attention on the cross during the stimulation period while refraining from unnecessary movements and frequent eye-blinks. Subjects attended to the target for 30 complete m-sequence cycles (31.5 s) while the segments of the ring simultaneously flashed with the respective lagged version of the m-sequence. After the 30-cycle stimulation interval, there was

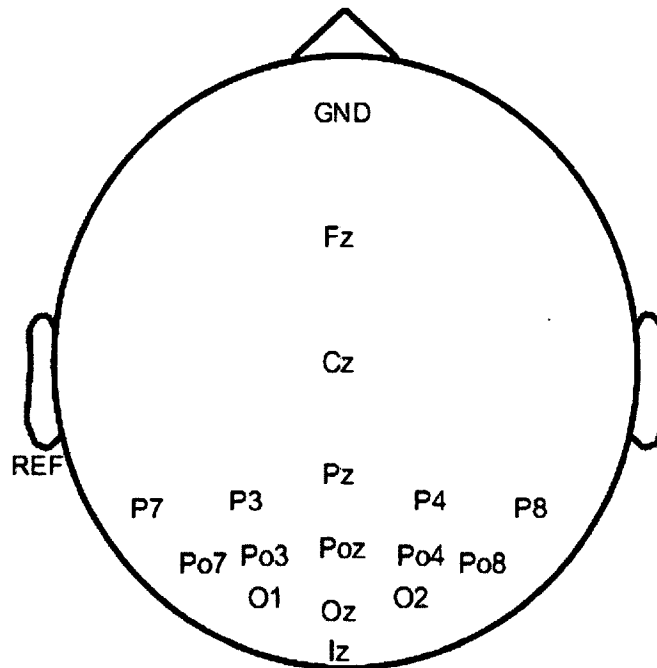


FIG. 31: The EEG electrode montage used for the study. The locations are based on the International 10-20 system.

a 4-second pause while the target appeared in a new location and the process was repeated. Each of the 25 target locations were presented in random order to mitigate any anticipation and order biases. After 8 consecutive 30-cycle stimulation periods, a 1-2 minute rest period was given. All 25 target locations were presented 4 times each totaling 126 seconds of data for each target location. The total session length for the offline experiment was approximately 1 hour.

Online Experiment

For the online experiment, two of the 4-class groups were used to evaluate the performance of the foveal and parafoveal target locations (groups 2 and 6, respectively, from the table in Figure 30c). A training and testing session were conducted during a single larger session for 5 subjects that previously participated in the offline experiment. Only two 4-class conditions were evaluated online to keep the overall session length (training and testing) manageable in comparison to the prior offline

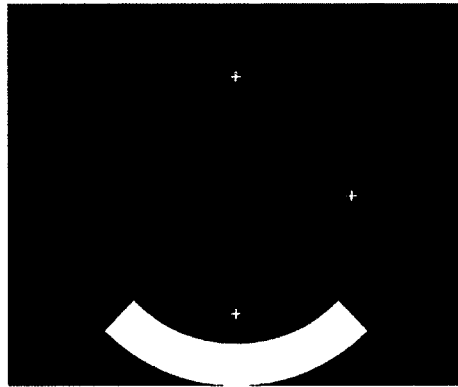
session.

The training session was used to generate the c-VEP template waveforms for target identification. The training session was similar to the offline experiment except that only 8 total target locations were trained (the union of groups 2 and 6 as shown in the table in Figure 30c). During training, only one target at a time was shown for 30 seconds with a 4-second blank interval. Presentation of each target position was again randomized. After completion of four repetitions of each of the 8 target locations, a custom Matlab script was used to generate the c-VEP templates as described in Section 6.2.3. These templates were then utilized for classification during the online testing session. The online training session lasted approximately 25 min including rest periods.

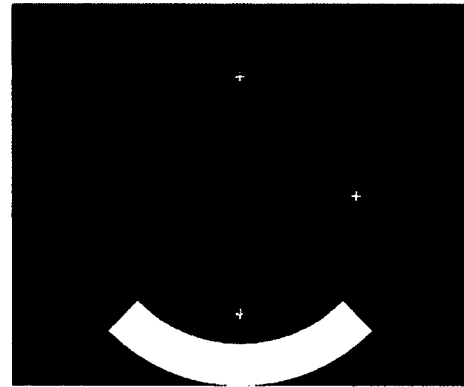
Each of the 4-class conditions (i.e., foveal and parafoveal) was tested separately. During a trial, all four target locations from the particular condition were simultaneously displayed to the subject. A trial commenced with a 2 s cue period that indicated the intended target by highlighting it in blue as shown in Figure 32b. Next, EEG data were collected during a 6-second stimulation period. This was followed by a 2-second feedback period where target classification was performed and the predicted target was presented to the subject by highlighting the target in green as shown in Figure 32c. The ring stimuli started flashing 1 second into the cue period and remained flashing throughout the stimulation period. This was done to mitigate any transient ERP responses from the stimulus onset. The total trial (Cue-Stimulation-Feedback) lasted 10 seconds. Figure 32a shows the timing protocol of a single online trial. After the feedback period, another trial commenced with a new target location. Sixteen trials constituted one run and two runs were performed for each 4-class condition. The online testing session lasted approximately 10 minutes, resulting in an overall online session length of approximately 45 minutes including a 10-minute interval for classifier calibration between the training and testing session.



(a) Timing Protocol



(b) Cue



(c) Feedback

FIG. 32: (a) Timing protocol for an online trial. A two second cue segment highlights the target to attend to in blue (b). One second into the cue period, the ring stimuli started to flash. Data is collected for 6 seconds during the stimulation followed by a two second feedback period where the selected target is highlighted in green (c).

Subjective Evaluation

Following the online study, each subject was asked to subjectively evaluate the direct-foveal and the parafoveal conditions in terms of degree of visual irritation. For each condition, the subjects provided a numeric response to the following statement: “On a scale from 1 to 10, please rate how visually irritating it is to continuously stare at the target, with 1 representing not at all irritating and 10 representing extremely irritating.”

6.2.3 DATA ANALYSIS

The analysis for this paradigm was based on Bin et al., [Bin et al., 2011], in which CCA was adopted for multichannel c-VEP classification. Modifications to the method described in [Bin et al., 2011] were made such that the asymmetries of the

ring paradigm could be exploited. Note that for the standard c-VEP BCI paradigm, which requires direct foveal fixation of the targets, the principle of equivalent neighbors [Bin et al., 2011] is employed; therefore, only one target template needs to be constructed. In contrast, the various target locations in the present paradigm do not have equivalently positioned neighboring stimuli, so optimal spatial weights were computed using CCA for each target location.

Canonical Correlation Analysis

To reliably detect EEG responses to the flashing stimuli, a multivariate processing technique known as Canonical Correlation Analysis (CCA) can be utilized to find linear correlations between EEG data and a stimulating signal. CCA has recently been adopted for multidimensional EEG analysis and has been shown to be extremely effective for SSVEP signal processing [Bin et al., 2009b, Lin et al., 2007] and has also been extended for c-VEP classification [Bin et al., 2011].

CCA is a multi-dimensional correlation analysis technique that finds underlying correlations between two sets of data. It creates linear combinations of two multi-dimensional data sets such that the mutual projection between the two data sets is maximized. Given two multi-dimensional data sets X , and Y , and their respective linear combinations $x = X^T W_x$ and $y = Y^T W_y$, CCA determines the weight vectors W_x and W_y that produce the maximum correlation between x and y . The projected vectors x and y are known as canonical variants and their correlation is known as the canonical correlation. The weight vectors W_x and W_y that produce the highest canonical correlation are found by solving the optimization problem:

$$\max_{W_x, W_y} \rho(x, y) = \frac{E[x^T y]}{\sqrt{E[x^T x]E[y^T y]}} = \frac{E[W_x^T X Y^T W_y]}{\sqrt{E[W_x^T X X^T W_x]E[W_y^T Y Y^T W_y]}} \quad (8)$$

In practice this can be solved using the singular-value decomposition method to diagonalize the covariance matrices as the maximum canonical correlation corresponds to the square-root of the largest eigenvalue.

Offline Experiment

Data from the offline experiment were zero-phase band-passed filtered from 0.5 – 30 Hz using a Chebychev type II IIR filter, as 30 Hz is the largest frequency produced by a monitor with a 60Hz refresh rate. All EEG channels were then re-referenced to channel Fz to eliminate potential hemispherical biases. Each 30-cycle stimulation trial for each target location was extracted and concatenated to create 126 s (4 trials x 31.5 s) EEG segments for each target.

Data from each of the target groups listed in Table from Figure 30c were aggregated, and target classification was performed to test the offline performance for each condition. For each condition, the 126 s data segments were separated into training and testing groups where 80% (96 cycles) was used for training and 20% (24 cycles) was used for testing. This ratio was selected because it gave sufficient training data to build the c-VEP templates for each target position. The c-VEP target templates, $M_k(t)$, were constructed using the training data by first averaging the multichannel EEG data, $X_k(t)$, across each m-sequence cycle to produce an averaged multichannel response, R_k , for each of the k target locations [Bin et al., 2011]. The resulting 1-second averaged responses were concatenated 100 times to produce a multichannel set S_k with the same dimensions as $X_k(t)$: $S_k = [R_k R_k R_k \dots R_k]$.

CCA was then applied to find the best linear transformations of S_k and $X_k(t)$ that maximize the mutual projection, i.e., W_{S_k} and W_{X_k} such that $\rho(W_{X_k}^T X, W_{S_k}^T S)$ is maximized. The resulting W_{X_k} are spatial weights that are used to combine the multichannel templates to form the final template response for each target position. The testing data were then utilized to evaluate the target predictions for different observation lengths.

The test data for each target location were separated into trials (simulated observations) with integer cycle lengths from 1 cycle (1.05 s) to 6 cycles (6.3 s). The EEG for each trial was processed using the spatial weights W_{X_k} and classified for target prediction [Bin et al., 2011]. For a given observation of test data, the spatially filtered EEG was linearly correlated with each of the target templates from a given

condition, and the template with the maximum correlation was classified as the predicted target. The average of a 6-fold cross-validation scheme was used to determine the unbiased classification accuracy.

In order to assess the relative contribution of each channel to classification performance, a leave-one-out scheme was employed in which 14 of the 15 occipital channels were used in the classification [Spüler et al., 2012]. The left-out channel was iterated through all channels. Left-out channels that resulted in a major drop in classification accuracy contributed more to the c-VEP response than left-out channels that resulted in little to no drop in accuracy. Because it was observed that excluding the worst performing channel generally boosted classification performance, the best 14 channels were selected for analysis. While CCA should theoretically assign an irrelevant channel a weight near zero, it is generally not identically zero, resulting in a noise component being added to the output of the spatial filter. Thus, an additional channel selection procedure may further boost CCA performance, particularly for larger channel sets. This simple channel exclusion procedure can be further optimized but is not expected to significantly affect the overall results of the present analysis.

Online Experiment

The online experiment consisted of a training and testing session as part of a larger session. After the training data were collected, the c-VEP target templates for the target locations were constructed using the same procedure described in the offline experiment shown in Section 6.2.3. The CCA spatial weights for each template were also constructed. During the online test, a 2-second cue instructed the subject to attend to a particular target location, after which 6 seconds of data were collected during the stimulation period. The 6-second observations were classified as described in Section 6.2.3 by filtering with W_{X_k} , correlating with each target template and selecting the target with maximum correlation. As with the offline analysis, the simulated performance was evaluated for cycle lengths 1-5, where a cycle length of 6 represents the actual online performance. However, unlike the 4-class offline analysis,

TABLE 2: Offline Accuracies

Distance from Ring	Group #	Avg. Accuracy
Direct-Foveal (locations 1-8)	1) 8-Class (all)	99.2%(±1.4)
	2) 4-Class (even)	100%(±0.0)
Near-Foveal (locations 9-16)	3) 8-Class (all)	96.6%(±6.0)
	4) 4-Class (even)	99.4%(±1.9)
Parafoveal (locations 17-24)	5) 8-Class (all)	89.7%(±10.1)
	6) 4-Class (even)	95.5%(±8.3)

no cross-validation was performed to provide a more realistic estimate of actual online performance.

6.3 RESULTS

6.3.1 OFFLINE EXPERIMENT

The average accuracies for the offline experiment for each condition are shown in Table 2. The accuracies are based on a 6-cycle observation length (6.3 s). The 8-class accuracies ranged from 89.7-99.2% and all of the 4-class conditions ranged from 95.5-100%. The average accuracies decreased with the distance from the target for all conditions. The 8-class parafoveal condition provided an average accuracy of 89.7% compared to 99.2% for the direct-foveal condition, which was statistically significant using a paired t-test ($p < 0.05$). The 4-class parafoveal condition provided an average accuracy of 95.5% compared to 100% for the direct-foveal condition, which was not statistically significant.

The two leftmost panels of Figure 33 show the average offline performance as a function of the number of stimulus cycles used for classification for the 8- and 4-class conditions, respectively. In general, the performance monotonically increases with the number of stimulus cycles, but this creates a trade-off in terms of information transfer rate. For the 8-class condition, there was a statistically significant difference in accuracies between the foveal and parafoveal targets across all observation lengths

($p < 0.05$ using a paired t-test). There was also a statistically significant difference between the near-foveal and parafoveal targets across all but the largest observation length. For the 4-class condition, there was a statistically significant difference in accuracy between the foveal and parafoveal targets only for the three shortest observation lengths.

In order to compare the relative classification performance of the targets at or near the boundaries of the stimuli, Figure 34 shows confusion matrices for each of the 8-class conditions at the 6.3 s observation length. It is observed that there is no apparent bias in performance for the boundary target locations (odd numbers). Figure 35 shows the CCA spatial weight topographies and template waveforms for the foveal and parafoveal conditions, respectively, from a representative subject (S1).

6.3.2 ONLINE EXPERIMENT

The accuracies of the online experiment for the direct-foveal and parafoveal conditions are shown in Table 3 for each subject. Both conditions provided average online accuracies of above 95%. The rightmost panel of Figure 33 shows the simulated average performance as a function of the number of stimulus cycles used for the online data. Using a paired t-test, there was a statistically significant difference in accuracies between the conditions for the two shortest observation lengths ($p < 0.05$). Table 3 also includes the responses to the subjective evaluation of the perceived visual irritation on a scale from 1(least)-10(most), termed the irritation index.

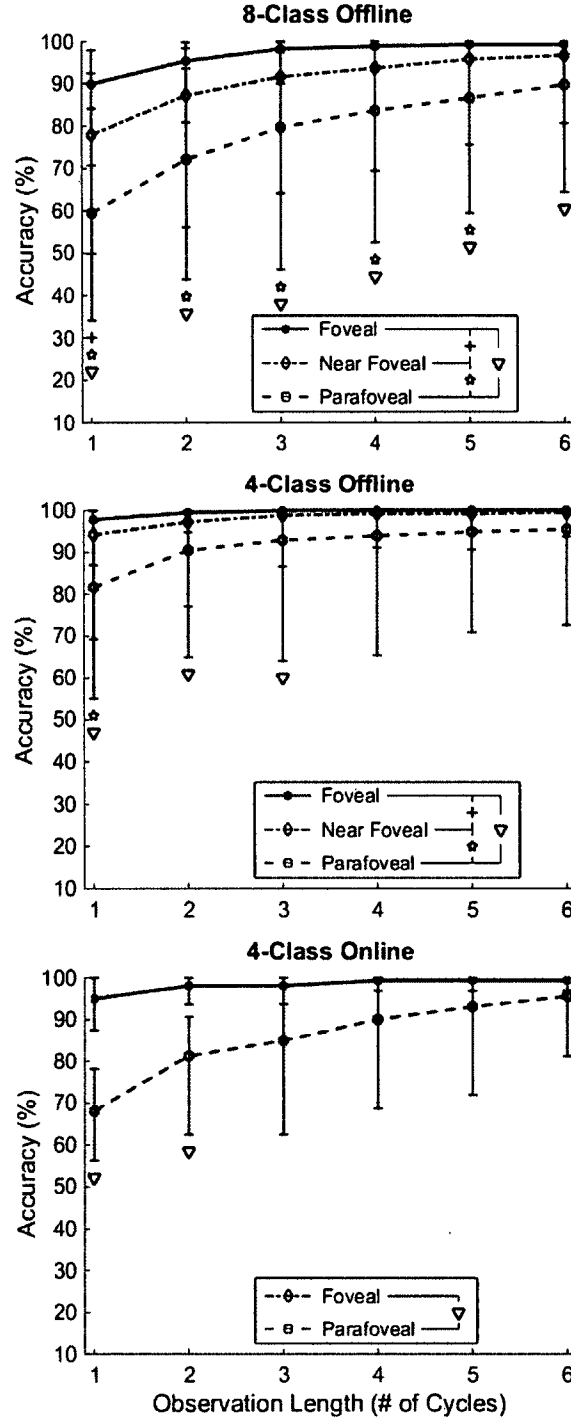


FIG. 33: Simulated average classification accuracies for the offline and online experiments as a function of observation length in # of complete m-sequence cycles. The limits of the error bars indicate the minimum and maximum subject performance. A single m-sequence cycle length is 1.05 s, thus the observation lengths range from 1.05 s to 6.3 s. The markers in the legend indicate statistically significant differences ($p < 0.05$) between each condition at each observation length.

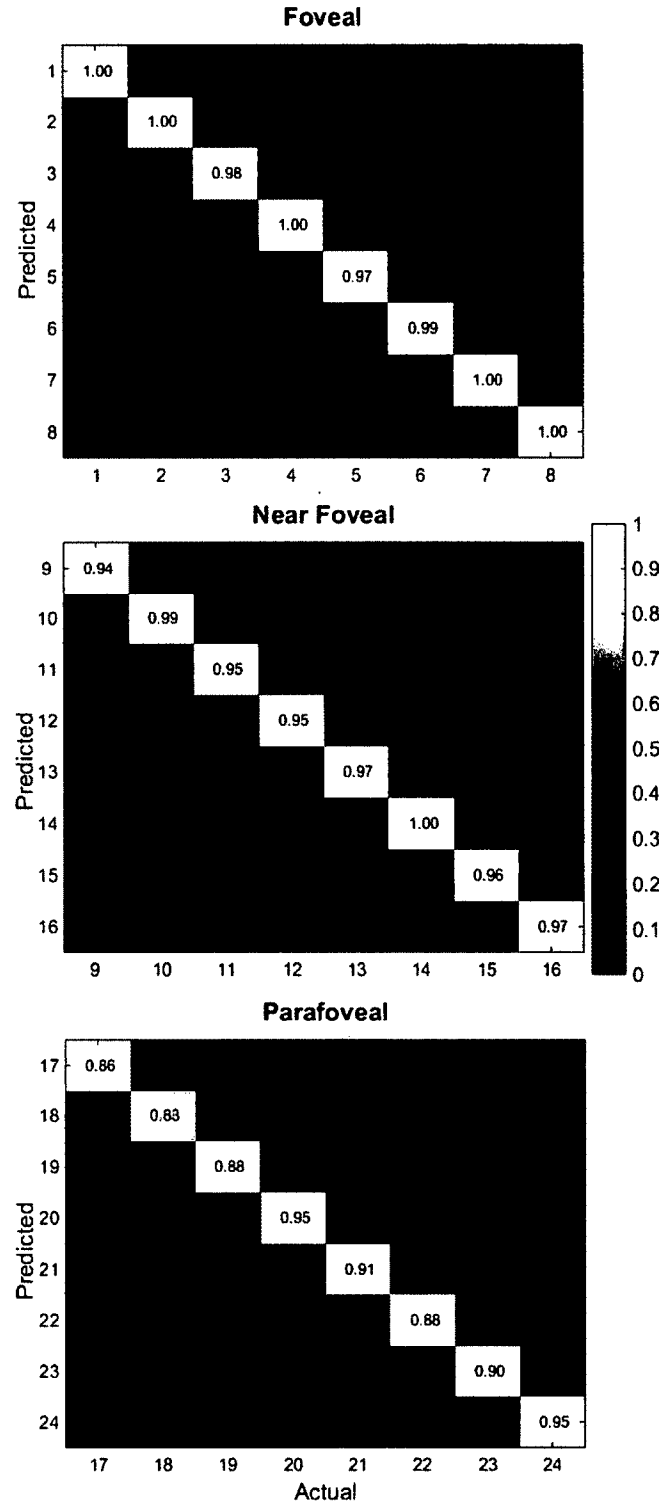


FIG. 34: Confusion matrices for the three offline 8-class conditions (direct-foveal, near-foveal, parafoveal) for the 6.3 s observation length. The color scale indicates the proportion of classifications, with the diagonals labeled with the proportion of correct classifications. It is observed that there is no apparent bias in performance for the boundary target locations (odd numbers).

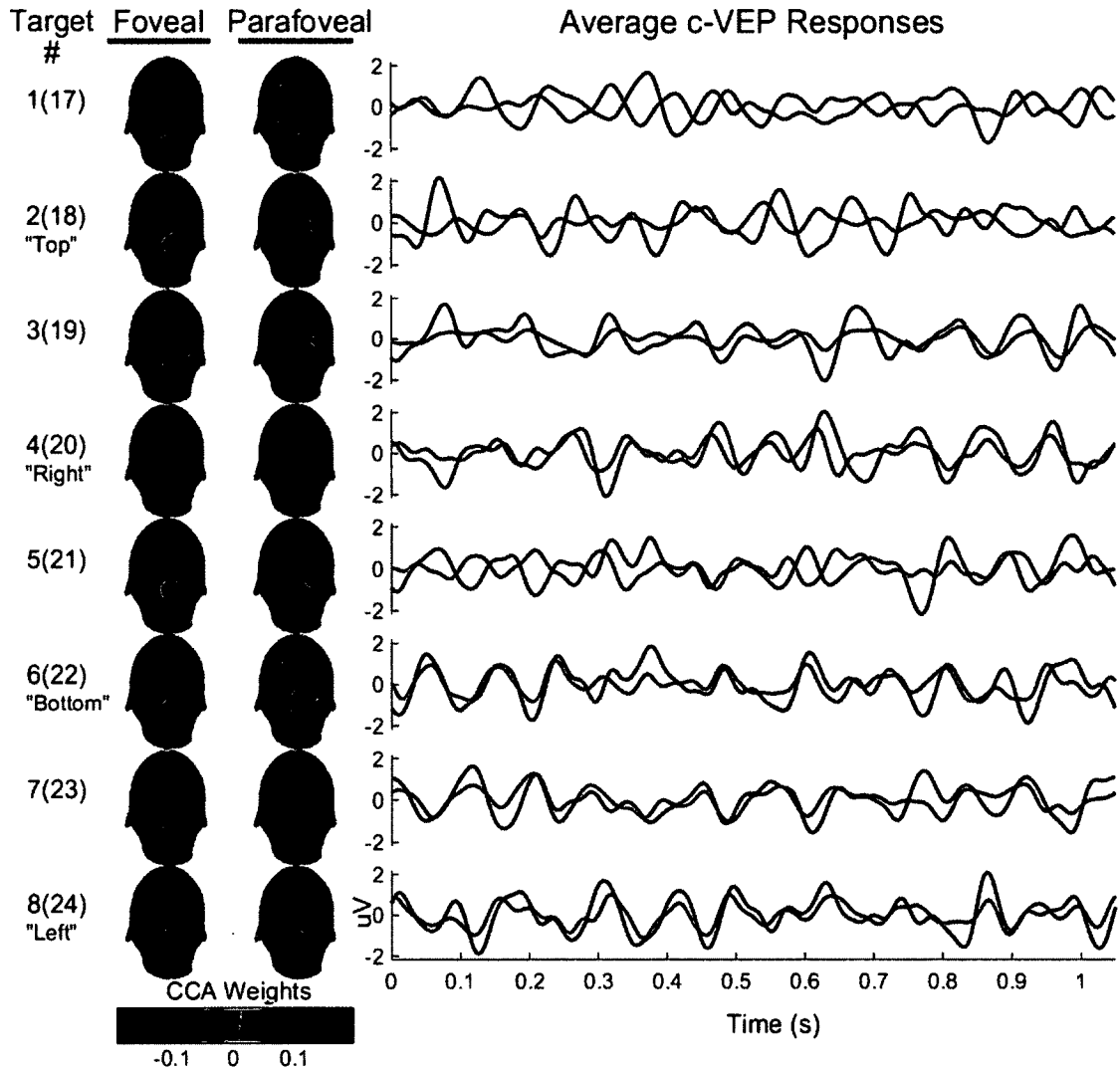


FIG. 35: The CCA spatial weight topographies and template waveforms for the foveal and parafoveal conditions, respectively, from a representative subject (S1). The leftmost column indicates the spatially paired foveal (parafoveal) target numbers according to Figure 30(b). The second and third columns show the CCA weight topographies for the foveal and parafoveal targets, respectively. The rightmost column shows the CCA template waveforms for the foveal (blue) and parafoveal (red) targets.

TABLE 3: Online Accuracies ($t = 6.3$ seconds) and Visual Irritation Index

	Foveal 4-Class	Irritation Index	Parafoveal 4-Class	Irritation Index
S1	100%	7	100%	5
S2	100%	8	100%	6
S9	96.9%	7	81.2%	3
S10	100%	8	96.9%	3
S11	100%	8	100%	5
Avg	99.4%	7.6	95.6%	4.4

6.4 DISCUSSION

While existing VEP BCI paradigms almost exclusively prescribe visual targets that overlay or embody a single flashing visual stimulus, this study demonstrates the potential for spatially decoupling targets from individual flashing stimuli. The offline results for the 4-class condition in Figure 33 indicate that there is no significant change in performance as the targets are positioned outside of direct foveal vision when an observation length greater than 4.2 seconds is used. The average performance across all conditions is above 80% after 3 (3.15 s) and 1 (1.05 s) stimulus cycles for the 8-class and 4-class scenarios, respectively. This indicates that the ring paradigm has the potential to achieve practical and competitive performance without requiring direct foveation of the targets.

Traditional VEP-BCIs generally associate a single target with a single, unique stimulus, which tends to create more visual discord for increasing numbers of targets. The proposed 8-class paradigm also introduces the novel concept of placing targets at or near the boundary of two adjacent stimuli. Figure 34 shows that there are no significant biases between the boundary and non-boundary classifications for a given condition. It can also be observed that misclassifications generally occur at adjacent targets along the diagonal, which is expected based on the design of the workspace.

The overall 8-class offline results demonstrate that it is possible to accurately detect and decode changes in the EEG due to multiple stimuli associated with a single target, although these results need to be verified using online experiments. While

EEG changes due to multiple non-foveal stimuli have been utilized in the past, particularly with the principle of equivalent neighbors from the c-VEP speller introduced by Bin et al. [Bin et al., 2011], the present study utilizes stimuli in a unique way such that there are more available targets than stimuli. This may help to mitigate the limits on the number of available traditional stimuli/targets imposed by the length of the m-sequence, monitor refresh rate, etc. Additionally, minimizing the number of required flashing stimuli may also have implications in terms of visual irritation and fatigue, although visual fatigue was not directly assessed in this study. Further investigations can be conducted to explore the effects of stimulus size, proximity, orientation, multiple boundaries, etc. on performance.

The CCA template waveforms presented in Figure 35 indicate that there is not a clear visual relationship between the foveal and parafoveal response templates. While the foveal and parafoveal templates for some corresponding target locations appear highly correlated (e.g., the bottom targets), others do not appear to have a distinct temporal relationship (e.g., the top targets). This is in contrast to Bin et al. (2011), where the responses for each target were consistent due to the principle of equivalent neighbors (i.e., each target had identical boundary stimulus configurations and timing) [Bin et al., 2011]. Related to this point, it is not obvious how the adjacent stimuli contribute to the boundary target responses. Again, each boundary stimulus has a different spatial orientation and further analysis is needed to quantify the relative contributions. Consistent with the differences in the CCA response templates, the CCA spatial weight topographies are similar between the foveal and parafoveal conditions for certain target locations (e.g., bottom) and dissimilar for other locations (e.g., top). The spatial weights with the largest magnitudes are generally focused over the central-occipital area for the foveal condition and more diffuse around the central-occipital area for the parafoveal condition, which is indicative of the contribution of peripheral vision. Similarities between adjacent patterns may provide some indication of the relative contributions of the adjacent stimuli to the boundary targets. These patterns were generally similar for the other subjects, but due to subtle differences between subjects, the patterns are most distinct when visualizing a single

subject's data compared to a grand average across subjects.

The 4-class online results show more of a deviation in performance between the conditions for shorter observation lengths compared to the equivalent offline condition. This can be partially attributed to the comparatively lower performance of Subject 9 for the parafoveal condition and that fewer subjects are represented in the average compared to the offline results. However, there is also a discrepancy in the relative performance ranges between the online and offline results, particularly for the parafoveal condition. One likely explanation is that the stimulus duration for the offline data was longer and the cross-validation procedure included segments of training data that did not begin from the stimulus onset and were from the middle of the trials. Therefore, it is likely that the simulated observations from the middle of the offline trials are fully entrained to the stimuli and do not include any transient effects of the stimulus onset. Thus, this offline training data is more representative of the entrained EEG of the later cycles and misleadingly indicates better performance compared to the online condition where the EEG of the early cycles may not be fully entrained. Nevertheless, the online parafoveal condition still attains an average accuracy above 80% after 2 (2.1 s) stimulus cycles. This may provide a favorable trade-off between performance and visual irritation since the online subjects universally rated the parafoveal condition as less irritating as indicated in Table 3.

In order to fully validate the paradigm, undirected free-choice online experiments should be conducted to account for practical use issues such as target scanning and reaction to task-related feedback. Future work will more thoroughly explore the effects of distance between the targets and stimuli, increasing the number of stimuli/boundaries along the ring, the use of shorter m-sequences, and larger N-class target configurations that further exploit the combined concepts of stimulus-target distance and boundaries. It is envisioned that these stimulus-target decoupling concepts introduced in the proposed paradigm will lead to the development of more practical and ergonomic BCIs by reducing visual irritation and potentially fatigue, as well as by increasing the number of available targets for a fixed number of stimuli.

CHAPTER 7

LARGE-SCALE TARGET DISCRIMINATION USING SPATIALLY DECOUPLED STIMULI

7.1 INTRODUCTION

The previous chapter introduced the concept of spatial decoupling for separating targets from flashing stimuli in a c-VEP BCI utilizing a novel ring paradigm: a segmented ring consisting of four time-delayed flashing m-sequence stimuli encompassing 25 non-flashing targets. The 25 non-flashing targets were grouped into several 8-class and 4-class conditions to test the spatial separation and boundary positioning decoupling techniques. The results show that targets could be discriminated when they were spatially separated from their flashing stimuli using parafoveal stimulation and that targets could also be discriminated when placed at or near the boundary of two adjacent stimuli.

These results demonstrate the concept of spatial decoupling in the context of 4-class and 8-class BCIs; however, the upper limit of spatial decoupling was not tested. This chapter extends upon the results of the previous chapter by performing a large-scale 25-class BCI in which all targets from the ring paradigm are discriminated simultaneously using only four flashing stimuli. Additionally, this chapter extends the c-VEP characterization from the previous chapter by analyzing the activations from all 25-target positions. The results show that it is feasible to obtain 25-class target discrimination from the ring paradigm with average accuracies above 80% from a 3.15 s observation window and accuracies above 90% from a 5.25 s observation window. Additionally, characterization analysis shows spatial c-VEP activations that are elicited contralaterally over the occipital regions from asymmetrical target/stimuli relationships from the ring stimulus.

7.2 METHODOLOGY

7.2.1 DATA COLLECTION AND EXPERIMENTAL PARADIGM

The data collection and experimental paradigm are described in the previous chapter. After a screening of the EEG data for discriminable c-VEP responses using the individual classification performance results from the previous chapter, one subject was excluded due to production of near-chance level classification accuracies for most of the 4-class and 8-class conditions. Thus, 10 (four females and six males, ages 21 to 28) of the original 11 subjects were included in the subsequent analysis.

7.2.2 PRE-PROCESSING

All data were band-passed filtered from 0.1-30 Hz using a zero-phase equiripple FIR filter. Data from each trial were extracted from all 25 target positions for analysis. All inter-trial data were discarded resulting in 126 s of data for each target.

7.2.3 25-TARGET CLASSIFICATION

Classification was performed with canonical correlation analysis using a similar method as described in section 6.2.3. The CCA algorithm was adapted for 25-target classification. Similarly to section 6.2.3, 25 cVEP templates $M_k(t)$ were constructed using training data by performing CCA between the two multichannel variables $X_k(t)$ and S_k where $X_k(t)$ is the raw multichannel EEG data and S_k is the concatenated average of $X_k(t)$ such that the S_k and $X_k(t)$ have the same dimensions. CCA is applied to find the best linear transformations of S_k and $X_k(t)$ such that the mutual projection, $\rho(W_{X_k}^T X, W_{S_k}^T S)$ is maximized. The weight vector that produces this maximization is used to filter the average template to produce a canonical template waveform for each of 25-targets. Testing data are then split into observations of length t and used for offline classification by linearly correlating the observations with each of the cVEP template waveforms and assigning the target class label C to

the template that produced the maximum p-value:

$$C = \arg \max_i \rho_i, i = 1, 2, \dots K$$

Data were split into training and testing according to a leave-one-out cross-validation scheme to give a thorough estimate of testing accuracy. The training data were utilized to construct the CCA spatial weights and the corresponding cVEP templates, and the testing data were used for classification.

The 25-Class ITR for all subjects vs. the observation length, shown in Figure 36(b), was computed using equation 9.

$$ITR = \left(\log_2 N + P \log_2 P + (1 - P) \log_2 \left(\frac{1 - P}{N - 1} \right) \right) * \frac{60}{T} \quad (9)$$

In order to simulate a practical ITR, an inter-epoch duration of 0.3 seconds was utilized based on the recent SSVEP BCI study from [Chen et al., 2014] which constitutes the time required to shift eye-gaze from one target to the next.

The confusion matrices were computed and averaged across all folds of the cross-validation. The results were plotted in the 25-target ring paradigm configuration where each target position contains a subplot showing the classifier predictions for the respective target.

7.2.4 C-VEP CHARACTERIZATION

A characterization of the c-VEP responses was performed by quantifying the contributing sources of the c-VEP responses from the four eliciting stimuli and also by extracting topographical head-plot activations. Since the majority of targets in the ring paradigm are spatially decoupled from the flashing stimuli, it is not fully known how each stimulus contributes to the c-VEP response for a given target. To quantify these relative source contributions, the c-VEP responses for each of the 25-targets were canonically correlated with the four template responses from the target positions that directly overlay each of the four flashing stimuli (i.e. the four

responses that came from the target positions 2, 4, 6 and 8 as shown in Figure 30(b)). These responses were from direct visual fixation of the flashing stimuli and thus are strongly representative of activity generated by those stimuli. The remaining targets are then canonically correlated with each these four targets responses, which constitutes the relative source contribution for each target. Targets that have high canonical correlation with a particular source stimulus are representative as having a large source contribution from that stimulus. The source contributions are computed from all target positions for each of the four sources and are plotted as mini-rings positioned at each of the 25 target locations (Figure 38). Each mini-ring is composed of four segments (representing the four flashing stimuli) whose shaded color represents the strength of the canonical correlation from that target response to the particular stimulus. This gives a visual representation relative source contributions for each of the target positions.

To characterize the topographical activations over the occipital and parietal regions of the scalp, the raw c-VEP responses $X_k(t)$ from each channel were correlated with the averaged evoked responses S_k from the corresponding channel. This gives a representation of the strength of the c-VEP responses contained within each channel. The single-channel correlations for each of the target responses are shown in Figure 39, where each topographic head-model corresponds to a target location and the head-models are plotted in the same 25-target configuration as the ring paradigm for intuitive visualization.

7.3 RESULTS

The average classification accuracies across all subjects are shown in Figure 36(a). The accuracies are plotted as a function of the observation length (i.e. number of m-sequence cycles), ranging from 1-6 cycles which corresponds to a time-window length ranging from 1.05 s to 6.3 s. The average accuracy is shown as the solid black line, and the minimum and maximum subject accuracies are shown with the solid blue lines. An average classification accuracy of over 90% is achieved with observation lengths ≥ 5 cycles. The accuracy monotonically decreases with decreasing

observation lengths as expected. Single trial target detection accuracies of 62% were achieved on average with the best subject reaching a 77% single trial accuracy which corresponds to a 1.05 s data window. The confusion plot in Figure 37 does not show any apparent classification biases in the 25-target detection. Figure 36(b) shows the average ITR across all subjects as a function of the stimulus cycle. As expected, the ITR for all subjects monotonically decreases as the observation length increases as the information rate is inversely proportional to the observation length. The average ITR obtained for a single cycle observation length is 88 bits/min, with the best performing subject achieving an ITR of 120 bits/min.

The c-VEP source correlation plot in Figure 38 shows a distinct pattern in the relative contribution of each source for the 25 targets. The pattern corresponds with the intuitive notion that targets have higher source contributions with adjacent stimuli than non-adjacent stimuli. The targets that lie on the vertical and horizontal axes of the ring, which have only one adjacent stimuli, show strong correlations with that stimuli. The targets that are at or near the boundary of stimuli (i.e. targets that are on the diagonals of the ring paradigm) show strong source correlations with the two adjacent stimuli that form the respective boundary. Additionally, there is a monotonic reduction in correlation strength as the target-stimulus distance increases.

The c-VEP activations plotted in Figure 39 show that the responses from direct foveal stimulation (outer ring) exhibit a focused activation over the primary visual cortex, while parafoveal responses are exhibited from the parietal-occipital regions of the visual cortex. Additionally, the activations from targets 24 (left-parafoveal) and 20 (right-parafoveal), according to Figure 30(b), show contralateral activations over the occipital regions from the left and right segments of the ring stimulus, respectively. The left visual field stimulation from target 24 produces activations in the right hemisphere of the occipital lobe, while right visual field stimulation from target 20 produces activations in the left hemisphere of the occipital lobe. This is consistent with the nature of information flow in the visual system pathway in which the optic chiasm contralaterally maps input from the right visual field to the left hemisphere and input from the left visual field to the right hemisphere [Rentschler et al., 1975].

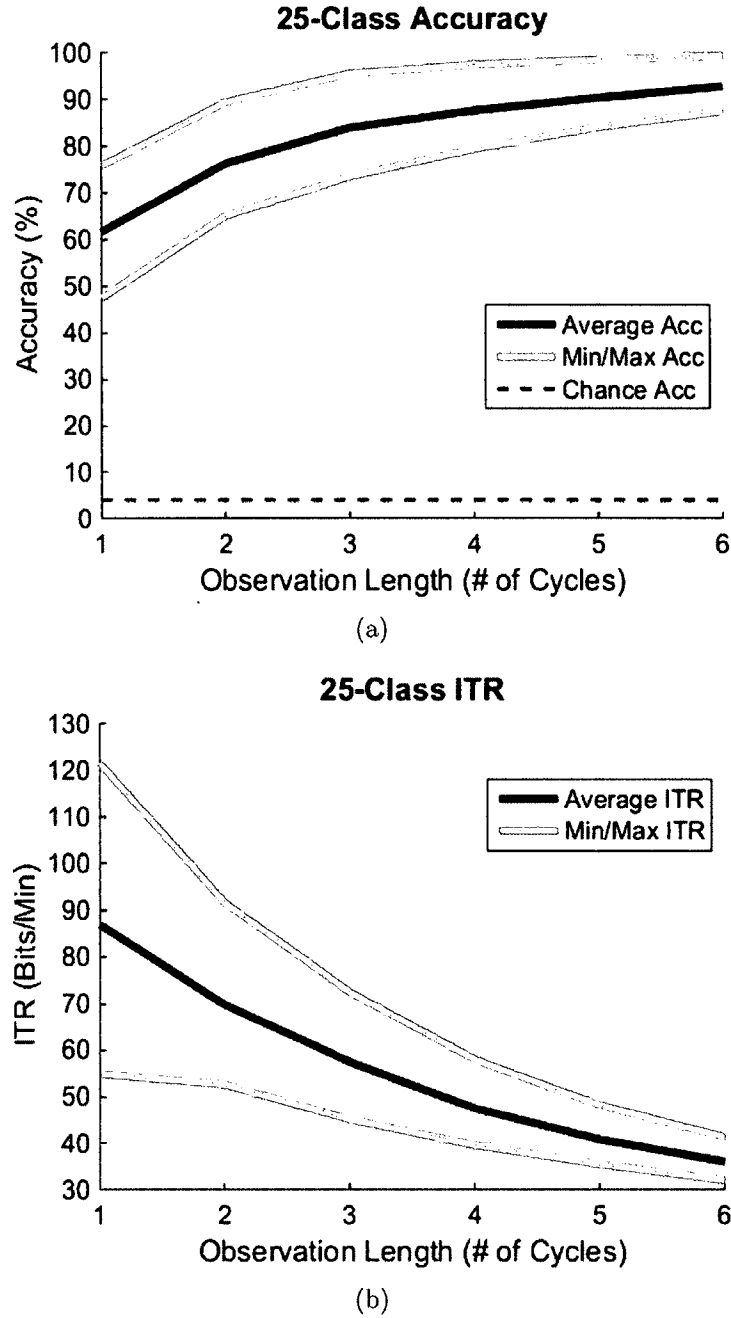


FIG. 36: (a) shows the average 25-class classification accuracies plotted as a function of observation length expressed in number of m-sequence stimulus cycles. (b) shows the 25-class information transfer rates also as a function of observation length. For both panels, the solid black lines show the average across all subjects while the blue lines show the minimum and maximum performing subjects. The shaded blue region therefore contains the distribution of the remaining subjects. In (a), the chance accuracy (4%) is shown as the gray dashed line.

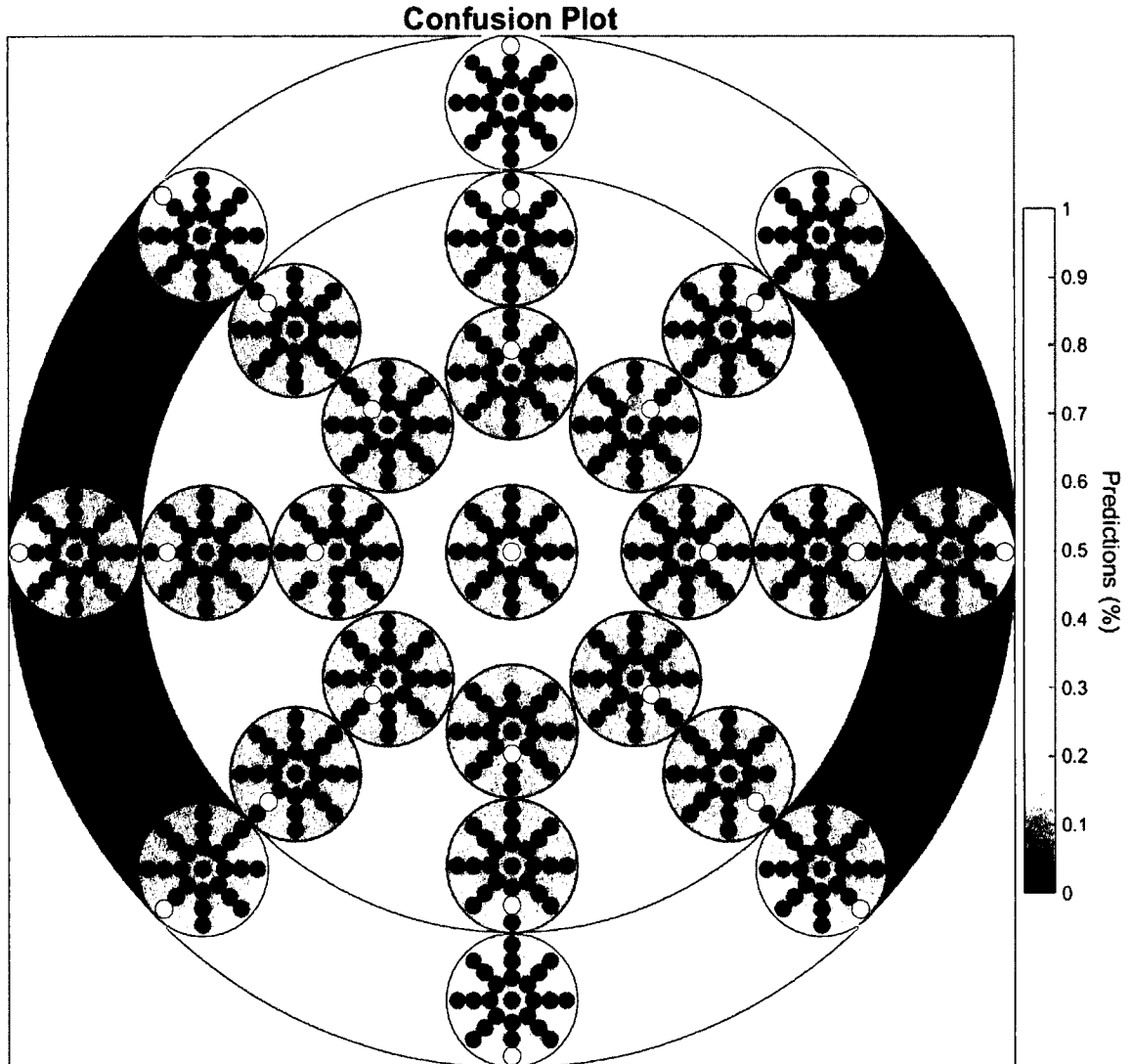


FIG. 37: Confusion matrix averaged across all subjects. The confusion matrix is plotted to match the same spatial configuration as the ring paradigm. Each of the mini-plots are positioned at each of the 25 target positions and represent the classification predictions for each target. The areas of bright yellow represent the correct classifications as the majority of predicted classes were the true target class. It can be seen that there is no apparent bias in the target classification.

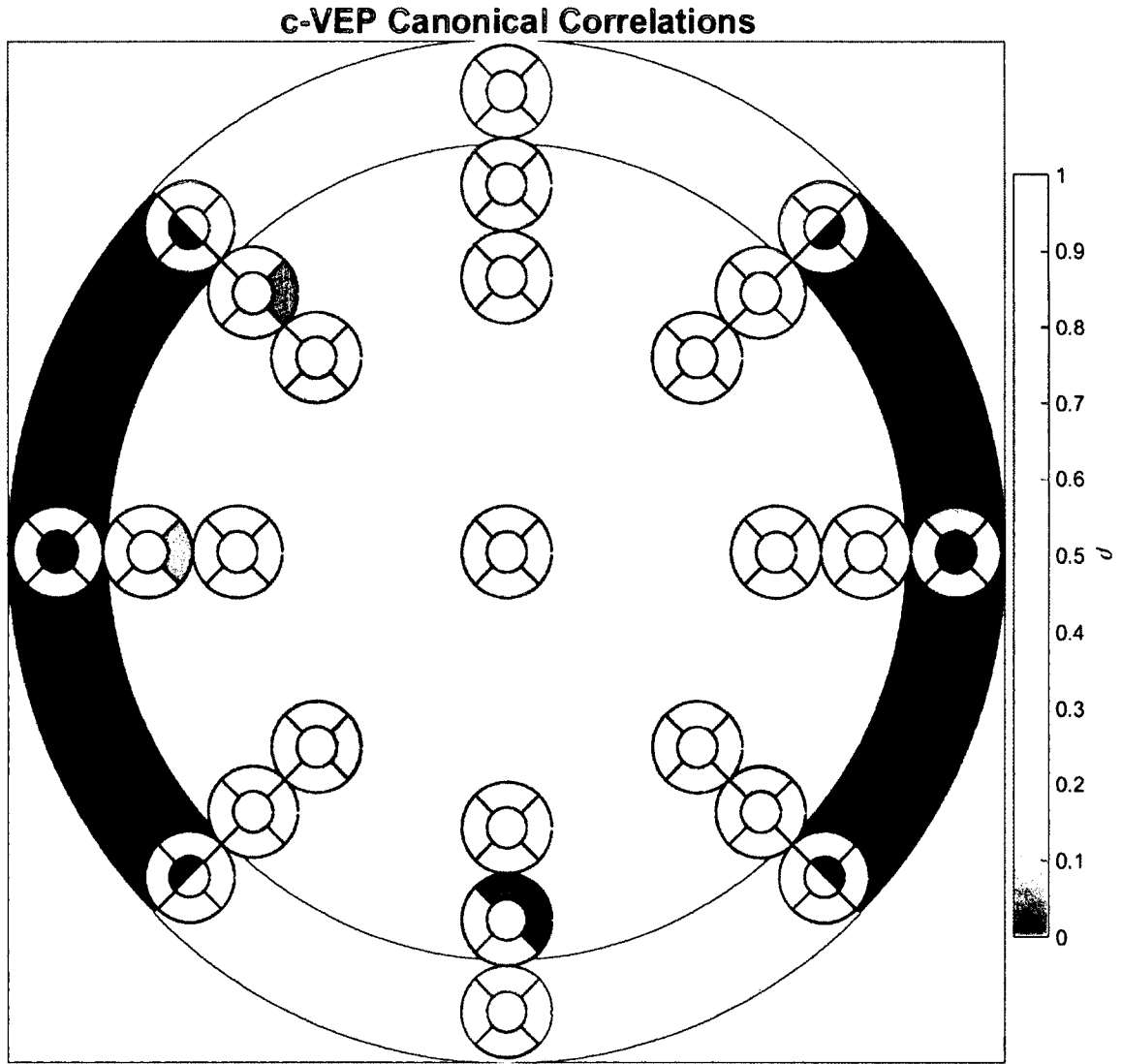


FIG. 38: 25-target source characterization plot averaged across all subjects. The c-VEP template response for each target was canonically correlated with the outer four target templates (targets: 2, 4, 6 and 8 as shown in Figure 30(b)). The relative contributions from the four stimuli for each target position can be seen as a function of the target location. For most boundary target positions (i.e. targets that lie at or near the boundary of two stimuli), the c-VEP response contributions are shown to be comprised of roughly equal parts of the two adjacent stimuli.

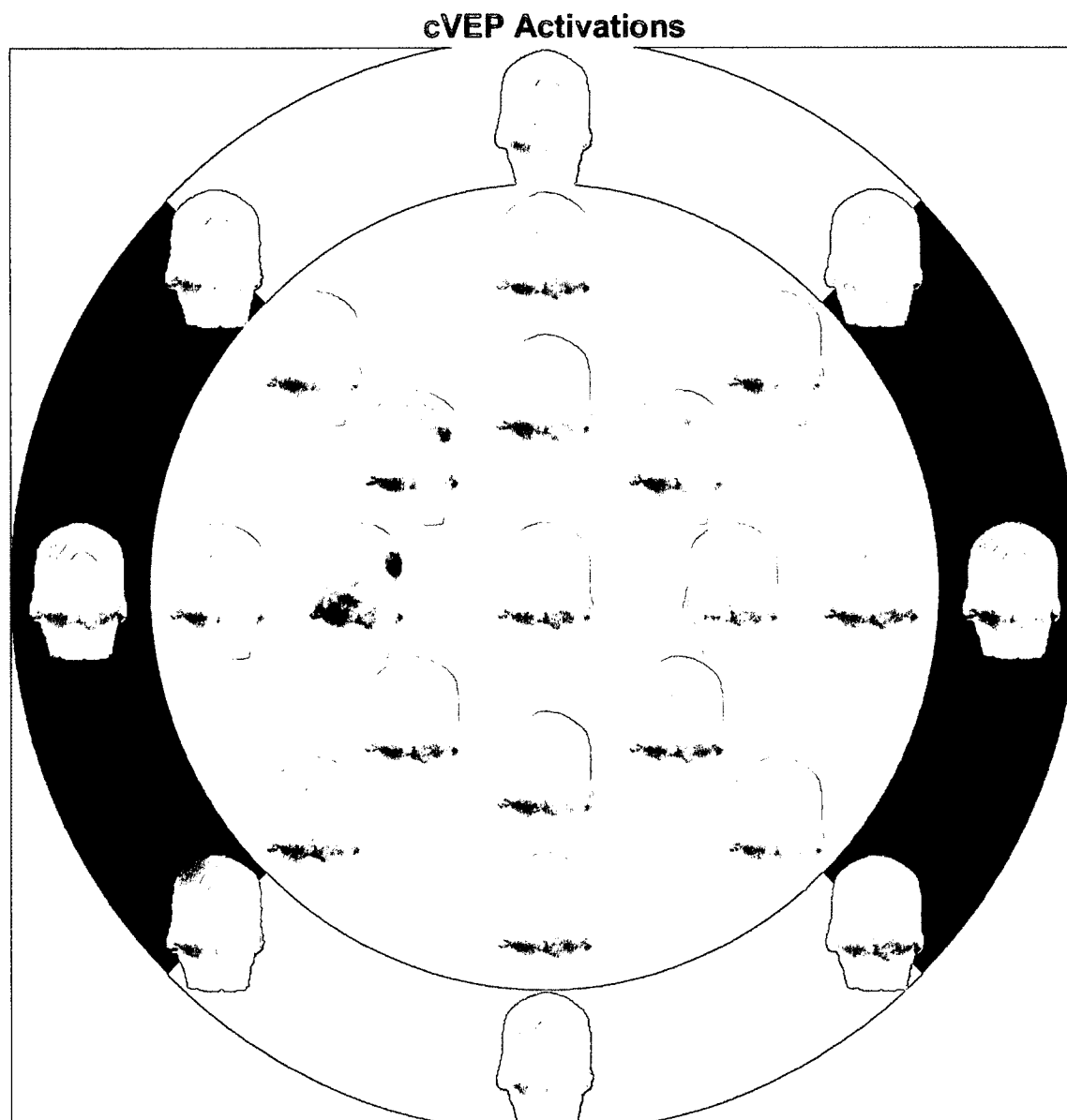


FIG. 39: Single channel correlation activations for each of the 25-target positions averaged across all subjects. The correlations are plotted topographically on head-models that are positioned at each of the 25-target positions. Each head-model is scaled to the minimum and maximum correlation value of the respective target position. The dark-red color indicates areas of high contributing activity for the c-VEP responses. It can be seen that the responses from direct foveal stimulation (outer ring) exhibit centrally over the primary visual cortex while parafoveal responses are exhibited from the parietal-occipital regions of the visual cortex.

7.4 DISCUSSION

The main objective of this offline analysis was to test the feasibility of 25-target detection using only 4 m-sequence stimuli. Currently, almost all VEP-based BCIs utilize a separate stimulus for each target or class. This work has the potential for not only leading to more practical VEP-BCIs from the reduction visual fatigue and irritation by reducing the number of flashing stimuli, but it can also potentially lead to the development of BCIs with higher ITRs. The average ITR of 88 bits/m for a single cycle observation length is comparable to the ITR results obtained in Gao's cornerstone c-VEP paradigm [Bin et al., 2011] but with only a fraction of the number of flashing stimuli used. The best subject was able to achieve an ITR of over 120 bits/min, which outperforms Gao's results. However, the present results need to be confirmed with an online implementation.

Nevertheless, these results represent an improvement in practicality as the a significant reduction of flashing stimuli is achieved. The target-to-stimulus ratio for the current ring paradigm is 6.25 targets per stimulus (25 targets / 4 stimuli) whereas the Gao's paradigm has a ratio of 0.53 targets per stimuli (32 targets / 60 stimuli). To the author's best knowledge, no study to date has attempted to increase the number of available targets to be larger than the number of flashing stimuli. Therefore, although the current results are from offline analysis and need to be repeated online, the obtained classification performance shows promise that VEP BCIs can utilize spatial decoupling of the targets and flashing stimuli to gain 3-fold increase in the number of target classes without increasing the number of flashing stimuli.

The concept of spatial decoupling can potentially increase the number of targets past a given physical limit on the bottlenecks the number of flashing stimuli for other existing paradigms. For example, Gao's paradigm owes its high information transfer rate to the 32 targets (and 32 + 28 corresponding flashing stimuli) it employs. However, that paradigm is unable to increase the number of targets further as the length of the m-sequence is unable to employ more than 32 distinct simultaneous flashing stimuli. Using this spatial decoupling technique, it is conceivable that Gao's

paradigm could be extended to employ more than 32 targets without increasing the number of flashing stimuli which would potentially lead to higher information transfer rates.

In addition to the 25-target detection, the present characterization analysis of the c-VEP responses elicited from the ring paradigm helps gain further insight on the nature of spatial decoupling. For instance, Figure 38 shows that when visually attending to (or near) the boundary of two adjacent m-sequence stimuli, the resulting c-VEP response is a combination of roughly equal proportions of the individual responses elicited innately by those two stimuli. Further, a predictable decrease in the response strength is shown as the distance between the target and stimulus is increased. A mathematical model representing VEP spatial decoupling can be made by modeling the correlation strength as a function of target-stimulus distance and as a function target adjacency relationships. This model could potentially be used as method to reduce the amount of training time needed for the BCI system. Currently, training data is needed from each target position in the BCI for construction of the template responses. A model describing the stimulus-target spatial decoupling could allow for a single master template to be made, requiring training data from only one target, and then constructing the remaining targets from the master template. Future analysis will test the efficacy of such model construction for BCI purposes.

Similar to the source correlations, the head-model topographies of the c-VEP responses shown in Figure 39 demonstrate the spatial activations that are elicited from the asymmetrical stimulation of the ring stimulus paradigm. The topographies show a noticeable pattern where targets that are positioned directly over the ring stimulus result in strong medial activations of the occipital lobe and targets that are positioned further away in the parafoveal stimulation region show more lateral activations. On the horizontal plane, the left and right parafoveal targets show strong right and left lateralizations, respectively. In future analysis, the knowledge channel-specific activations due to target-stimulus positional relationships can be used as a priori information for multi-class target detection.

CHAPTER 8

PRACTICAL IMPLEMENTATION AND DEVELOPMENT

The final chapter of this dissertation applies the results and insights gained from the previous chapters for development and implementation of practical VEP-based BCI software and applications. Many BCI paradigms work in the laboratory but fail to translate practically when used in real-world applications. VEP-based BCIs are particularly vulnerable to this issue as they require constant external stimulation that generally: 1) is not portable, 2) is visually fatiguing and irritating, 3) requires the user to focus gaze on the stimuli, not the task, and 4) has predefined parameters and configurations that are often suboptimal for individual users.

These issues are especially problematic for the target population of individuals with severe movement disorders or locked-in syndrome. For example, a paralyzed individual who wants to use a VEP-based BCI to control a motorized wheelchair currently has limited options of available systems that would be feasible. Most VEP-BCIs require computer monitors or LCD screens to display the stimuli that are not practical for wheelchair use. Additionally, the stimuli that are commonly utilized in the BCI may be visually irritating and may not give optimal response characteristics, which would not be conducive for practical long-term use. Furthermore, the ability to safely control a wheelchair and navigate is highly dependent upon the user's ability to see and react to the environment. Users currently need to directly visually attend to flashing stimuli to achieve VEP control, which consequently diverts eye-gaze away from the immediate surroundings when navigating the wheelchair. Additionally, for most VEP-BCI research, there is a lack of standardized software options that allow for flexible configurations for stimulus specificity as well as a lack of controllable BCI applications.

A practical implementation of a VEP-based BCI software system is needed to address these issues. This chapter describes the development of a practical VEP-BCI system consisting of an extensible VEP-BCI software platform called VESSELS, and the implementation and validation of that system with hardware and software interfacing for various BCI-control mechanisms of both computer-based and peripheral device control applications.

8.1 DEVELOPMENT OF FLEXIBLE SOFTWARE

Flexible and user-friendly software is rarely found in the context of BCI systems, particularly outside of laboratory settings. As such, the underlying software that controls the visual stimulation and control is usually predefined and fixed to the parameters of the associated study. This rigid system model is not optimal for VEP BCIs as seen in the results in Table 3.3.2 from Chapter 2, where subjects preformed sub-optimally with arbitrarily defined stimulus characteristics. Stimuli that are individually tailored to each user can greatly increase the detection accuracy and robustness of the VEP-BCI. Additionally, flexible software allows the user to preferentially favor either BCI usability by adjusting stimulus parameters that they find visually appealing (such as stimulus frequency, color, size and position), or they can favor BCI performance by adjusting stimulus parameters that maximize detectability. With this capability, BCI users can find an optimal configuration that balances BCI comfort and performance and ultimately increases the overall usability of the system. Thus, this last chapter focuses on the design and development of a sophisticated software platform with configurable parameters to allow for real-time tailoring of VEP stimuli as well as allowing for easily implementable control of various BCI applications.

8.1.1 VESSELS: VISUAL EVOKED STIMULATION AND SELECTION SOFTWARE

The Visual Evoked Stimulation and SElection Software (VESSELS) is an extensible software platform for VEP-BCI applications that allows for configuration of VEP stimuli and provides control of various software and hardware applications. VESSELS is a cross platform system designed around a single codebase software model that can be run natively on Windows, Mac, Android, and iOS operating systems. VESSELS is written in C# and uses the Mono runtime framework allowing it to run Microsoft .NET code using the Common Language Runtime (CLR) to compile natively on various operating systems and architectures.

VESSELS is designed around the integration of four major components: the stimulation interface (SI), the BCI2000 Interface (BI), the application interface (AI), and the control architecture (CA). Each component is an individual module that handles various duties relating to either system timing, application control, communication or visual stimulation. A diagram of the VESSELS software architecture is shown in Figure 40. The CA component is the main hierarchical GUI system that manages a menu-driven interface and facilitates the communication between all component interfaces. The SI manages and renders all flashing stimuli according to their configured shape, size, frequency, color, etc. The BI handles full-duplex communication between VESSELS and the BCI2000 General Purpose BCI software. The BI sends and receives state information to and from BCI2000. The primary state is the classification output from the BCI2000 signal processing filter. The selected classifier output is sent to the AI for device command translation according to the specific application task. The AI component handles all aspects of the BCI application. If the application is a self-contained software application, such as BCI Pacman, Google Maps, or 3-d virtual navigation (see Figure 42), then all aspects of the application logic and rendering are managed internally by the AI. If the application involves control of an external device, then the AI manages the communication between VESSELS and the device, such as sending device commands over Bluetooth or Wi-Fi to

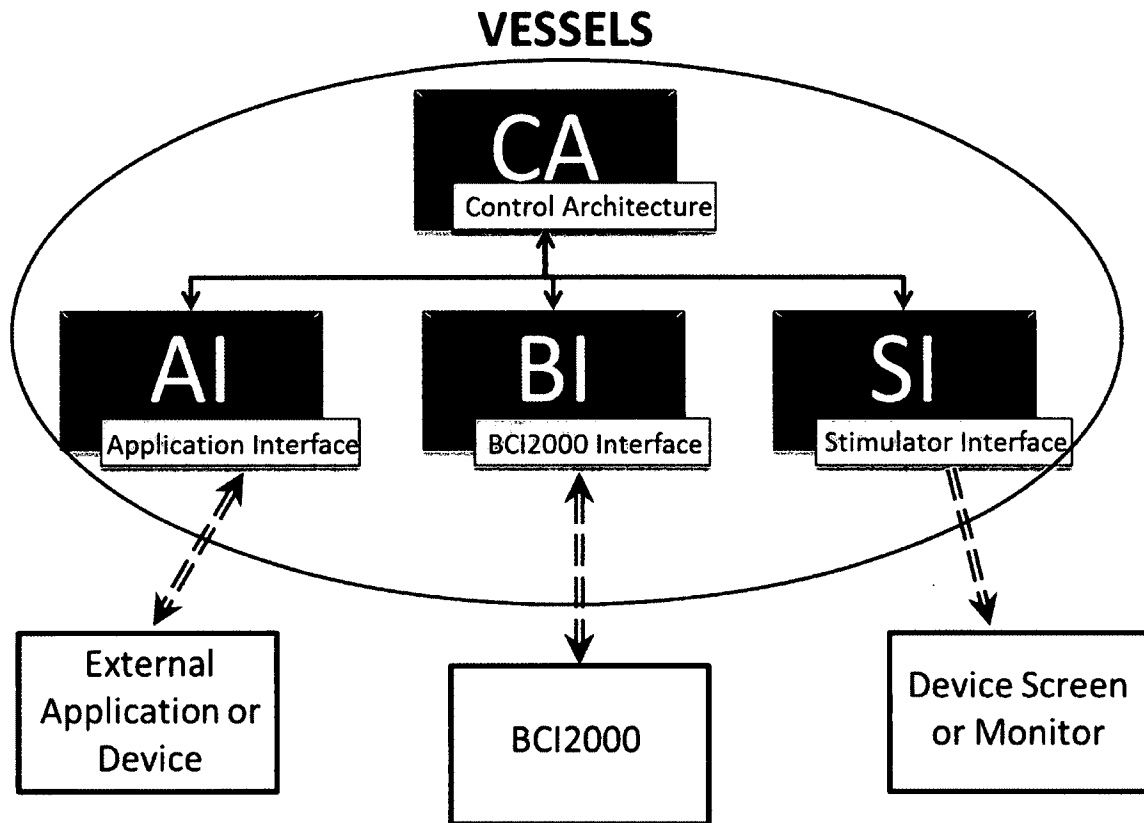


FIG. 40: Diagram of the software architecture for the VESSELS platform which consists of four major components: the control architecture (CA), the application interface (AI), the BCI2000 interface (BI) and the stimulator interface (SI). The CA component contains the main GUI system and handles communication between the three sub-components. The AI controls the BCI application and performs BCI command device translation. The BI handles communication between VESSELS and the BCI2000 software. The SI manages the timing and rendering of the flashing stimuli.

a microcontroller or a smartphone.

Figure 41 shows VESSELS's main graphical user interface system exemplifying the various menu and options screens. The stimulus characteristics as well as application parameters can be configured using VESSELS GUI system. Figure 41(a) shows the potential flexibility of VESSELS as the user can select between any of the current list applications and settings. Additionally, new application modules can easily be added to VESSELS's extensible framework.

A few examples of the applications employed by VESSELS's AI component are

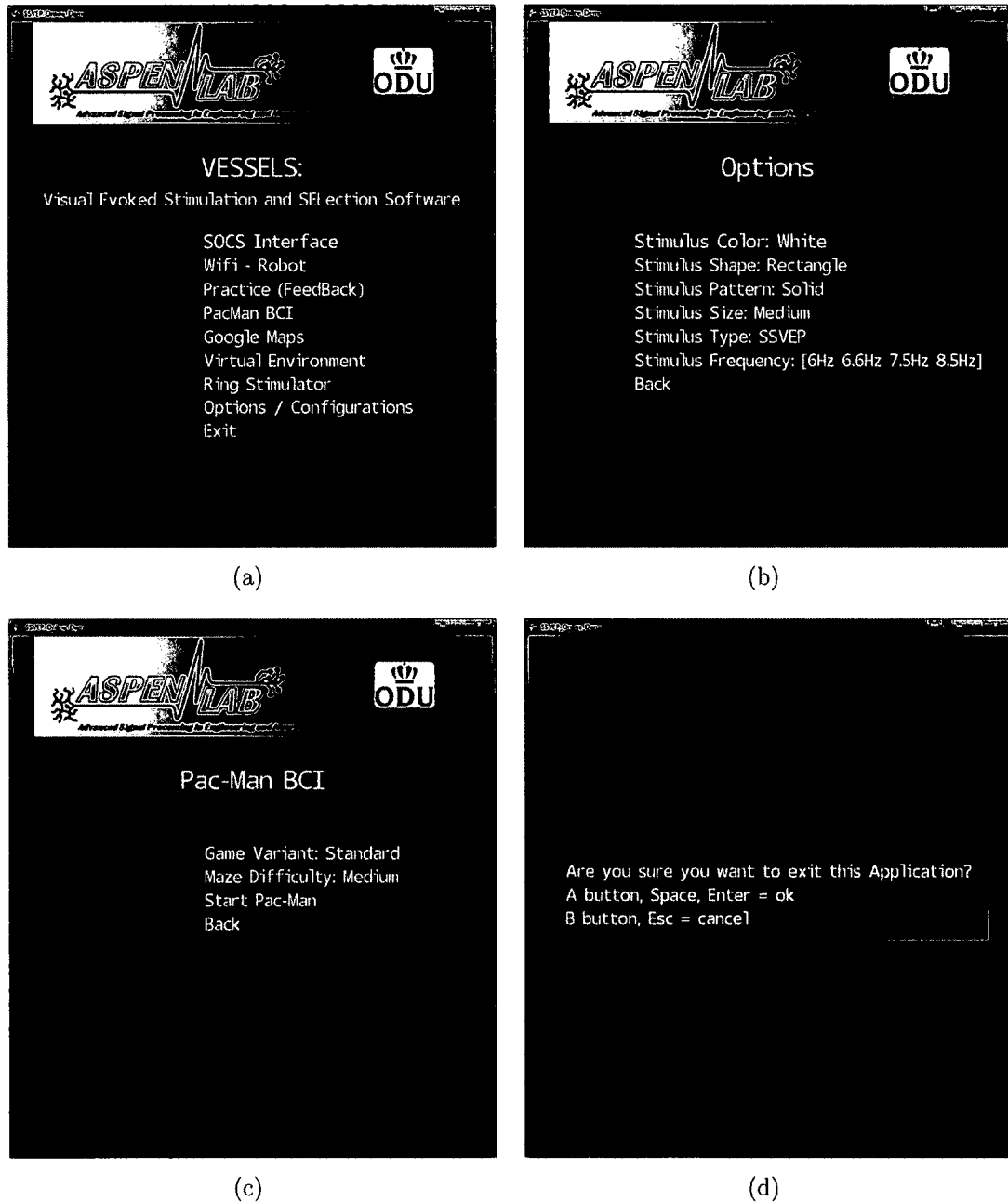


FIG. 41: Main GUI system for the VESSELS framework. (a) a screenshot of the main menu screen for BCI application selection. (b) the SI configuration screen for setting visual stimulus parameters. (c) an example configuration screen for one of the built-in AI applications (PacMan). (d) demonstrates a message box pop-up window for obtaining user confirmation.

shown in Figure 42. For each application shown, the SI component is currently configured with white rectangular stimuli which are rendered in the same window as the AI application. Figure 42(a) shows a map navigation task in which VESSELS renders and scrolls through Google Maps. Figure 42(b) shows a BCI game application using a simplified version of PacMan. A 3-d spatial navigation application with a virtual avatar is shown in Figure 42(c). Figure 42(d) shows the 4-target ring paradigm described in chapter 5 which is used to control a small web-cam robot over a Wi-Fi connection for a telepresence application. This particular application illustrates the potential ubiquitousness of the ring paradigm as the task space and the control space are merged together, encompassed by the ring stimuli.

SOCS: Screen Overlay Control System

The Screen Overlay Control System (SOCS) is a rendering system embedded within VESSELS that allows for a screen overlay of the stimuli onto any application window. The standard VESSELS configuration involves the rendering of the stimuli and the application graphics in the same window. This requires VESSELS's AI component to completely manage and render any embedded application. Overall, this presents a limiting factor on the amount of applications that can be controlled by VESSELS as each new application has to be created as a separate AI module. SOCS allows the SI component of VESSELS to render stimuli as window-less, free-floating objects that are overlayed onto whatever application is running on the host computer. With SOCS, the AI component does not have to render its own application; instead, it controls whatever current application is running on the host machine by translating the BCI output to emulated keyboard commands. This allows VESSELS to control virtually any application on the host computer ranging from web browsers, explorers, video games, typing programs, and any other third-party software.

The VESSELS platform's effectiveness for VEP-BCI control has been tested to some degree as it has been utilized numerous times to give BCI demonstrations at Old Dominion University. It has been tested primarily on Windows and Android systems, and is capable of fully running on an Android smart-phone. The software has been

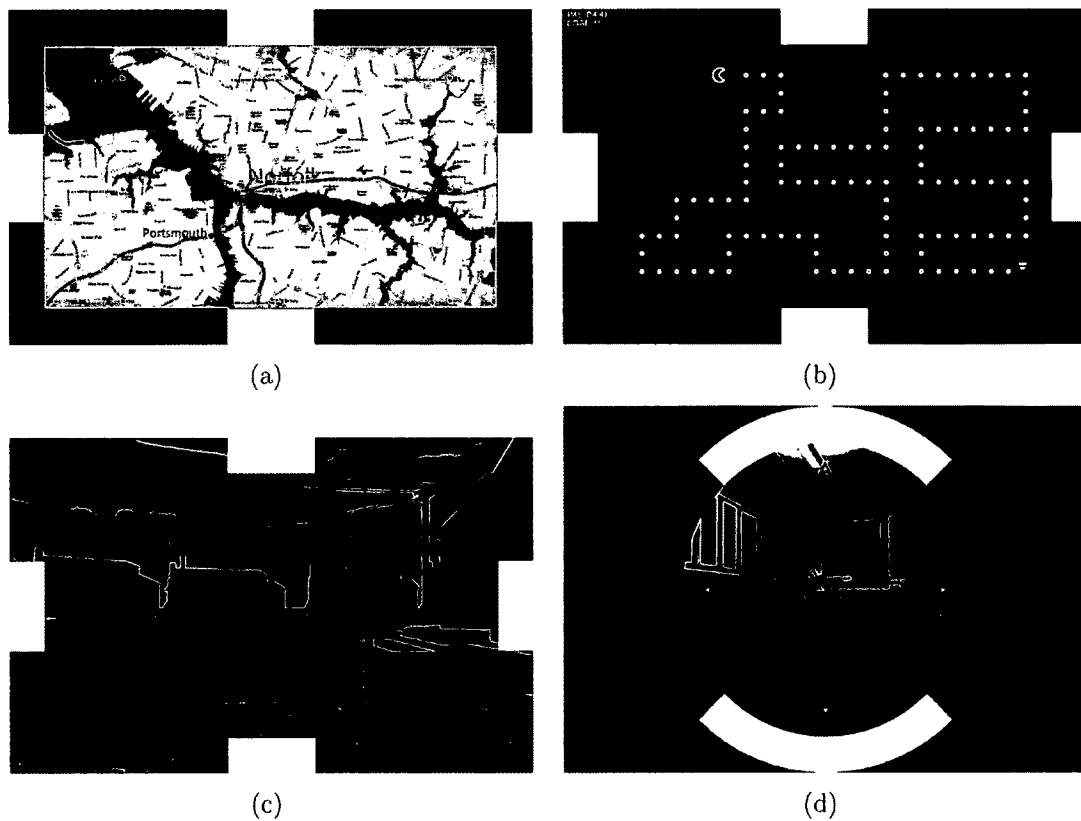


FIG. 42: Screenshots of several native applications built into VESSELS. (a) shows the map navigation application using Google maps. (b) shows the PacMan maze navigation Game. (c) shows a virtual navigation task through a 3-d environment. (d) shows the ring paradigm implemented to control a mobile web-cam robot in a telepresence application.

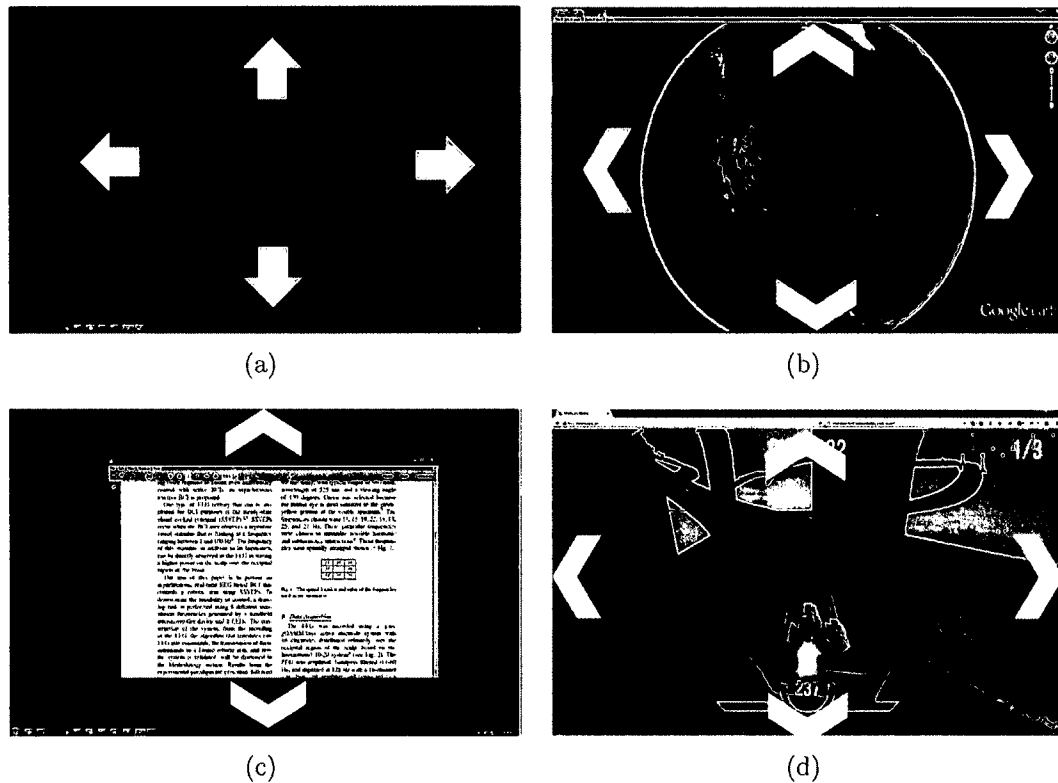


FIG. 43: (a) a screen-shot of four free-floating stimuli rendered with VESSELS using the SOCS interface. The stimuli from SOCS can be manually positioned anywhere on the desktop or on top of any application window. (b) the SOCS interface controlling a popular application known as Google Earth. (c) a PDF scrolling application. (d) a web-browser based racing game with the SOCS stimuli overlaid.

tested with many volunteers, most of which were new to BCI control. VESSELS has also been presented in front of Google’s rapid evaluation team at their headquarters in Mountain View, CA where a successful demonstration of an SSVEP-BCI with real-time control of Google Earth was given using SOCS (Figure 43(b)).

8.2 IMPLEMENTATION AND VALIDATION

The VESSELS system described in the previous section is a fully-fledged BCI stimulation and control program capable of controlling virtually any software application on the computer. However, it is also common to control external hardware and peripheral devices with the BCI system. Applications that extend beyond the computer are potentially beneficial to the target population, such as motorized wheelchair navigation, robotic telepresence control, and neuroprosthetics. Each of these requires a layer of hardware interfacing and communication for incorporation into a BCI system. The next few sections in this chapter describe several BCI hardware and communications interfacing applications in which VESSELS was extended to control peripheral devices such as motorized wheelchairs, telepresence robots, and anthropomorphic robotic manipulator arms.

8.2.1 HARDWARE INTERFACING

Hardware interfacing is an important application domain for BCI control systems and has been performed extensively in the field of brain-computer interfaces ranging from environmental control of thermostats, TV’s, smartphones, wheelchairs, and robotic or prosthetic arms [Diez et al., 2013, Gao et al., 2003, Valbuena et al., 2007, Müller-Putz and Pfurtscheller, 2008, Al-maqtari et al., 2009, Kapeller et al., 2013].

Microcontrollers are small programmable computers embedded on a single integrated circuit containing a processing core, memory and programmable input/output peripherals. The general purpose input/output pins (GPIOs) on a microcontroller allow for low-level hardware interfacing through digital logic circuits or binary serial communication. The Arduino microcontroller board is an open-source electronics

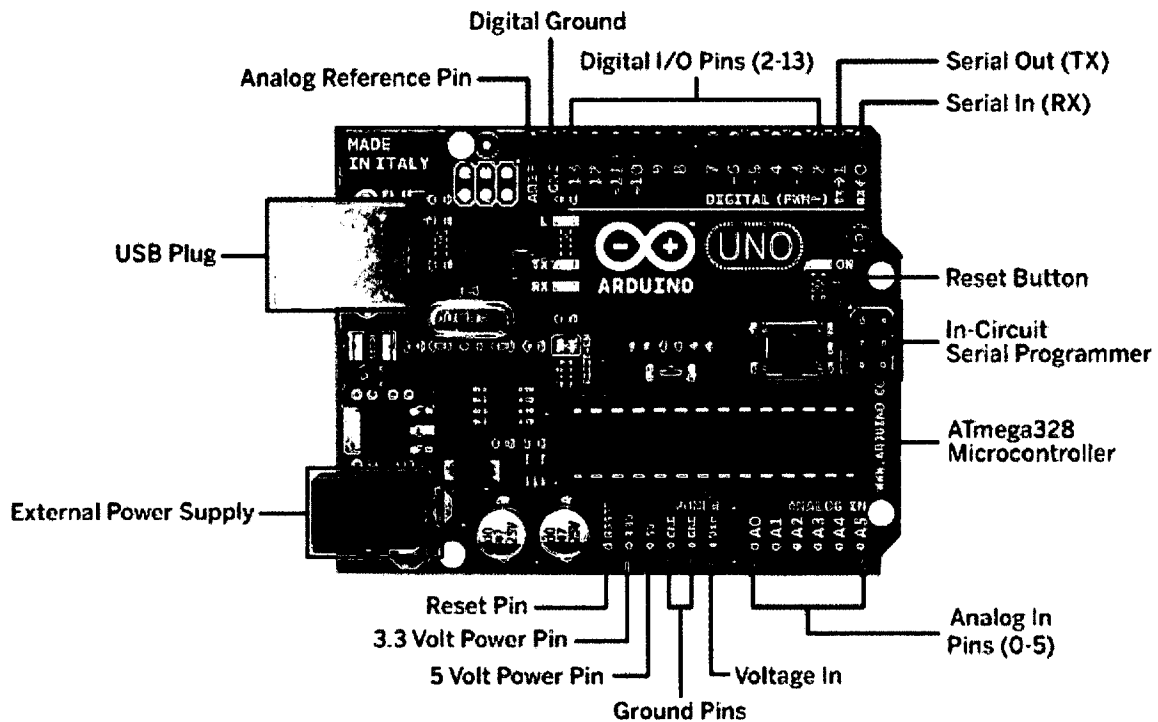


FIG. 44: Standard configuration of the Arduino UNO development board with ATmega328 chip with on-board voltage regulation, 14 digital input/output pins, 6 pulse-width modulation (PWM) pins, 6 analog input pins and Serial communication pins.

platform with extensible hardware and software. The Arduino microcontrollers have several advantages for use in hardware interfacing. The Arduino board is a self-contained module that facilitates rapid prototyping and hardware development with the integration of standard connection pins that allow for digital input/output interfacing. Additionally, the Arduino boards contain pre-programmed boot loaders with flash memory, interchangeable add-on modules known as shields and several packaging layouts with various form factors to handle a wide range of electronic applications. A diagram of the standard Arduino UNO board is shown in Figure 44. The Arduino microcontroller is used for all of the hardware interfacing applications described in the following sections. The digital I/O pins on the Arduino board are wired to the peripheral device to be controlled, such as the controller unit of a motorized wheelchair or a motor-driver circuit for controlling servos and actuators.

8.2.2 COMMUNICATIONS

When interfacing a BCI system with peripheral devices, the data containing the device commands need to be transmitted from the BCI computer to the external hardware. Depending on the nature of the application, this is usually done over a wired Ethernet connection, or a wireless connection using either Bluetooth communication protocols or local area networking over Wi-Fi. RFCOMM is a bluetooth communication protocol in which a direct connection is established between the serial ports of two devices which are first 'paired' together. Network based communication via Ethernet or Wi-Fi channels utilize either a connection-oriented protocol, such as TCP (Transmission Control Protocol) or a connectionless protocol such as UDP (Universal Datagram Protocol). TCP is a high reliability communication protocol where data loss is critically avoided at the expense of potentially increased data-transmission time. UDP, on the other hand, is a stateless connection where data transmission is always real-time with the possibility of potential loss of packets. The UDP protocol, shown in Figure 45, requires no connection between the server and client. The server handles each UDP packet independently of other packets and performs no error-checking on packets. UDP communication is primarily used in the applications presented in this chapter and is the protocol of choice for BCI control as command buffering from TCP communication can potentially lead to severely time-delayed interactions which negatively interfere with the 'closed-loop' nature of the BCI system.

8.2.3 WHEELCHAIR BCI SYSTEM

BCI control of a motorized wheelchair is an important device application for patients with locked in syndrome and ALS as it has the potential to restore a significant level of independence and quality of life for the patient. Previous work involving BCI wheelchair control with VEP based BCI systems require the use of an LCD monitor for stimulus rendering. In this work, a 4-class SSVEP BCI system was interfaced with

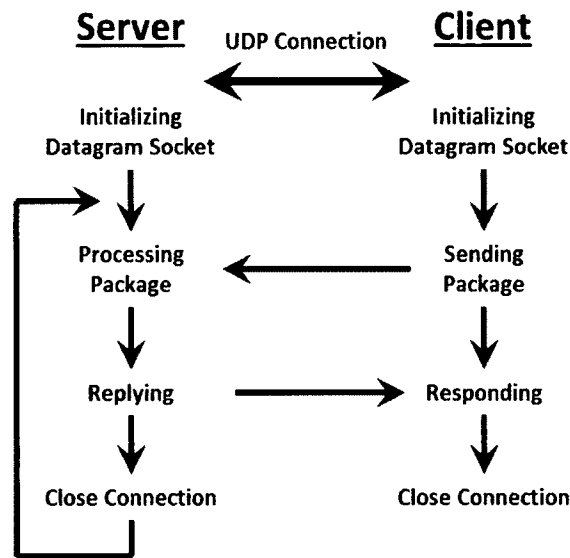


FIG. 45: Universal Datagram Protocol (UDP) communication architecture. UDP is a connectionless interface in which data packets are sent and received in a stateless fashion. UDP is useful for BCI applications as no buffering of potential device commands is performed.

an android smartphone using VESSELS for control of a motorized wheelchair. A calibrationless classifier was implemented with BCI2000's Matlab filter using the CCA classification method described in Section 2.5.1. Additionally, a low-profile headband with 5 dry electrodes was used for signal acquisition for a practical implementation of a BCI controlled Wheelchair.

System Overview

A diagram of the implemented BCI wheelchair system is shown in Figure 46. The system uses five g.Sahara active dry electrodes (Guger Technologies, Austria) placed at Po7, O1, Oz, O2 and Po8 using a custom made headband. The electrode signals are amplified using a g.MOBILab+ wireless amplifier which sends digitized EEG signals over Bluetooth to a laptop computer placed in a sleeve behind the wheelchair. BCI2000 was used to process and classify the buffered EEG signals using CCA. Output selections are made and sent over UDP to the VESSELS platform also running on the laptop. The AI component within VESSELS translates the BCI

Wheelchair Control Diagram

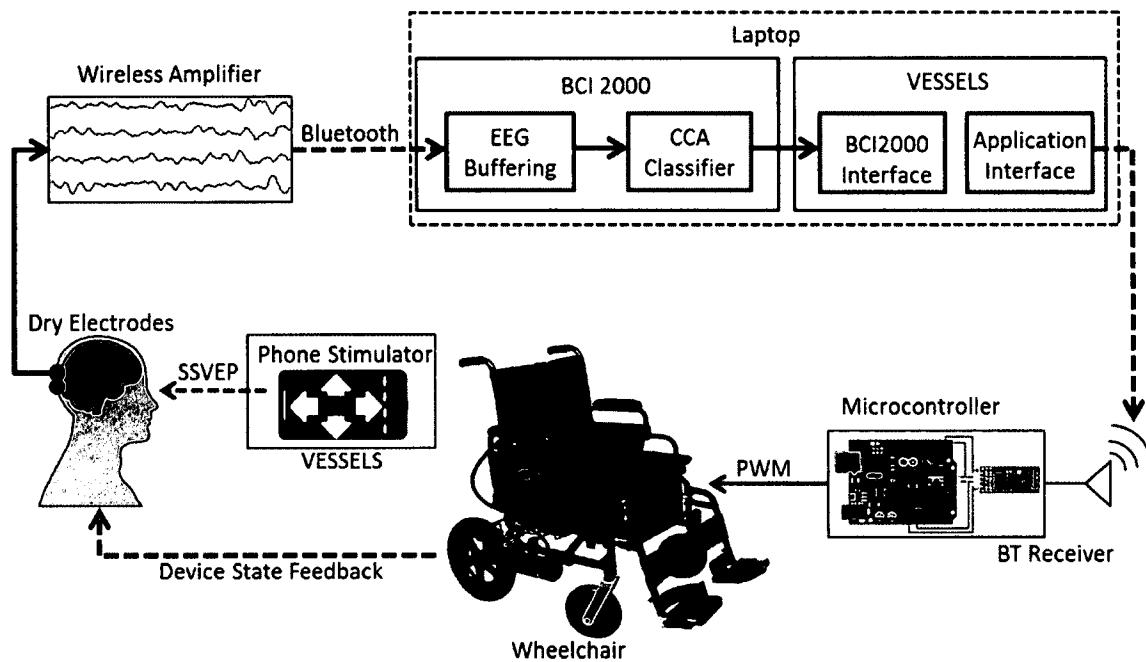


FIG. 46: SSVEP BCI Diagram for Motorized Wheelchair Control. Signals are collected from five active dry electrodes and sent wirelessly to a laptop computer. The BCI classification module classifies the signals using CCA and sends the output to VESSELS over UDP. The VESSELS application interface translates the output to device commands which are sent via bluetooth to an Arudino Microcontroller whose PWM ports are used to control the wheelchair's directional movements. The VESSELS's SI component runs on an android smartphone for SSVEP stimulation while overlaid on video feed from the back-facing camera.

output into one of four wheelchair commands: move forward, rotate left, rotate right and stop movement. The output commands are sent through Bluetooth to an Arduino microcontroller wired to the wheelchair input control system. The Arduino was fitted with an HC06 BT transceiver to receive bluetooth commands. Based on the command received from VESSELS, the corresponding PWM signals are sent to the wheelchair controller indicating the direction of movement. The Metro Power 3 wheelchair employs a zero-turn drive system which allows the wheelchair to 180 degree turns and thus eliminating the need for a backward movement command. The speed of wheelchair movement and turning are controlled with a master speed switch on the wheelchair controller. As a safety precaution, a joystick override and

kill switch were placed on the wheelchair controller allowing the user to override BCI control and/or turn off power to the wheelchair. The VESSELS stimulator interface was run separately on an android smart-phone (Samsung Galaxy S4) to render the stimuli using a 60Hz refresh rate. Four SSVEP stimuli, representing the four wheelchair commands, were flashed at 6 Hz, 6.66 Hz, 7.5 Hz and 8.57 Hz. The Android phone was mounted on the wheelchair and positioned 12 inches in front of the user's head. Using VESSELS, the stimuli were placed on the peripheral edges of the phone's 5 inch LCD screen and were overlaid on top of the video feed from the phone's back-facing camera. This allows the user to visually attend to the control stimuli while also viewing the space in front of the wheelchair. Figure 47(a) shows a picture of the developed wheelchair BCI system in use.

8.2.4 TELEPRESENCE BCI SYSTEM

Telepresence applications allow for the remote control of devices using virtual reality technology for participation in distant events. These applications are especially useful for individuals that are confined to their home or to a bed. A telepresence BCI system was developed by modifying the Wheelchair BCI system already in place. A diagram of the Telepresence control scheme is shown in Figure 48. For the telepresence BCI system, the user is fixed to a stationary location, and thus a wired amplifier is used with the dry electrode band. The EEG signals are transferred through USB to a desktop PC running BCI2000 and VESSELS. Communication from VESSELS to the wheelchair device is handled using bluetooth communication in the same way as described in section 8.2.3. The Android phone camera mounted on the wheelchair wirelessly transmits a video stream over Wi-Fi to the VESSELS application interface. The video feed and VEP stimuli are overlaid and rendered on a standard computer monitor attached to the desktop PC. The wireless camera feed provides feedback to the user about the device state of the wheelchair from a distance. This allows the user to remotely control and navigate the wheelchair from a fixed location. Figure 47(b) shows a picture of the Telepresence BCI system in use.



(a)



(b)

FIG. 47: Part (a) shows the developed wheelchair BCI system in use. Part (b) shows the motorized wheelchair being navigated remotely using the telepresence BCI system.

Telepresence Control Diagram

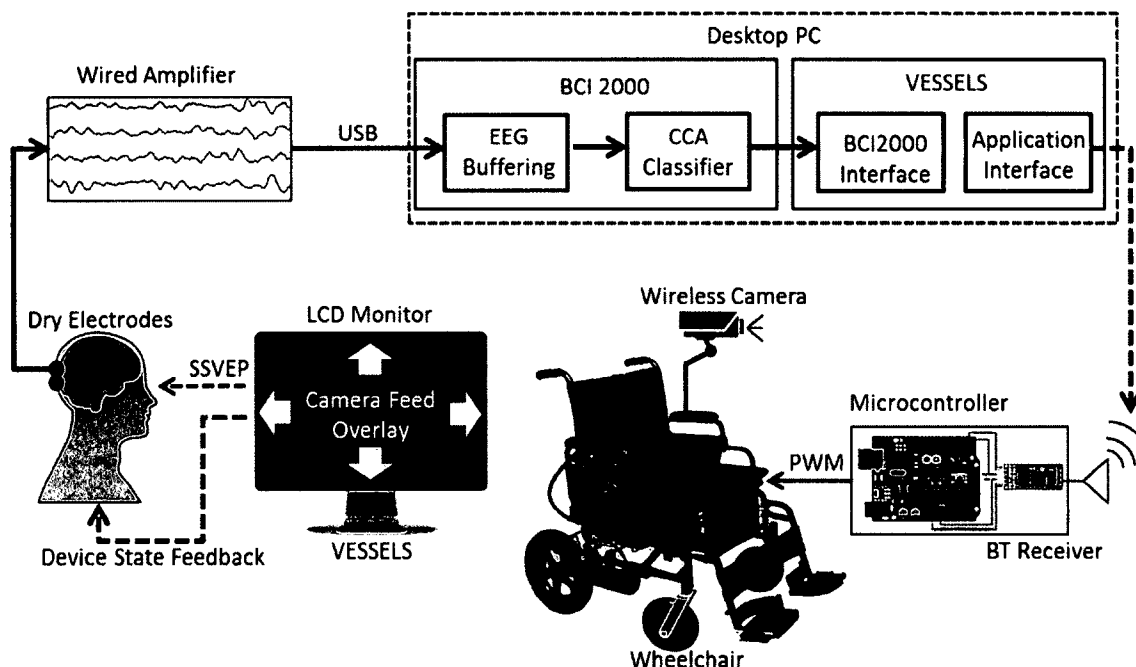


FIG. 48: SSVEP BCI Diagram for Telepresence BCI Control. Signals are collected from five active dry electrodes and sent through USB to a Desktop computer. The BCI classification module classifies the signals using CCA and sends the output to VESSELS over UDP. The VESSELS application interface translates the output to device commands which are sent via bluetooth to an Arudino Microcontroller whose PWM ports are used to control the wheelchair directional movements. The VESSELS's SI component renders the stimuli on a computer monitor and are overlayed on a wirelessly transmitted video feed from a phone-camera mounted on the remotely operated wheelchair.

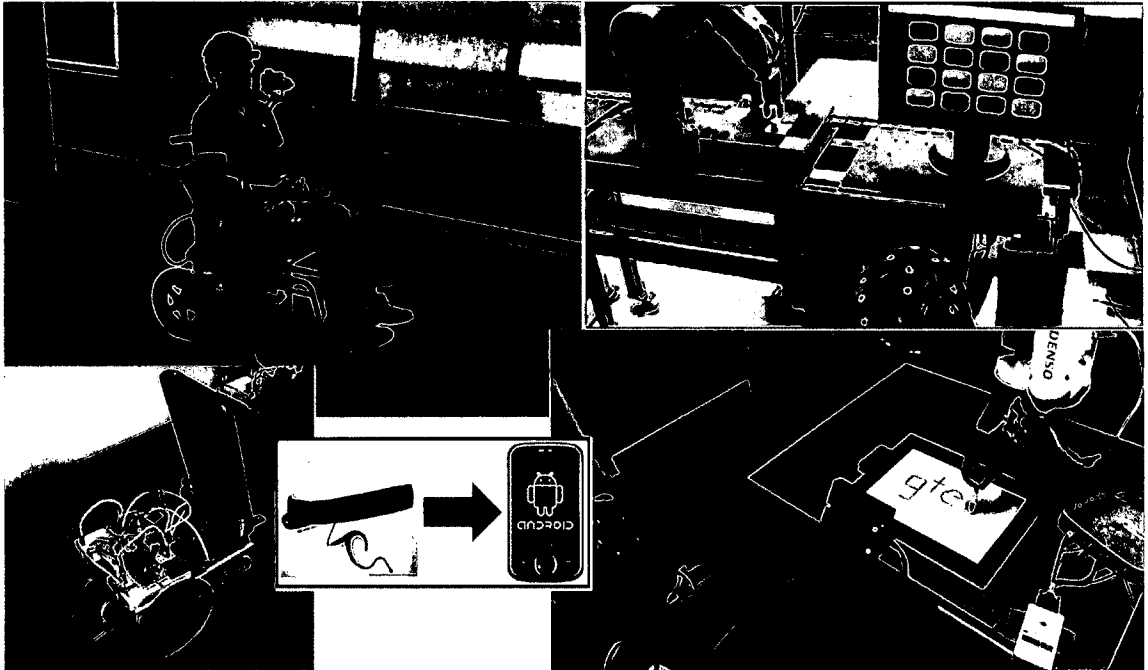


FIG. 49: Developed BCI systems from left to right: BCI Wheelchair system using VESSELS, P300 pick-and-place BCI using a Staubli robotic manipulator arm [Waytowich et al., 2010], custom made Wi-fi robot using the Arduino Micro paired with an Android phone for remote sensing, EMG controlled music player on an Android phone, and a 10-class SSVEP BCI drawing application using a Denso arm and prosthetic hand.

8.2.5 OTHER PROJECTS

Figure 49 shows a compilation of other BCI related projects that were developed. A 10-class SSVEP BCI was implemented for controlling of a 6-DOF robotic manipulator arm with an attached prosthetic hand that holds a marker for drawing applications (shown in the bottom right of Figure 49). A P300 BCI system controlling a Staubli robotic arm during an object pick-and-place task is shown in the upper right of Figure 49 [Waytowich et al., 2010, Johnson et al., 2010]. The bottom left shows a custom made Wi-fi robot using the Arduino Micro paired with an android phone for remote sensing applications.

8.3 FUTURE DIRECTIONS WITH MODERN VISUAL OVERLAY DEVICES

The true mark of practicality of a BCI system is to make it as transparent as possible to the user. For VEP-based BCIs, this is hardly attainable as external visual stimulation is required which generally requires the use of LCD computer monitors that are not portable and not a transparent mode of stimulation. Recent advances in mobile technology have made modern visual overlay devices portable, lightweight, unobtrusive, and more accessible than ever. Such devices present a novel avenue for implementing practical VEP-BCIs. Visual overlay devices have the potential to dramatically improve the overall mobility of the VEP-BCI system as the overlay devices are typically small enough to be worn on the user. The main advantage of utilizing a visual overlay device is that the stimuli can be directly overlaid in the user's visual field in an augmented reality sense. A BCI system of this type would allow the user to seamlessly view his or her environment while also having access to the control stimuli of the VEP-BCI in a intuitive manner.

8.3.1 GOOGLE GLASS

Although any modern overlay device can be utilized, Google Glass (Google Inc.) has many attractive properties that make it a suitable choice for VEP-BCI implementation. Google Glass represents a leap forward in the field of wearable computing because of its ergonomic and ubiquitous design. It provides users with instant access to a mobile device capable of virtually any application ranging from sending/receiving emails, taking pictures/videos, web surfing, etc. As such, Google Glass has the hardware and software requirements to meet the technical specifications for implementing a VEP stimulation paradigm with a 1 Ghz processor and 30 Hz screen refresh rate. An image of the Google Glass components and its visual overlay is shown in Figure 50. The overlay mechanism in Google Glass works by projecting an image directly onto the fovea part of the retina through a prism. This creates a sharp image that is visible to the user. The display can be adjusted to cover different parts of the user's vision. This is important for VEP-BCI implementation because

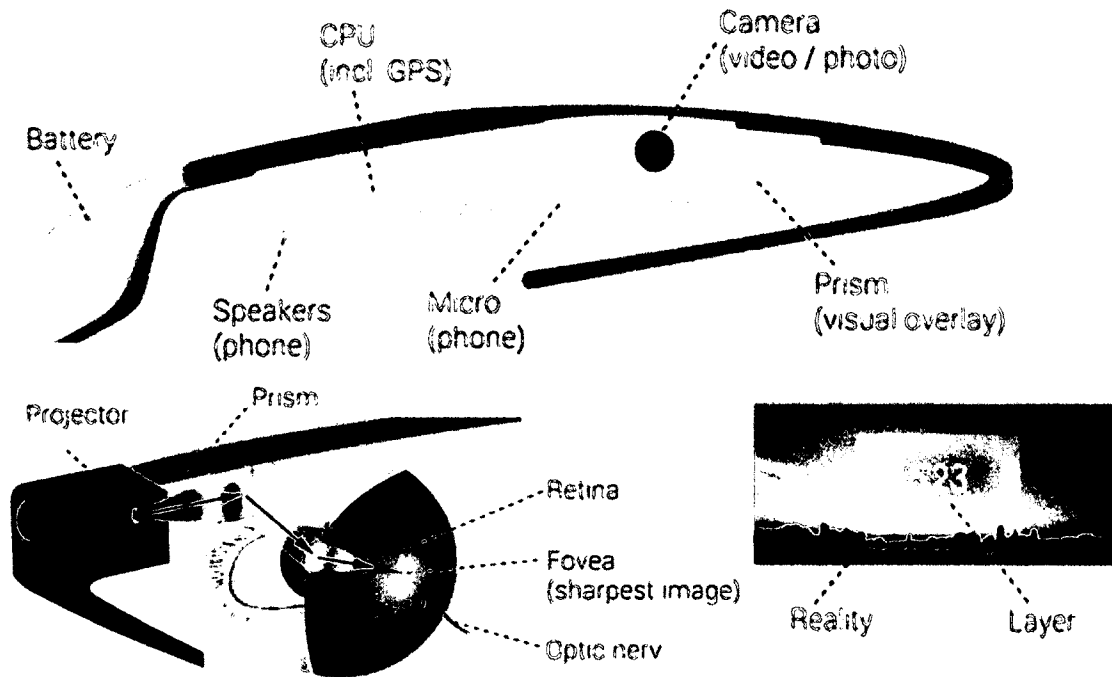


FIG. 50: Google Glass visual overlay device. The top image shows the Google Glass with labeled components. The bottom left demonstrates how the overlay system works. An image from a projector is presented directly on the retina from a prism. The bottom right image shows how the Google Glass looks from a user's perspective.

it allows for the user to adjust the position of the visual stimuli, thus controlling its prominence. The bottom-right of Figure 50 shows an example view of the overlay itself. The overlay layer has a translucent background with opaque images. This characteristic is especially beneficial as this system would allow for the user to view both the VEP stimuli and the environment simultaneously; a characteristic that has never been fully realized for a VEP-BCI.

8.3.2 GOOGLE GLASS EVALUATION STUDY

Two studies are planned utilizing the visual overlay device. The first study will test the feasibility of the visual overlay device itself by implementing a 2-class BCI using SSVEP stimuli. The results from Chapters 3 and 4 will be used to select optimal stimuli characteristics. Figure 51 shows a diagram of the SSVEP system for the first

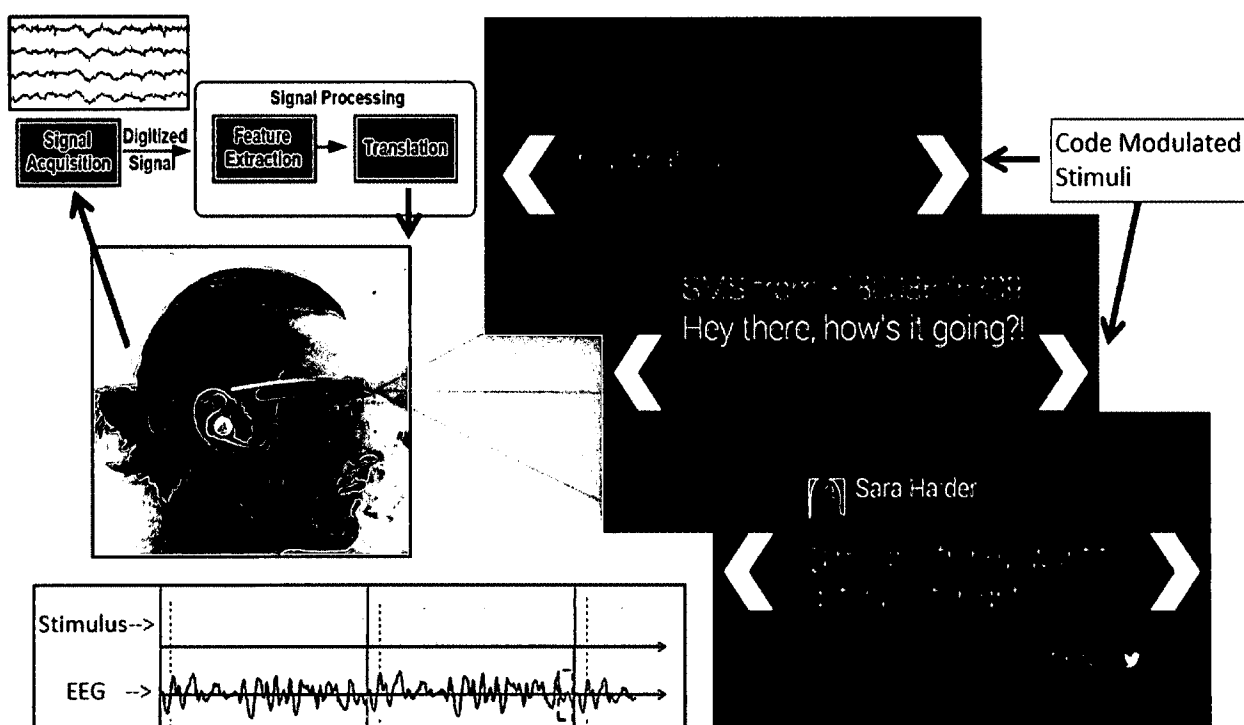


FIG. 51: Diagram of the proposed system setup using a VEP based BCI with a visual overlay device. The overlay device depicted is the Google Glass although, in practice, any overlay device can be used. The VEP stimuli can be modulated by either c-VEP or SSVEP stimuli.

CHAPTER 9

CONTRIBUTIONS AND FUTURE DIRECTIONS

The presented work shows the initial steps towards developing a practical VEP BCI by characterizing and optimizing visual stimuli, improving ergonomic design, reducing visual fatigue, and implementing a practical VEP based BCI using flexible software and modern mobile device platforms. Considerable work remains to be done in aggregating and extending the results from this work to further increase the practicality of brain-computer interfaces. The major contributions from the work presented in this dissertation as well as the future directions are summarized below.

STIMULUS CHARACTERIZATION AND OPTIMIZATION

Contributions

1. Inherent SSVEP response differences that exist between subjects were shown to have a significant effect on performance. This demonstrates the degree of importance of subject-specific frequency optimization as BCI classification can be significantly increased.
2. A framework for a rapid optimization of subject-specific frequency profiles was established using chirp-modulated stimuli. This method can be used as an efficient way to characterize the response of the SSVEP spectrum for an individual, which can now be achieved much more rapidly than evaluating individual frequencies independently.
3. Distinct frequency feature groupings for optimal performance exist for different multiclass scenarios. This information can provide a guide for generalized stimulus frequency selection for SSVEP-based BCIs with an arbitrary number of targets. This is particularly useful for scenarios where subject-specific optimization is not feasible.

4. The spatial frequency of checkerboard stimuli was shown to have a major effect on performance for SSVEP BCIs with two distinct spatial frequency conditions showing optimal results. This optimization of the spatial frequency can lead to increased SSVEP performance over current studies which arbitrarily predefine the spatial frequency.
5. The use of high spatial frequency stimuli, which are perceptually less irritating to subjects, can achieve comparable classification performance as the traditional low spatial frequency stimuli. This has significant implications for the designing of more practical VEP BCIs as less obtrusive and more visually appealing stimuli can be used for BCI stimulation and control.
6. Neural mechanisms of spatial frequency tuning and spatial frequency adaptation, which were originally shown in the context of clinical studies using a single stimulus, have been shown to be present in the context of SSVEP BCIs. These mechanisms, which are generally unknown in the BCI field, should be considered when designing SSVEP BCIs as further understanding can potentially lead to improved VEP BCI performance.

Future Directions

Because of the limitation of monitor refresh rates, LEDs were used for chirp-signal stimulation. However, it is desirable to implement stimuli using more practical and ubiquitous LCD screens. An identical follow-up study using an LCD monitor will be conducted in the future, although it is not expected that the results will significantly differ from the results in this dissertation. Additionally, the long-term stability of the stimulus characterization and optimization results from this dissertation have yet to be assessed and longitudinal experiments should be conducted.

The results from chapters 3 and 4 have some limitations in terms of generalizing to an online BCI. Additionally, the analysis from those chapters do not account for the potential simultaneous interference or attentional issues present in a practical online scenario. Thus, an additional online study should be performed with data

collected from a multi-class BCI. Another future stimulus characterization study is planned to evaluate other classification schemes as the current optimization results may be specific to the CCA approach.

Finally, the relationship between spatial frequency and temporal frequency is not well understood, and additional work should investigate a joint-optimization between these two variables.

SPATIAL DECOUPLING OF VEP STIMULI

Contributions

1. A novel c-VEP stimulation paradigm was developed that showed practical classification accuracies for non-foveal VEP stimulation that are comparable to the traditional direct-foveal stimulation. This significant finding demonstrates that adequate classification performance can be obtained without requiring direct visual fixation of flashing stimuli. This provides an avenue for the development of more practical BCIs that are less visually irritating to operate.
2. BCI targets that are positioned at or near the boundaries of two stimuli can be classified with the same accuracy as traditional targets that are superimposed over a single stimulus. This shows that it is possible to increase the number of targets beyond the number of stimuli without degrading performance. This can lead to increased information transfer rates for BCI communication as well lead to the development of more practical and ergonomic BCIs.
3. A 25-class c-VEP BCI using the ring-stimulator achieved favorable classification performance. These results are the first to demonstrate that large-scale target discrimination can be obtained using spatial decoupling in which there are 6-fold more targets than flashing stimuli. This provides a significant and novel avenue for the development of more practical BCIs that utilize minimal visual stimulation.
4. The c-VEP characterization analysis shows spatial activations that are elicited

contralaterally over the occipital regions from asymmetrical target/stimuli relationships from the ring stimulus. This provides insights into the information flow of the visual system that can potentially be used for developing more accurate classifiers, as well as for developing new ways to measure inter-hemispheric transfer time.

Future Directions

In order to fully validate the spatial decoupling ring paradigm, undirected free-choice online experiments need to be conducted to account for practical use issues such as target scanning and reaction to task-related feedback. Future work will more thoroughly explore the effects of distance between the targets and stimuli, increasing the number of stimuli/boundaries along the ring, the use of shorter m-sequences, and larger N-class target configurations that further exploit the combined concepts of stimulus-target distance and boundaries. It is envisioned that these stimulus-target decoupling concepts introduced in the proposed paradigm will lead to the development of more practical and ergonomic BCIs by reducing visual irritation and potentially fatigue, as well as by increasing the number of available targets for a fixed number of stimuli.

Future analysis will further investigate the topographical activations of c-VEP responses due to the asymmetrical stimulation of the ring stimulus pattern. Additional characterization is planned to model the channel specific activations due to target-stimulus positional relationships for the potential use as a priori information in multi-class target detection.

PRACTICAL IMPLEMENTATION AND DEVELOPMENT

Contributions

1. A flexible and extensible software platform for the stimulation of flashing stimuli and versatile control of various VEP BCI applications called VESSELS was

developed and tested. This is a cross-platform software designed for the implementation and control of SSVEP and c-VEP BCI applications that is currently not available in the standard BCI2000 software package.

2. A practical implementation of a BCI controlled motorized wheelchair was developed that uses a calibrationless classifier, a minimal form-factor dry electrode band, a wireless amplifier, and a mobile smart-phone running the VESSELS software overlayed on a camera video feed for SSVEP stimulation and control. The combination of the signal acquisition, decoding algorithm, and augmented reality-style mobile stimulation makes this a novel implementation of a BCI wheelchair that is both ergonomic and practical.
3. Finally, a practical implementation of a telepresence BCI was developed and implemented using the motorized wheelchair and VESSELS software which allows a stationary individual to control the wheelchair remotely using real-time video feed from a wireless camera. This system utilizes dry electrodes, requires no user calibration, and achieves quick and robust control that can allow immobile individuals to independently explore and interact with their surroundings.

Future Directions

Future work is planned to test the VESSELS software in multiple large-scale research studies. Additionally, work will be done towards packaging the VESSELS software with the popular BCI2000 software platform so that it can be utilized by other BCI research groups.

Future work will also involve the testing of the VESSELS software on Google Glass and other head-mounted displays to achieve an ergonomic visual overlay of the VEP stimuli. A study will be conducted testing the efficacy of using Google Glass for BCI control as well as eventually implementing the Google Glass with the BCI controlled wheelchair for a truly intuitive and transparent BCI.

BIBLIOGRAPHY

- [Al-maqtari et al., 2009] Al-maqtari, M. T., Taha, Z., and Moghavvemi, M. (2009). Steady state-VEP based BCI for control gripping of a Robotic hand. In *International Conference for Technical Postgraduates 2009, TECHPOS 2009*.
- [Allison et al., 2010] Allison, B., Luth, T., Valbuena, D., Teymourian, A., Volosyak, I., and Graser, A. (2010). Bci demographics: how many (and what kinds of) people can use an ssvep bci? *IEEE transactions on neural systems and rehabilitation engineering*, 18(2):107–116.
- [Allison and Sugiarto, 2008] Allison, B. and Sugiarto, I. (2008). Display optimization in SSVEP BCIs. *Computer-Human Interaction*, pages 2–5.
- [Allison et al., 2008] Allison, B. Z., McFarland, D. J., Schalk, G., Zheng, S. D., Jackson, M. M., and Wolpaw, J. R. (2008). Towards an independent brain-computer interface using steady state visual evoked potentials. *Clinical neurophysiology*, 119(2):399–408.
- [Armington, 1977] Armington, J. C. (1977). Psychophysical applications of human electroretinography. *Journal of the Optical Society of America*, 67(11):1458–1465.
- [Armington et al., 1971] Armington, J. C., Corwin, T. R., and Marsetta, R. (1971). Simultaneously recorded retinal and cortical responses to patterned stimuli. *Journal of the Optical Society of America*, 61(11):1514–1521.
- [Armington et al., 1967] Armington, J. C., Gaarder, K., and Schick, a. M. (1967). Variation of spontaneous ocular and occipital responses with stimulus patterns. *Journal of the Optical Society of America*, 57(12):1534–1539.
- [Baas et al., 2002] Baas, J. M. P., Kenemans, J. L., and Mangun, G. R. (2002). Selective attention to spatial frequency: An ERP and source localization analysis. *Clinical Neurophysiology*, 113(11):1840–1854.

- [Bakardjian et al., 2010] Bakardjian, H., Tanaka, T., and Cichocki, A. (2010). Optimization of SSVEP brain responses with application to eight-command Brain-Computer Interface. *Neuroscience letters*, 469(1):34–8.
- [Baluja and Caruana, 1995] Baluja, S. and Caruana, R. (1995). Removing the genetics from the standard genetic algorithm. *International Society of Machine Learning*, pages 1–11.
- [Bin et al., 2009a] Bin, G., Gao, X., Wang, Y., Hong, B., and Gao, S. (2009a). Vep-based brain-computer interfaces: time, frequency, and code modulations [research frontier]. *Computational Intelligence Magazine, IEEE*, 4(4):22–26.
- [Bin et al., 2011] Bin, G., Gao, X., Wang, Y., Li, Y., Hong, B., and Gao, S. (2011). A high-speed BCI based on code modulation VEP. *Journal of neural engineering*, 8(2):025015.
- [Bin et al., 2009b] Bin, G., Gao, X., Yan, Z., Hong, B., and Gao, S. (2009b). An online multi-channel ssvep-based brain-computer interface using a canonical correlation analysis method. *Journal of neural engineering*, 6(4):046002.
- [Blakemore and Sutton, 1969] Blakemore, C. and Sutton, P. (1969). Size adaptation: a new aftereffect. *Science (New York, N.Y.)*, 166(902):245–247.
- [Boksem et al., 2005] Boksem, M. a. S., Meijman, T. F., and Lorist, M. M. (2005). Effects of mental fatigue on attention: an ERP study. *Brain research. Cognitive brain research*, 25(1):107–16.
- [Burkitt et al., 2000] Burkitt, G. R., Silberstein, R. B., Cadusch, P. J., and Wood, a. W. (2000). Steady-state visual evoked potentials and travelling waves. *Clinical neurophysiology : official journal of the International Federation of Clinical Neurophysiology*, 111(2):246–58.
- [Celesia et al., 1982] Celesia, G. G., Middleton, W. S., and Veterans, M. (1982). Steady-state and transient visual evoked potentials in clinical practice. *Annals of the New York Academy of Sciences*, 388:290–307.

- [Chen et al., 2014] Chen, X., Chen, Z., Gao, S., and Gao, X. (2014). A high-ITR SSVEP-based BCI speller. *Brain-Computer Interfaces*, (December):1–11.
- [Cheng et al., 2002] Cheng, M., Gao, X., Gao, S., and Xu, D. (2002). Design and implementation of a brain-computer interface with high transfer rates. *Biomedical Engineering, IEEE Transactions on*, 49(10):1181–1186.
- [Diez et al., 2013] Diez, P. F., Torres Müller, S. M., Mut, V. A., Laciari, E., Avila, E., Bastos-Filho, T. F., and Sarcinelli-Filho, M. (2013). Commanding a robotic wheelchair with a high-frequency steady-state visual evoked potential based brain-computer interface. *Medical Engineering and Physics*, 35:1155–1164.
- [Duszyk et al., 2014] Duszyk, A., Bierzyska, M., Radzikowska, Z., Milanowski, P., Ku, R., Suffczynski, P., Michalska, M., abcki, M., Zwoliski, P., and Durka, P. (2014). Towards an optimization of stimulus parameters for brain-computer interfaces based on steady state visual evoked potentials. *PLoS ONE*, 9(11):e112099.
- [Ficke and Science Management Corp. Washington, 1992] Ficke, R. C. and Science Management Corp. Washington, D. C. (1992). *Digest of Data on Persons with Disabilities [microform] / Robert C. Ficke*. Distributed by ERIC Clearinghouse [Washington, D.C.].
- [Galloway, 1990] Galloway, N. (1990). Human Brain Electrophysiology: Evoked Potentials and Evoked Magnetic Fields in Science and Medicine. *The British Journal of Ophthalmology*, 74(4):255.
- [Gao et al., 2003] Gao, X., Xu, D., Cheng, M., and Gao, S. (2003). A bci-based environmental controller for the motion-disabled. *Neural Systems and Rehabilitation Engineering, IEEE Transactions on*, 11(2):137–140.
- [Garcia-Molina and Zhu, 2011] Garcia-Molina, G. and Zhu, D. (2011). Optimal spatial filtering for the steady state visual evoked potential: BCI application. *2011 5th International IEEE/EMBS Conference on Neural Engineering*, pages 156–160.

- [Goldberg and Others, 1989] Goldberg, D. E. and Others (1989). *Genetic algorithms in search, optimization, and machine learning*, volume 412. Addison-Wesley Professional, 1 edition.
- [Grill-Spector et al., 2006] Grill-Spector, K., Henson, R., and Martin, A. (2006). Repetition and the brain: Neural models of stimulus-specific effects. *Trends in Cognitive Sciences*, 10(1):14–23.
- [Guo et al., 2008] Guo, F., Hong, B., Gao, X., and Gao, S. (2008). A brain-computer interface using motion-onset visual evoked potential. *Journal of neural engineering*, 5(4):477–85.
- [Haslwanter, 2011] Haslwanter, T. (2011). Magno parvocellular pathways [online image]. retrieved from http://commons.wikimedia.org/wiki/File:with_permissions_under_by-sa_3.0_liscence.
- [Heinrich and Bach, 2001] Heinrich, S. P. and Bach, M. (2001). Adaptation dynamics in pattern-reversal visual evoked potentials. *Documenta Ophthalmologica*, 102(2):141–156.
- [Herrmann, 2001] Herrmann, C. S. (2001). Human EEG responses to 1100 Hz flicker: resonance phenomena in visual cortex and their potential correlation to cognitive phenomena. *Experimental Brain Research*, 137(3-4):346–353.
- [Hinterberger et al., 2004] Hinterberger, T., Schmidt, S., Neumann, N., Mellinger, J., Blankertz, B., Curio, G., and Birbaumer, N. (2004). Brain-computer communication and slow cortical potentials. *IEEE Transactions on Biomedical Engineering*, 51(6):1011–1018.
- [Hong et al., 2009] Hong, B., Guo, F., Liu, T., Gao, X., and Gao, S. (2009). N200-speller using motion-onset visual response. *Clinical neurophysiology*, 120(9):1658–66.

- [Hwang et al., 2013] Hwang, H.-J., Hwan Kim, D., Han, C.-H., and Im, C.-H. (2013). A new dual-frequency stimulation method to increase the number of visual stimuli for multi-class SSVEP-based brain-computer interface (BCI). *Brain research*, 1515:66–77.
- [Jia et al., 2011] Jia, C., Gao, X., and Hong, B. (2011). Frequency and Phase Mixed Coding in SSVEP-Based Brain-Computer Interface. *Biomedical Engineering, IEEE*, (c):1–7.
- [Jin et al., 2011] Jin, J., Zhang, Y., and Wang, X. (2011). A novel combination of time phase and EEG frequency components for SSVEP-based BCI. *Neural Information Processing*, pages 273–278.
- [Johnson et al., 2011] Johnson, G., Waytowich, N., and Krusienski, D. J. (2011). The challenges of using scalp-EEG input signals for continuous device control. *Lecture Notes in Computer Science*, 6780 LNAI:525–527.
- [Johnson et al., 2010] Johnson, G. D., Waytowich, N. R., Cox, D. J., and Krusienski, D. J. (2010). Extending the discrete selection capabilities of the P300 Speller to goal-oriented robotic arm control. *2010 3rd IEEE RAS and EMBS International Conference on Biomedical Robotics and Biomechatronics, BioRob 2010*, pages 572–575.
- [Kapeller et al., 2013] Kapeller, C., Hintermuller, C., Abu-Alqumsan, M., Pruckl, R., Peer, A., and Guger, C. (2013). A bci using vep for continuous control of a mobile robot. *Conference proceedings: IEEE Engineering in Medicine and Biology Society.*, 2013:5254–5257.
- [Kelly et al., 2004] Kelly, S. P., Lalor, E., Finucane, C., and Reilly, R. B. (2004). A comparison of covert and overt attention as a control option in a steady-state visual evoked potential-based brain computer interface. *Conference proceedings: IEEE Engineering in Medicine and Biology Society.*, 7:4725–4728.

- [Klein et al., 1974] Klein, S., Stromeyer, C. F., and Ganz, L. (1974). The simultaneous spatial frequency shift: a dissociation between the detection and perception of gratings. *Vision Research*, 14(12):1421–1432.
- [Ko, 2013] Ko, S. (2013). On multi-class classification through the minimization of the confusion matrix norm. *JMLR: Workshop and Conference Proceedings*, (2004):277–292.
- [Kubler et al., 2004] Kubler, A., Neumann, N., Wilhelm, B., Hinterberger, T., and Birbaumer, N. (2004). Predictability of Brain-Computer Interfaces. *Journal of Psychophysiology*, 18(2-3):130–139.
- [Kuś et al., 2013] Kuś, R., Duszyk, A., Milanowski, P., abecki, M., Bierzyska, M., Radzikowska, Z., Michalska, M., Zygierecz, J., Suffczynski, P., and Durka, P. J. (2013). On the Quantification of SSVEP Frequency Responses in Human EEG in Realistic BCI Conditions. *PLoS ONE*, 8(10).
- [Lalor and Foxe, 2009] Lalor, E. C. and Foxe, J. J. (2009). Visual evoked spread spectrum analysis (VESPA) responses to stimuli biased towards magnocellular and parvocellular pathways. *Vision research*, 49(1):127–33.
- [Lalor et al., 2005] Lalor, E. C., Kelly, S. P., Finucane, C., Burke, R., Smith, R., Reilly, R. B., and McDarby, G. (2005). Steady-state VEP-based brain-computer interface control in an immersive 3D gaming environment. *Eurasip Journal on Applied Signal Processing*, 2005(19):3156–3164.
- [Lalor et al., 2007] Lalor, E. C., Kelly, S. P., Pearlmutter, B. a., Reilly, R. B., and Foxe, J. J. (2007). Isolating endogenous visuo-spatial attentional effects using the novel visual-evoked spread spectrum analysis (VESPA) technique. *The European journal of neuroscience*, 26(12):3536–42.
- [Lee et al., 2011] Lee, P.-L., Yeh, C.-L., Cheng, J. Y.-S., Yang, C.-Y., and Lan, G.-Y. (2011). An SSVEP-based BCI using high duty-cycle visual flicker. *IEEE transactions on bio-medical engineering*, 58(12):3350–9.

- [Leguire and Rogers, 1985] Leguire, L. E. and Rogers, G. L. (1985). Pattern electroretinogram: Use of noncorneal skin electrodes. *Vision Research*, 25(6):867–870.
- [Lesenfants et al., 2014] Lesenfants, D., Habbal, D., Lugo, Z., Lebeau, M., Horki, P., Amico, E., Pokorny, C., Gómez, F., Soddu, a., Müller-Putz, G., Laureys, S., and Noirhomme, Q. (2014). An independent SSVEP-based brain-computer interface in locked-in syndrome. *Journal of neural engineering*, 11(3):035002.
- [Lesenfants et al., 2011] Lesenfants, D., Partoune, N., Soddu, A., Lehembre, R., Noirhomme, Q., and Muller-Putz, G. (2011). Design of a covert SSVEP-based BCI for the diagnosis of unresponsive patients. *In: 5th Int. Brain-Computer Interface Conf.*, pages pp:1–4.
- [Li et al., 2013] Li, Y., Pan, J., Wang, F., and Yu, Z. (2013). A hybrid BCI system combining P300 and SSVEP and its application to wheelchair control. *IEEE transactions on bio-medical engineering*, 60(11):3156–66.
- [Lin et al., 2007] Lin, Z., Zhang, C., Wu, W., and Gao, X. (2007). Frequency recognition based on canonical correlation analysis for SSVEP-based BCIs. *IEEE transactions on bio-medical engineering*, 54(6 Pt 2):1172–6.
- [Lotte et al., 2007] Lotte, F., Congedo, M., Lécuyer, a., Lamarche, F., and Arnaldi, B. (2007). A review of classification algorithms for EEG-based brain-computer interfaces. *Journal of neural engineering*, 4(2):R1–R13.
- [Mackay et al., 2003] Mackay, A. M., Bradnam, M. S., and Hamilton, R. (2003). Rapid detection of threshold VEPs. *Clinical Neurophysiology*, 114(6):1009–1020.
- [McKeefry et al., 1996] McKeefry, D. J., Russell, M. H., Murray, I. J., and Kulikowski, J. J. (1996). Amplitude and phase variations of harmonic components in human achromatic and chromatic visual evoked potentials. *Visual neuroscience*, 13(4):639–53.

- [Middendorf et al., 2000] Middendorf, M., McMillan, G., Calhoun, G., and Jones, K. S. (2000). Brain-computer interfaces based on the steady-state visual-evoked response. *IEEE transactions on rehabilitation engineering*, 8(2):211–4.
- [Movshon and Lennie, 1979] Movshon, J. A. and Lennie, P. (1979). Pattern-selective adaptation in visual cortical neurones. *Nature*, 278(5707):850–852.
- [Müller et al., 2011] Müller, S. M. T., Diez, P. F., Bastos-Filho, T. F., Sarcinelli-Filho, M., Mut, V., and Laciari, E. (2011). SSVEP-BCI implementation for 37-40 Hz frequency range. *Conference proceedings : IEEE Engineering in Medicine and Biology Society.*, 2011:6352–5.
- [Müller-Putz and Pfurtscheller, 2008] Müller-Putz, G. R. and Pfurtscheller, G. (2008). Control of an electrical prosthesis with an ssvep-based bci. *IEEE transactions on bio-medical engineering*, 55(1):361–364.
- [Ng et al., 2012] Ng, K. B., Bradley, A. P., and Cunnington, R. (2012). Stimulus specificity of a steady-state visual-evoked potential-based braincomputer interface. *Journal of neural engineering*, 9(3):036008.
- [Peterson et al., 2005] Peterson, D. a., Knight, J. N., Kirby, M. J., Anderson, C. W., and Thaut, M. H. (2005). Feature Selection and Blind Source Separation in an EEG-Based Brain-Computer Interface. *EURASIP Journal on Advances in Signal Processing*, 2005(19):3128–3140.
- [Pfurtscheller et al., 2010] Pfurtscheller, G., Solis-Escalante, T., Ortner, R., Linortner, P., and Müller-Putz, G. R. (2010). Self-paced operation of an SSVEP-Based orthosis with and without an imagery-based ”brain switch:” a feasibility study towards a hybrid BCI. *IEEE transactions on neural systems and rehabilitation engineering*, 18(4):409–14.
- [Ralaivola, 2012] Ralaivola, L. (2012). Confusion-based online learning and a passive-aggressive scheme. *In: Neural Information Processing Systems Conference*, pages 1–9.

- [Rentschler et al., 1975] Rentschler, I., Hilz, R., and Grimm, W. (1975). Processing of positional information in the human visual system. *Nature*, 253(5491):444–445.
- [Saetang et al., 2013] Saetang, J., Punsawad, Y., and Wongsawat, Y. (2013). On the performance comparison of using checkerboard and flash ball visual stimulators for SSVEP-based BCI system. *IFMBE Proceedings*, 39 IFMBE:1549–1552.
- [Schalk, 2004] Schalk, G. (2004). BCI2000, a general-purpose brain-computer interface (BCI) system. *IEEE Trans. Biomed Eng*, 51:1034–1043.
- [Schroeder, 2014] Schroeder, K. (2014). Visual system diagram [online image]. retrieved from <http://commons.wikimedia.org/wiki/file:gray722-svg.svg> with permissions under by-sa 3.0 liscence.
- [Sharbrough et al., 1991] Sharbrough, F., Chatrain, C. E., Lesser, R. P., Luders, H., Nuwer, M., and Picton, T. W. (1991). Amearican Electroencephalographic Society guidelines for standard electrode position nomenclature. *J. Clin Neurophysiol*, 8:200–202.
- [Sokol and Bloom, 1977] Sokol, S. and Bloom, B. (1977). Macular ergs elicited by checkerboard pattern stimuli. In Lawwill, T., editor, *ERG, VER and Psychophysics*, volume 13 of *Documenta Ophthalmologica*, pages 299–305. Springer Netherlands.
- [Spüler, 2012] Spüler, M. (2012). One class SVM and Canonical Correlation Analysis increase performance in a c-VEP based Brain-Computer Interface (BCI). In: *Proceedings of 20th European Symposium on Artificial Neural Networks (ESANN 2012)*. Bruges, Belgium,, (April):pp:103–108.
- [Spüler et al., 2012] Spüler, M., Rosenstiel, W., and Bogdan, M. (2012). Online adaptation of a c-VEP Brain-computer Interface(BCI) based on error-related potentials and unsupervised learning. *PloS one*, 7(12):e51077.

- [Srihari Mukesh et al., 2006] Srihari Mukesh, T. M., Jaganathan, V., and Reddy, M. R. (2006). A novel multiple frequency stimulation method for steady state VEP based brain computer interfaces. *Physiological measurement*, 27(1):61–71.
- [Sutter, 1992] Sutter, E. E. (1992). The brain response interface: communication through visually-induced electrical brain responses. *Journal of Microcomputer Applications*, 15(1):31 – 45. Special Issue on Computers for Handicapped People.
- [Tanaka, 1996] Tanaka, K. (1996). Inferotemporal cortex and object vision. *Annual review of neuroscience*, 19:109–39.
- [Tobimatsu et al., 1993] Tobimatsu, S., Kurita-Tashima, S., Nakayama-Hiromatsu, M., and Kato, M. (1993). Effect of spatial frequency on transient and steady-state VEPs: stimulation with checkerboard, square-wave grating and sinusoidal grating patterns. *Journal of the neurological sciences*, 118(1):17–24.
- [Tomoda et al., 1991] Tomoda, H., Celesia, G. G., and Toleikis, S. C. (1991). Effect of spatial frequency on simultaneous recorded steady-state pattern electroretinograms and visual evoked potentials. *Electroencephalography and Clinical Neurophysiology - Evoked Potentials*, 80(2):81–88.
- [Tu et al., 2012] Tu, T., Xin, Y., Gao, X., and Gao, S. (2012). Chirp-modulated visual evoked potential as a generalization of steady state visual evoked potential. *Journal of neural engineering*, 9(1):016008.
- [Valbuena et al., 2007] Valbuena, D., Cyriacks, M., Friman, O., Volosyak, I., and Graser, A. (2007). Brain-computer interface for high-level control of rehabilitation robotic systems. In *Rehabilitation Robotics, 2007. ICORR 2007. IEEE 10th International Conference on*, pages 619–625.
- [Vialatte et al., 2010] Vialatte, F.-B., Maurice, M., Dauwels, J., and Cichocki, A. (2010). Steady-state visually evoked potentials: focus on essential paradigms and future perspectives. *Progress in neurobiology*, 90(4):418–38.

- [Wang et al., 2008] Wang, Y., Gao, X., Hong, B., Jia, C., and Gao, S. (2008). Brain-computer interfaces based on visual evoked potentials. *IEEE engineering in medicine and biology magazine*, 27(5):64–71.
- [Waytowich et al., 2010] Waytowich, N., Henderson, a., Krusienski, D., and Cox, D. (2010). Robot application of a brain computer interface to staubli TX40 robots - early stages. *World Automation Congress (WAC)*, 2010.
- [Waytowich and Krusienski, 2014] Waytowich, N. R. and Krusienski, D. J. (2014). Novel Characterization of the Steady-State Visual Evoked Potential Spectrum of EEG. *Braink KDD: International Workshop on Data Mining for Brain Science*.
- [Waytowich and Krusienski, 2015] Waytowich, N. R. and Krusienski, D. J. (2015). Spatial decoupling of targets and flashing stimuli for visual brain-computer interfaces. *Journal of Neural Engineering*, 12(3).
- [Westheimer, 1982] Westheimer, G. (1982). The spatial grain of the perifoveal visual field. *Vision Research*, 22(1):157–162.
- [Wolpaw and Wolpaw,] Wolpaw, J. and Wolpaw, E. W. Oxford: Oxford University Press.
- [Wolpaw et al., 2002] Wolpaw, J. R., Birbaumer, N., McFarland, D. J., Pfurtscheller, G., and Vaughan, T. M. (2002). Brain-computer interfaces for communication and control. *Clinical neurophysiology : official journal of the International Federation of Clinical Neurophysiology*, 113(6):767–91.
- [Wolpaw et al., 1991] Wolpaw, J. R., McFarland, D. J., Neat, G. W., and Forneris, C. a. (1991). An EEG-based brain-computer interface for cursor control. *Electroencephalography and clinical neurophysiology*, 78(3):252–259.
- [Xie et al., 2012] Xie, J., Xu, G., Wang, J., Zhang, F., and Zhang, Y. (2012). Steady-state motion visual evoked potentials produced by oscillating Newton’s rings: implications for brain-computer interfaces. *PloS one*, 7(6):e39707.

- [Yan et al., 2011] Yan, Z., Gao, X., and Gao, S. (2011). Right-and-left visual field stimulation: A frequency and space mixed coding method for SSVEP based brain-computer interface. *Science China Information Sciences*, 54(12):2492–2498.
- [Zerafa et al., 2013] Zerafa, R., Camilleri, T., Falzon, O., and Camilleri, K. P. (2013). Comparison of plain and checkerboard stimuli for brain computer interfaces based on steady state visual evoked potentials. *International IEEE/EMBS Conference on Neural Engineering, NER*, pages 33–36.
- [Zhang et al., 2012] Zhang, Y., Jin, J., Qing, X., Wang, B., and Wang, X. (2012). LASSO based stimulus frequency recognition model for SSVEP BCIs. *Biomedical Signal Processing and Control*, 7(2):104–111.
- [Zhu et al., 2010] Zhu, D., Bieger, J., Garcia Molina, G., and Aarts, R. M. (2010). A survey of stimulation methods used in SSVEP-based BCIs. *Computational intelligence and neuroscience*, 2010:702357.

VITA

Nicholas R. Waytowich
 Department of Biomedical Engineering
 Old Dominion University
 Norfolk, VA 23529

Nicholas Waytowich recieved a B.S. in Mechanical Engineering in 2010 at the University of North Florida with a specialization in Robotics, and a Masters in Electrical and Computer Engineering in 2013 at Old Dominion University with an emphasis in neural signal processing and machine learning. During his Ph.D. studies, he worked as a graduate research assistant in the Advanced Signal Processing in Engineering and Neuroscience (ASPEN) Lab under the advisement and mentorship of Dr. Dean J Krusienski. His research areas of interest include signal processing and machine learning, image processing, brain-computer interface development and experimental design.

Waytowich, N. R. and Krusienski, D. J. Spatial Decoupling of Targets and Flashing Stimuli for Visual Brain-Computer Interfaces. *Journal of Neural Engineering*, vol. 12, no. 3, 2015.

Waytowich, N. R. and Krusienski, D. J. Multiclass Steady-State Visual Evoked Potential Frequency Evaluation using Chirp-Modulated Stimuli. Submitted for review, Dec 2014.

Waytowich, N. R. and Krusienski, D. J. Novel Characterization of the Steady-State Visual Evoked Potential Spectrum of EEG. In: BrainKDD: International Workshop on Data Mining for Brain Science, 2014.

Waytowich, N. R. and Krusienski, D. J. Control of a Brain-Computer Interface using Parafoveal Code-modulated Visual Stimuli. In: Society for Neuroscience Abstracts, 2014.

Waytowich, N. R. and Krusienski, D. J. Characterizing the SSVEP Spectrum using a Broadband Noise Stimulus. In: The International Brain-Computer Interface Conference, 2013.